Long-term video monitoring of aeolian activity on a narrow beach

Lange-termijnvideomonitoring van eolische activiteit op een smal strand

(met een samenvatting in het Nederlands)

P R O E F S C H R I F T

ter verkrijging van de graad van doctor aan de Universiteit Utrecht
op gezag van de rector magnificus, prof. dr. H.R.B.M. Kummeling,
ingevolge het besluit van het college voor promoties in het openbaar te verdedigen
op maandag 21 september 2020 des ochtends te 11.00 uur

door

Pam Margaretha Hage
geboren op 10 juni 1991 te Kampen

Promotor:
Prof. dr. B. G. Ruessink

Copromotor:
Dr. J. J. A. Donker

This work was financially supported by the Dutch Technology Foundation STW, which is part of the Netherlands Organisation for Scientific Research (NWO), and is partly funded by the Ministry of Economic affairs (project number 13709).

Long-term video monitoring of aeolian activity on a narrow beach

Promotor:
Prof. dr. B. G. Ruessink

Copromotor:
Dr. J. J. A. Donker

Examination committee:
Prof. dr. I. Delgado-Fernandez
Edge Hill University, United Kindom

Prof. dr. K.M. Wijnberg
University of Twente, The Netherlands

Prof. dr. D. van der Wal
University of Twente, The Netherlands

Prof. dr. ir. S.G.J. Aarninkhof
TU Delft, the Netherlands

Dr. S.M Arens
Arens Bureau voor Strand- en Duinonderzoek

ISBN 978-90-6266-580-8

Published by Faculty of Geosciences, Universiteit Utrecht, The Netherlands, in:
Utrecht Studies in Earth Sciences (216), ISSN 2211-4335

Typeset using XeLaTeX

Printed by Ipskamp Printing || www.proefschriften.net
Cover and artwork by Pam Hage.

Utrecht Studies in Earth Sciences 206

Long-term video monitoring of aeolian activity on a narrow beach

P.M. Hage

Utrecht 2020

Faculty of Geosciences, Utrecht University

Even blond als de duinen

loopt ze te struinen

op het strand,

emmer in haar hand.

Met de zon in de rug

loopt ze heen en weer terug.

Ze zoekt niet, ze vindt,

van alles, dit zomerkind.

Daar duikt ze de zee weer in,

die kleine zeemeermin.

- Opa Zee, uit mijn poëziealbum

Contents

Summary

Aeolian sand transport takes place when the wind is strong enough to lift a grain of sand. Predicting aeolian transport for beaches is difficult, as existing predictive models, which usually only have the wind velocity as a variable, are designed for ideal circumstances with a steady wind flow, a homogeneous grain size, and a dry and flat sand surface. Sandy beaches show different conditions. When wind-only models are applied, the resulting amount of sand that is predicted to be deposited on the foredune often exceeds the measured amount considerably, especially when the beach is less than several tens of metres wide. This is caused by transport limiting factors, such as surface moisture, the formation of salt or algae crusts, the presence of vegetation, or snow and ice cover. The aeolian transport rate increases downwind until it reaches its maximum at a distance termed the critical fetch length. When the available distance, or maximum fetch, cannot reach this critical fetch, aeolian transport will not reach its potential value. This is particularly relevant for narrow beaches. As a consequence, the moment of largest potential transport does not necessarily coincide with the moment of largest actual transport. When the actual transport is smaller than expected, the transport is limited. When this is not the case, the transport is unlimited. When transport events are limited and unlimited, and what factors control this, is not well understood. Accordingly, we also have limited capabilities in accurately predicting the long-term (>months) amount of wind-blown sand to the foredune.

Improved understanding of long-term aeolian sand transport is important as the sand contributes to dune growth and recovery from storms, which is a relatively slow process and takes months to years (long-term). In contrast, erosive storm events last only a few hours or days. Coastal dunes have been strengthened and encouraged to grow to protect densely populated hinterlands by planting marram grass or placing fences to catch the sand and keep it in place. This, however, has created an unnaturally high foredune that prevents sand from being transported further inland. The input of sand into the dunes contributes to a diverse ecosystem, as the sand can bury climax vegetation and make it possible for pioneer vegetation to recolonise. Ideally, coastal dunes should combine both: provide safety from marine flooding and have a diverse ecosystem. To do this, measures to change sand dikes into dynamic systems are increasingly being implemented. This requires us knowing when to expect aeolian sand transport. The main aim of this thesis is therefore to better understand the timing of aeolian transport on a narrow beach, and to identify and elucidate key factors that determine this timing, with a focus on timescales from months to years.

To reach this aim, I examined a long-term data set of video images of Egmond aan Zee, the Netherlands. Video monitoring captures signs of aeolian sand transport in the shape of sand strips, which are stripe-like, slipfaceless bedforms with a wavelength of approximately 12 m that move slowly in the downwind direction; and streamers, which are clouds of sand that move rapidly across the surface. The Argus station at Egmond is a coastal video monitoring system with a good view on the beach and makes photographs every half an hour. These images were used together with weather data to determine the physical characteristics of sand strips, and how they change under a wide range of wind conditions; and to determine how transport limiting factors affect aeolian sand transport on long time scales at this beach.

Finally, the Argus imagery was used to test the timing of limited and unlimited aeolian sand transport predicted by a fetch model, building on the work of Delgado-Fernandez (2011).

Despite being common features in wet aeolian systems, sand strips have not been studied extensively before, even though they can provide valuable insight into wind conditions that favour transport on narrow beaches. Aeolian transport, and therefore sand strip development, can only take place when the wind velocity surpasses a certain threshold value. In Chapter 2, this threshold value was determined by studying 6 months of Argus imagery (October 2011 to March 2012). It was found that signs of aeolian transport usually appear when the wind velocity (measured at 10-m height at a nearby meteorological station operated by the Royal Netherlands Meteorological institute) is 8 m/s or higher. This threshold was used to select aeolian transport events with well-developed sand strips from the 2005 to 2012 Argus dataset to find how their wavelength and migration velocity depend on the wind velocity. As sand strips have a lighter colour than the surface they travel over, a sinusoid signal could be found in the images' pixel values. Auto- and cross-correlation were applied to these pixel values to find the sand strips' wavelength and migration velocity. It was found that these characteristics were 12.0 m and 1.24 m/h on average, respectively, and showed only a slight, barely significant increase with wind velocity. What mattered more was the wind direction; sand strips fully developed only when the wind was (almost) alongshore. During cross-shore winds, the sand strips often developed no further than a cluster of irregular patches of migrating sand. The beach sometimes became inundated due to storm surges, which made the beach very narrow or completely flooded. This made aeolian sand transport almost impossible, as reflected by the absence of sand strips. The maximum available fetch therefore seems to be an important limiting factor.

In order to eventually improve predictions of aeolian sand transport, it is important to find moments where the actual aeolian sand transport is lower than the potential transport and to determine what factors contribute to this mismatch. In Chapter 3, this was pursued by first classifying the Argus imagery from October 2011 to March 2012 based on their visual transport intensity. Weak signs of visual aeolian transport include small migrating patches of sand and/or some streamers, while strong signs of transport show well-developed, migrating sand strips that cover the entire beach. The corresponding wind was then classified according to its velocity. Strong wind velocities were expected to cause strong visual signs of aeolian transport quickly. When this was not the case, the transport was considered to be limited. Weaker winds were expected to have visual signs of aeolian transport that were not as strong, but when very weak or no signs of transport could be seen, the transport was also considered to be limited. The opposite was possible as well; weak winds could cause well-developed sand strips. The results illustrate that limited transport events were more common for high wind velocities with a cross-shore direction. Unlimited events had a large range of wind velocities, but the strongest winds had an alongshore direction. The winter months showed more high wind velocity events, but these events resulted in limited transport when the wind is not blowing alongshore, which happened often. The summer was characterised by unlimited events with a relatively low wind velocity. The summer/winter variability could imply that aeolian transport dynamics also depends on air temperature, affecting evaporation and moisture content, but it remains unclear if this is truly the case.

A fetch-based model can be used to predict whether aeolian transport is limited or unlimited and hence to predict the timing of aeolian sand transport events. The model used in this thesis, called Aeolus, incorporates the effect of the fetch distance and surface moisture in order to make better long-term aeolian transport predictions than the wind only (potential) predictions. With Argus data, I checked if the model's timing is indeed correct. In Chapter 4, the Argus images taken between October 2011 and March 2012 were classified according to their visual signs of aeolian sand transport, and the same period of time was modelled by

Aeolus. It was found that the timing of non-zero Aeolus results coincided quite well with the timing of transport visible on the Argus images. Strong differences between the modelled actual and potential transport indicate limited transport, which were more common for strong, cross-shore winds. This corresponds with the findings in Chapter 3, indicating that the model results are in line with observations. Thirty of the 183 examined days had no visual signs of aeolian transport on the Argus imagery, while Aeolus predicted non-zero transport. The actual transport calculated by Aeolus was very small for 27 of these 30 days, and could probably not be seen on the Argus images. Additionally, the Argus imagery sometimes showed signs of rain or snow. These factors are not incorporated in Aeolus and could have hindered aeolian transport. On 3 of the 30 days, Aeolus predicted transport but none was observed. On 5 other days, transport was observed while non was predicted. All of these mismatches could be the result of incorrect classification due to unclear Argus imagery. According to Aeolus, limited transport did not happen often. It is still important, however, as limited transport happened during strong, cross-shore winds, which under unlimited circumstances would result in large aeolian transport to the foredune.

The three chapters have provided insights into the factors that limit aeolian transport on a narrow beach and thus affect the timing of transport. Video monitoring has illustrated that wind speed and direction as well as beach width play a critical role in determining whether an event is limited or unlimited. The timing of limited and unlimited events can be predicted with reasonable accuracy with a fetch-based model that uses groundwater-induced surface-moisture dynamics as a transport limiting factor. The next step will be to test the model quantitatively with in-situ measurements. Using other field sites will help generalising the model results for beaches with different slopes, grain sizes, wind climates, and foredune morphologies. Studying aeolian sand transport with video monitoring will also benefit from the use of different sites. Combining imagery with in-situ data can lead to estimating aeolian sand transport rates without needing to visit the field site. These steps lead to a better prediction of long-term aeolian sand transport on beaches and how much of this sand can enter the dunes, where it can contribute to flood protection and to a diverse ecosystem.

Samenvatting

Eolisch zandtransport vindt plaats wanneer de wind sterk genoeg is om een zandkorrel op te tillen. Het voorspellen van eolisch transport voor stranden is moeilijk, omdat bestaande voorspellende modellen, die meestal alleen de windsnelheid als variabele hebben, zijn ontworpen voor ideale omstandigheden met een constante wind, een homogene korrelgrootte en een droge en vlakke ondergrond van zand. Zandstranden hebben echter andere omstandigheden. Wanneer transportmodellen op basis van alleen de wind worden gebruikt, dan zal de hoeveelheid zand dat naar verwachting op het voorduin wordt afgezet vaak de gemeten hoeveelheid overschrijden. Dit gebeurt vooral wanneer het strand minder dan enkele tientallen meters breed is. Dit wordt veroorzaakt door transportbeperkende factoren, zoals het vochtgehalte van het strandoppervlak, de vorming van zout- of algenkorsten, de aanwezigheid van vegetatie of sneeuw- en ijsbedekking. Het eolisch transport neemt toe in de richting van de wind tot het zijn maximum bereikt op een afstand die de kritische strijklengte wordt genoemd. Wanneer de beschikbare afstand of maximale strijklengte korter is dan deze kritieke strijklengte, dan zal het eolisch transport zijn potentiële waarde niet bereiken. Dit is vooral relevant voor smalle stranden. Als gevolg hiervan valt het moment van het grootste potentiële transport niet noodzakelijk samen met het moment van het grootste daadwerkelijke transport. Wanneer het daadwerkelijke transport kleiner is dan verwacht, dan is het transport gelimiteerd. Wanneer dit niet het geval is, is het transport ongelimiteerd. Het is onduidelijk wanneer transportgebeurtenissen gelimiteerd of ongelimiteerd zijn en welke factoren dit beheersen. Hierdoor hebben we ook beperkte mogelijkheden om de hoeveelheid zand dat naar het voorduin geblazen wordt nauwkeurig te voorspellen op de lange termijn (> maanden).

Het beter begrijpen van eolische zandtransport op de lange termijn is belangrijk omdat het zand bijdraagt aan de groei van duinen en hun herstel van stormen, wat een relatief langzaam proces is en maanden tot jaren duurt (lange termijn). Daarentegen duren erosieve stormmomenten slechts een paar uur of dagen. Om het dichtbevolkte achterland te beschermen, worden kustduinen versterkt en gestimuleerd om te groeien door het planten van helmgras of het plaatsen van hekken om het zand op te vangen en op zijn plaats te houden. Hierdoor is echter een onnatuurlijk hoog voorduin ontstaan dat voorkomt dat zand verder landinwaarts wordt getransporteerd. De toevoeging van zand aan de duinen draagt bij aan een divers ecosysteem, omdat het zand de climaxvegetatie kan begraven en het voor pioniervegetatie mogelijk maakt om te koloniseren. Idealiter zouden kustduinen dit combineren: bescherming bieden tegen overstromingen van zee en het hebben van een divers ecosysteem. Hiervoor worden steeds meer maatregelen genomen om zanddijken te veranderen in dynamische systemen. Dit vereist dat we weten wanneer we eolisch zandtransport kunnen verwachten. Het belangrijkste doel van dit proefschrift is dan ook om de timing van eolisch transport op een smal strand beter te begrijpen, en om sleutelfactoren die deze timing bepalen te identificeren en op te helderen. De focus ligt op tijdschalen van maanden tot jaren.

Om dit doel te bereiken heb ik een lange-termijndataset van videobeelden van Egmond aan Zee, Nederland, onderzocht. Videomonitoring ziet eolisch zandtransport in de vorm van zandstrips (streepachtige bodemvormen zonder storthelling en met een golflengte van ongeveer 12 m die langzaam in de richting van de wind bewegen) en streamers (zandwolken die snel over het oppervlak bewegen). Het Argusstation in Egmond is een videomonitorings-

systeem van de kust met een goed zicht op het strand en maakt elk half uur foto's. Deze beelden werden samen met weergegevens gebruikt om de fysieke kenmerken van zandstrips te bepalen en hoe die kenmerken veranderen onder een breed scala van windomstandigheden; en om te bepalen hoe transportlimiterende factoren het eolische zandtransport op dit strand beïnvloeden op lange tijdschalen. Ten slotte werden de Argusbeelden gebruikt om de timing van gelimiteerd en ongelimiteerd eolisch zandtransport te testen die waren voorspeld door een model dat rekening houdt met strijklengte. Dit model bouwt voort op het werk van Delgado-Fernandez (2011).

Ondanks dat zandstrips veel voorkomen in natte eolische systemen, zijn ze niet uitgebreid bestudeerd, terwijl ze waardevol inzicht kunnen geven in de windomstandigheden die transport op smalle stranden bevorderen. Eolisch transport, en dus zandstripontwikkeling, vindt alleen plaats wanneer de windsnelheid een bepaalde drempelwaarde overschrijdt. In Hoofdstuk 2 werd deze drempelwaarde bepaald door 6 maanden (oktober 2011 tot maart 2012) aan Argusbeelden te bestuderen. Hieruit bleek dat tekenen van eolisch transport meestal optreden wanneer de windsnelheid (gemeten op 10 m hoogte bij een nabijgelegen meteorologisch station van het Koninklijk Nederlands Meteorologisch Instituut) 8 m/s of hoger is. Deze drempel werd gebruikt om uit de Argus-dataset van 2005 tot 2012 eolische transportmomenten te selecteren met goed ontwikkelde zandstrips. Met deze transportmomenten werd achterhaald hoe golflengte en migratiesnelheid van zandstrips afhangen van de windsnelheid. Omdat zandstrips een lichtere kleur hebben dan het oppervlak waarover ze migreren, kan er een sinusvormig signaal worden gevonden in de pixelwaarden van de afbeeldingen. Auto- en kruiscorrelatie werden toegepast op deze pixelwaarden om de golflengte en migratiesnelheid van de zandstrips te bepalen. Deze kenmerken bleken respectievelijk 12,0 m en 1,24 m/u te zijn en vertoonden slechts een geringe, nauwelijks significante toename met de windsnelheid. De windrichting was belangrijker; zandstrips zijn pas volledig ontwikkeld als de wind (bijna) kustlangs was. Bij kustdwarse wind ontwikkelden de zandstrips zich vaak niet verder dan een cluster van migrerende, onregelmatige zandhoopjes. Het strand werd soms overspoeld door stormvloeden, waardoor het strand erg smal of volledig overspoeld was. Dit maakte eolisch zandtransport bijna onmogelijk, zoals blijkt uit de afwezigheid van zandstrips. De maximaal beschikbare strijklengte lijkt daarom een belangrijke limiterende factor.

Om uiteindelijk de voorspellingen van eolisch zandtransport te verbeteren, is het belangrijk om momenten te vinden waarop het daadwerkelijke eolische zandtransport lager is dan het potentiële transport en om te bepalen welke factoren bijdragen aan dit verschil. In Hoofdstuk 3 werd dit nagestreefd door eerst de Argus-beelden van oktober 2011 tot maart 2012 te classificeren op basis van hun visuele transportintensiteit. Zwakke tekenen van visueel eolisch transport zijn onder meer kleine migrerende hoopjes zand en/of enkele streamers, terwijl sterke tekenen van transport goed ontwikkelde, migrerende zandstrips vertonen die het hele strand bedekken. De bijbehorende wind werd vervolgens geclassificeerd op basis van snelheid. Van hoge windsnelheden werd verwacht dat ze sneller sterke visuele tekenen van eolisch transport konden veroorzaken. Wanneer dit niet het geval was, werd het transport als gelimiteerd beschouwd. Van zwakkere winden werd verwacht dat ze meer visuele tekenen van eolisch transport vertoonden die minder sterk waren. Wanneer er echter zeer zwakke of geen sporen van transport te zien waren, werd het transport ook als gelimiteerd beschouwd. Het tegendeel was ook mogelijk; een zwakke wind kan ook goed ontwikkelde zandstroken veroorzaken. De resultaten illustreren dat gelimiteerde transportmomenten vaker voorkwamen bij wind met een hoge snelheid en een kustdwarse richting. Ongelimiteerde momenten kwamen voor bij verschillende windsnelheden, maar de sterkste winden hadden een kustlangse richting. In de wintermaanden waren er meer momenten met hoge windsnelheden, maar deze momenten resulteerden in gelimiteerd transport wanneer de wind niet langs de

kust waait, wat vaak gebeurde. De zomer werd gekenmerkt door ongelimiteerde momenten met een relatief lage windsnelheid. De variabiliteit tussen zomer en winter zou kunnen betekenen dat de eolische transportdynamiek ook afhangt van de luchttemperatuur, wat de verdamping en het vochtgehalte beïnvloedt, maar het blijft onduidelijk of dit echt het geval is.

Een model gebaseerd op strijklengte kan worden gebruikt om te voorspellen of eolisch transport gelimiteerd of ongelimiteerd is en kan daarom de timing van eolische zandtransportmomenten voorspellen. Het model dat in dit proefschrift wordt gebruikt, Aeolus, gebruikt het effect van de strijklengte en het vochtgehalte van het strandoppervlak om betere eolische transportvoorspellingen voor de lange termijn te maken dan voorspellingen gebaseerd op de wind alleen (het potentiële transport). Met Argus-gegevens heb ik gecontroleerd of de timing van het model inderdaad correct is. In Hoofdstuk 4 werden de Argus-beelden van oktober 2011 tot en met maart 2012 geclassificeerd op basis van hun visuele tekenen van eolisch zandtransport. Dezelfde periode werd gemodelleerd door Aeolus. Het bleek dat de timing van transport die door Aeolus was voorspeld vrij goed samenviel met de timing van transport die zichtbaar was op de Argus-beelden. Sterke verschillen tussen het gemodelleerde werkelijke en potentiële transport duiden op gelimiteerd transport en kwam vaker voor bij sterke kustdwarse winden. Dit komt overeen met de bevindingen in Hoofdstuk 3, wat aangeeft dat de modelresultaten in lijn zijn met de waarnemingen. Dertig van de 183 onderzochte dagen vertoonden geen visuele tekenen van eolisch transport op de Argus-beelden, terwijl Aeolus wel transport voorspelde. Het daadwerkelijke transport dat door Aeolus werd berekend, was gedurende 27 van deze 30 dagen erg klein en was waarschijnlijk niet te zien op de Argus-beelden. Bovendien vertoonden de Argus-beelden soms tekenen van regen of sneeuw. Deze factoren zijn niet verwerkt in Aeolus en zouden het eolisch transport kunnen hebben belemmerd. Op 3 van de 30 dagen voorspelde Aeolus transport, maar dit werd niet waargenomen op de Argus-beelden. Op 5 andere dagen werd wel transport waargenomen terwijl dit niet werd voorspeld door Aeolus. Al deze discrepanties kunnen het gevolg zijn van een onjuiste classificatie vanwege onduidelijke Argus-beelden. Op 5 van de 183 dagen waren er visuele tekenen van transport aanwezig, maar het Aeolus-model voorspelde geen zandtransport. Nogmaals, dit kan het gevolg zijn van een onjuiste classificatie vanwege onduidelijke Argus-beelden. Volgens Aeolus kwam ongelimiteerd transport weinig voor. Het is echter nog steeds belangrijk, aangezien het gelimiteerde transport plaatsvond tijdens sterke, kustdwarse winden die met ongelimiteerde omstandigheden zouden resulteren in een hoog eolisch transport naar het voorduin.

De drie hoofdstukken hebben inzicht gegeven in de factoren die het eolisch transport op een smal strand limiteren en dus de timing van het transport beïnvloeden. Videomonitoring heeft aangetoond dat de windsnelheid en -richting en strandbreedte een cruciale rol spelen bij het bepalen of een transportmoment gelimiteerd of ongelimiteerd is. De timing van gelimiteerde en ongelimiteerde momenten kan met redelijke nauwkeurigheid worden voorspeld met een op strijklengte gebaseerd model dat de door grondwater-geïnduceerde dynamiek van het vochtgehalte aan het oppervlak gebruikt als transportbeperkende factor. De volgende stap is het kwantitatief testen van het model met in-situ metingen. Het gebruik van andere onderzoekslocaties zal helpen bij het generaliseren van de modelresultaten voor stranden met andere hellingen, korrelgroottes, windklimaten en morfologieën van het voorduin. Het bestuderen van eolisch zandtransport met videomonitoring zal ook baat hebben bij andere locaties. Het combineren van beelden met in-situ gegevens kan resulteren in het schatten van eolische zandtransportsnelheden zonder het onderzoeksgebied te hoeven bezoeken. Deze stappen leiden tot een betere voorspelling van eolisch zandtransport op stranden op de lange termijn en hoeveel van dit zand de duinen kan binnendringen, waar het kan bijdragen aan bescherming tegen overstromingen vanuit zee en aan een divers ecosysteem.

Chapter 1

Introduction

1.1 Societal context

Sandy coasts are diverse landscapes that show a strong variability in vegetation, morphology and dynamics (Martínez and Psuty, 2004). Together with gravel beaches, they make up 40% of the world's coastlines (Bird, 2011; Luijendijk et al., 2018). Dunes have developed along many of the world's coastlines, provided there is a sufficient supply of sand transported by an onshore wind and burial-tolerant vegetation to capture the sand grains (Hesp, 2012). The largest dunes (10 to 100 m high, 1 to 10 km wide) are generally found along high-energy surf zones, while low-energy beaches may have dunes not higher and broader than 1 and 10 m, respectively (Short and Hesp, 1982; Durán and Moore, 2013). The most seaward dune can erode during relatively short (hours to days) storm events, which can result in a scarped dune face, dune overtopping, or even inundation (Sallenger Jr, 2000; Stockdon et al., 2007; Roelvink et al., 2009). For example, the west coast of Europe suffered from severe erosion during the unusually stormy winter in 2013/2014 (Masselink et al., 2016), which brought monitored sites in England back to their most eroded state since records started 5 to 10 years earlier (Scott et al., 2016), and the Gironde coast in France developed dune scarps over 10 m high (Castelle et al., 2015). In contrast, dune recovery and growth due to landward aeolian transport of beach sand takes months to years, or even longer, and is predominantly due to aeolian sediment transport of beach sand.

The growth and retreat of coastlines depend on the demand and supply of sediment, or in other words, the relative importance of erosion versus accretion. When erosion exceeds accretion in the long term, the coastline will retreat and undermine the dunes' strength. When accretion is dominant, the coastline extends, and new dunes might develop (Hesp, 2002). Structural erosion may threaten many densely populated, low-lying areas. Climate change threatens these coastal zones, as sea level rise increases the frequency and impact of erosion events, even if wave conditions remain unaltered (e.g. De Winter and Ruessink (2017)). High-end predictions by the Intergovernmental Panel on Climate Change (IPCC) estimate a sea level rise of 90 cm through 2099 (Pachauri et al., 2014), but a stronger rise up to 270 cm is physically possible (Sweet et al., 2017). According to the most conservative calculations, about 177 million people worldwide live in areas that are or will be vulnerable to chronic flooding within the next 100 years (Kopp et al., 2014). When assuming an extreme change in climate due to high carbon emissions, the number of people living below high tide levels can reach 630 million in 2100, versus 250 million today (Kulp and Strauss, 2019).

Natural dunes show a mosaic of habitats, with high and dry dune crests, moist valleys, and a stronger input of sand and sea spray when close to the shore. This causes plant succession to be more developed or developed differently in some coastal areas than in others. As a result, there are different habitats for a stunning variety of plant and animal species (Avis and Lubke, 1996; Martínez and Psuty, 2004). In the Netherlands, for example, coastal dunes contain 70% of all plant species (Kooijman, 2008). The hardest conditions for vege-

tation to survive can be found at embryo dunes and blowouts, where there is little moisture and nutrition. The plants are often exposed to salt spray and strong winds. Pioneer vegetation adapted to these circumstances, like sand couch (*Elytrigia juncea*) and marram grass (*Ammophila arenaria*), colonise here, and with time, they improve soil conditions by adding nutrients. More landward, other vegetation grows, like heather and later coniferous forest, which form climax communities for coastal dunes. The relatively wet dune valleys are often more developed than the dune tops and, when waterlogged, may contain marsh plants like willows, reeds and aquatic weeds (Chapman, 2016). When enough beach sand enters an area with climax vegetation (after a storm erodes the seaward dune that shelters the hinterland, for example), the climax vegetation disappears, and pioneer vegetation will replace it.

In order to protect densely populated hinterlands, coastal dunes have been strengthened and encouraged to grow, a process that started centuries ago for some locations. To strengthen a dune, marram grass has been planted or branches have been placed as fences to catch the sand and keep it in place, stabilising the dune (Arens, 1994; Nordstrom et al., 2004; Jackson et al., 2011). This has resulted in an unnaturally high foredune with little to no variation in vegetation. The planted vegetation is sometimes not a local species, and thus invasive (Martínez et al., 2013). Ideally, nature development and coastal safety have to be combined to have a dynamic and flood-resistant coast, but with an artificially stabilised dune, there can be no strong ecological diversity, as no beach sands can enter the dune area (Arens et al., 2013). This stimulates the growth of climax vegetation, resulting in a monotone landscape.

In order to maintain or enhance diversity in coastal dune areas, beach sand must be brought into the system. This can be done by removing vegetation that holds the sand in place, or by digging artificial blow outs (Martínez et al., 2013; Wondergem, 2005; Meerkerk et al., 2007). Aeolian sediment transport plays a crucial role in this, as it transports sands from the beach to the hinterland. The sand buries the climax vegetation and makes it possible for pioneer vegetation to recolonise. Dune restoration has been done for various places around the world, mostly in the USA, the Netherlands, and South-Africa (Lithgow et al., 2013) with promising results. A single restoration effort might not be enough, as roots of deep-rooting plant species and rhizomes of perennials are hard to remove all at once. Furthermore, the input of sand to the hinterland must be large enough to prevent sand-covered climax vegetation from recovering (Martínez et al., 2013).

Whereas knowledge about erosional storm-wave processes are extensive, the process of aeolian sand transport on beaches is less well-known and mostly conceptual (Short and Hesp, 1982; Houser, 2009; Bauer and Davidson-Arnott, 2002). Especially when aeolian sediment transport for longer time scales (months to years) is studied, there is often a large mismatch between transport predictions and measurements of foredune growth (Delgado-Fernandez, 2011; Keijsers et al., 2014). It is necessary to find the cause behind this mismatch, as aeolian transport is part of a broadening set of functions that coastal dunes fulfil. Dunes still provide protection against marine flooding, but having a diverse ecosystem is growing more valuable as well. Understanding aeolian sediment transport means a better comprehension of the dunes' dynamic ecological development.

1.2 Nature of aeolian transport on beaches

Aeolian processes involve the entrainment, transport and deposition of sediment particles by the wind. The first step, entrainment, takes place when the wind is strong enough to overcome the weight of the sand particle and the cohesive forces that keep it in place (Owen, 1964; Nickling and Neuman, 2009). When air flows over an exposed sand grain, it creates a

zone of low pressure above the grain. This, together with a steep velocity gradient close to the surface, causes a lift force. The shear wind velocity is the wind velocity near the surface and it has to exceed a certain threshold shear wind velocity u_{*t} to entrain sand. This threshold is created by the weight of the particle and the cohesion between adjacent particles (Bagnold, 1941). For dry sand, it can be found with

$$u_{*t} = A[\frac{\rho_s - \rho_a}{\rho_a} gD]^{1/2} \tag{1.1}$$

where A is an empirical coefficient which depends on the characteristics of the sand grains, ρ_s is the density of the sand, ρ_a is the density of the air, D is the median grain size, and g is gravitational acceleration.

Early, extensive research of sand dunes and the processes of aeolian sediment transport was performed by R.A. Bagnold. He described three ways for a sediment particle to move (Bagnold, 1941): suspension (grain size < 70 µm), where the particle will stay airborne for relatively long periods of time (minutes to several days); saltation, where the particle hops across a surface in parabolic arcs (grain size= 70–500 µm); and creep, where the particle is so heavy it rolls or is pushed along without losing contact with the surface (grain size >500µm). On beaches, the most common form of transport is saltation, making up 95% of all transport. The velocity and momentum of saltating grains increase before they fall back to the surface, where the impact ejects other sand particles in the air. These particles require a lower shear velocity to become airborne (Nickling and Neuman, 2009). The saltating grains also subtract momentum from the wind, which lowers wind velocity with distance when the saltating intensity is high. After some distance, saltation saturates (Gillette et al., 1996).

When the wind blows from the sea to the beach, the aeolian sand transport rate will thus not reach its maximum transport rate instantly. The transport rate will be zero at the shoreline and increase with distance (Owen, 1964; Gillette et al., 1996; Bauer and Davidson-Arnott, 2002; Delgado-Fernandez, 2010). This is called the fetch effect. Sediment particles strike the surface and their impact causes other particles to become airborne. This creates an exponential increase in transported sediment particles. The wind loses momentum, and therefore wind velocity, due to the saltating sand grains. This slows down the sand grains and stops the exponentially growing number of sand particles, reaching an equilibrium (Owen, 1964; Anderson and Haff, 1988). The distance at which this equilibrium saltation rate is reached is called the critical fetch distance. The maximum fetch is the total distance the wind can blow across the beach. It will be the shortest when the wind is cross-shore, and infinitely long when the wind is alongshore. The amount of transport will be the largest when the maximum fetch distance is equal to or larger than the critical fetch distance. When the critical fetch distance is larger than the maximum fetch distance, transport will be smaller than its potential amount. The critical fetch distance increases with increasing wind velocity, and is usually a few tens of metres long (Delgado-Fernandez, 2010).

Bagnold's work on desert dunes showed that potential aeolian sediment transport rates depend on the wind velocity to the power of three. Many other Bagnold-type equations have been since then developed (Kawamura, 1951; Zingg, 1953; Owen, 1964; Kadib, 1965; Hsu, 1974; Lettau, 1978; Sørensen, 2004). These Bagnold-type equations work well under controlled environments where the sand is uniform and dry, the sand supply is endless, and the wind is steady (Gares, 1988; Sherman and Hotta, 1990; Bauer et al., 2009; Sherman and Li, 2012). On beaches, however, the predicted amount of transport is almost always lower than the measured amount. This is caused by transport limiting factors that are common for beaches, but are not present in deserts or controlled conditions like wind tunnels. A high moisture content, for example, increases the adhesive forces between the sand grains. With gravimetric moisture contents higher than 4 to 10% (Namikas and Sherman, 1995;

Jackson and Nordstrom, 1997; Wiggs et al., 2004; Nield and Wiggs, 2011), transport is often no longer possible. Algae (Arens, 1996) and salt crust layers (Poortinga et al., 2014) keep the sand grains together as well and prevent the sand grains to be entrained by the wind. Snow and ice cover (Delgado-Fernandez, 2010) and extensive seashell beds (Van der Wal, 1998; Hoonhout and de Vries, 2017) or other beach litter prevent entrainment of sand as well. Finally, vegetation is able to capture sand grains, lowering aeolian sediment transport rates. These limiting factors affect the amount of sand available by either capturing sand and/or protecting it from the wind or increasing the cohesion between sand particles. When limiting factors are present, the critical fetch length will become larger, which makes it more likely for it to be longer than the maximum fetch, especially when the beach is narrow (30 to 100 m wide). This can therefore cause a transport rate at the beach-dune interface lower than what is potentially possible; in this thesis, I will call this a limited transport event. In order to make aeolian sediment transport rates predicted for longer timescales (months to years) and deposition on the foredune more accurate, it must be known when transport is limited.

Bauer and Davidson-Arnott (2002) proposed a series of explicit parametrisations of the fetch effect to improve aeolian sediment transport rates on a seasonal to annual scale, as simply long-term predictions of small-scale physical processes is unlikely to give accurate results. This would require extensive computation run times and there could be a strong temporal accumulation of error, or errors caused by the sensitivity to the initial conditions because of model non-linearity (Pape et al., 2010), or because of schematising of boundary conditions (Walstra et al., 2013). Bauer and Davidson-Arnott (2002)'s modelling framework is capable of calculating the spatial distribution of the sediment transport rate as a function of the critical fetch distance, beach geometry, and wind angle, but was not formulated so as to predict actual transport amounts. Data from a 9-month field campaign at Greenwich Dunes, Canada, was used by Delgado-Fernandez (2011) to test the framework in a more quantitative sense. Firstly, she extended the model and filtered out all moments when no transport was possible, either due to low wind velocities, a short fetch length, and/or too much snow, ice, or moisture, and, secondly, used transport equations that would decrease aeolian transport rates for the days that showed limited transport. This strongly improved predictions; where the originally predicted transport rate was 29 times higher compared to the deposited values on the foredune, the new result was only 6.2 times higher. The beach at Greenwich Dunes is arctic, and a large part of the difference between predicted and measured transport may have been caused by the presence of snow (Delgado-Fernandez and Davidson-Arnott, 2011). Beaches at temperate climates can also show a large difference between predicted and measured transport (Keijsers et al., 2014), which must have different causes and might be more common during all seasons.

1.3 Monitoring of aeolian sand transport

Aeolian sediment transport can be measured in various ways, both passive and active. An example of a passive method is a sediment trap, where sand gets blown into a container (Rasmussen and Mikkelsen, 1998; Dong et al., 2004; Sterk and Raats, 1996; Basaran et al., 2011; Mendez et al., 2011). Active methods include laser samplers, where sand grains are counted when they pass a laser (Hugenholtz and Barchyn, 2011; Sherman et al., 2011); acoustic samplers, where the sediment flux is determined by counting the impact sounds created by sand grains hitting a microphone (Spaan and Van den Abeele, 1991; Yurk et al., 2013; Ellis et al., 2009; Schönfeldt, 2012); piezoelectric samplers, in which sand grains hit a crystal and cause a recording of the kinetic energy of the impacts (Stout, 1998; Baas, 2004; de Winter et al., 2018), pressure sensitive samplers (Ridge et al., 2011); and finally, terrestrial laser scanners, where a laser reflects on the saltation cloud, and the return signal holds information about

Figure 1.1: Development of sand strips at Egmond aan Zee, the Netherlands. Small patches of sand grow into sand strips. Streamers can be seen further downwind, blowing over fully developed sand strips.

the location and height of the saltation cloud (Nield and Wiggs, 2011). These types of research are often done for relatively short periods of time, as the tide would submerge the instruments when placed on the intertidal beach. Furthermore, rain could make sand stick to the instruments, making the measurements highly inaccurate.

Aeolian sediment transport can be observed visually as well. Saltation causes the initiation and growth of aeolian bedforms. At the intertidal beach, where the surface is relatively moist and packed, the bedforms start as patches of dry, transported sand, sometimes covered with wind ripples with a wavelength of a few centimetres (Kocurek et al., 1992; Baddock et al., 2017). The patches can grow into much larger, slipfaceless ripples, which are known as sand strips (Figure 1.1). These bedforms have a wavelength of metres, move with only a few metres per hour, and mainly develop on the upper intertidal beach. When undisturbed, sand strips can grow into protodunes, which in turn can develop into dunes (Kocurek et al., 1992). Another visual sign of aeolian sediment transport are streamers, which are snake-like clouds of sand that move over and between patches of sand, or can be observed when no patches of sand have developed yet. Streamers move much faster than sand strips.

Video monitoring has been used to observe sand strips, protodunes, and streamers (Delgado-Fernandez, 2010; Guimarães et al., 2016; Williams et al., 2018; Montreuil et al., 2018). Delgado-Fernandez (2010) observed that the moments with the strongest wind were not necessary the moments with the highest visual signs of transport and volumes of transported sand; out of the 9 days with strong winds, only one day resulted in high transport rates and strong visual transport signs. Her research strongly suggests that a large part of the total transported sediment may be caused by moments with low to medium wind velocities, and that the wind direction may matter more than wind velocity. Winds of medium strength are more common than strong winds and could therefore contribute more to the total amount of sand transport. Furthermore, strong winds often cause a storm surge and inundate large portions of the beach. This was also found by Guimarães et al. (2016), where they used an Argus video monitoring station to study the behaviour of protodunes.

Argus video monitoring is used to study beaches worldwide. An Argus station consists of multiple cameras that, when mounted on a tall structure, can photograph the beach at regular intervals (Holman and Stanley, 2007). Argus was originally intended to sample breaking waves in the nearshore. However, when the beach is in view of the cameras, it can be used to study the beach's dry part as well. Both sand strips and streamers can be observed, but mainly on the intertidal beach, where the dark, moist surface offers a strong contrast with the relatively dry, wind-blown sand. Wind ripples, which develop on dry, loose sand, are usually not visible on Argus video monitoring imagery. The Argus system makes three types of images: snapshot, timex, and variance images. Snapshots are ordinary photographs, taken at regular intervals (usually an hour or 30 minutes) during daylight hours. The timex images are time-averaged, made by taking the mean pixel values of images taken for 10 minutes with a frequency of 2 Hz. This causes all movement to be smoothed out. A variance image shows the standard deviation of a pixel in the same 10-minute period. Dark colours indicate a low standard deviation, and therefore little change, while light colours indicate the opposite. As the migration velocity of sand strips is slow, the sand strips appear in both the snapshot and the timex image. Images of subsequent hours need to be studied to see sand strips move. Streamers, on the other hand, move so quickly that they get blurred out on the timex images, and can therefore only be seen on snapshot images. Both sand strips and streamers can be used to identify moments of aeolian transport. Where other measurement methods can usually be used for only a few hours on the intertidal beach, an Argus station can be used for decades. In this research, the intensity of aeolian transport visible on Argus imagery will be used to find moments with limited and unlimited transport.

1.4 Research objectives and outline

The main aim of this thesis is to better understand the timing of aeolian transport on a narrow beach, and to identify and elucidate key factors that determine this timing, with a focus on timescales from months to years. To do this, three research questions were defined. The first two questions use Argus imagery as their main source of data, while the third is based on a fetch model, building on Delgado-Fernandez (2011).

1. *What are the physical characteristics of sand strips on a narrow beach under a wide range of wind conditions?*
   Sand strips are common bedforms in wet aeolian systems (Bauer and Davidson-Arnott, 2002; Jackson et al., 2006; Davidson-Arnott and Bauer, 2009; Montreuil et al., 2018). They have often been observed, but not studied in great detail, even though they could provide valuable insight into the timing of aeolian transport events on beaches. Nield et al. (2011) have conducted the most extensive field study, where sand strip patterns were measured using terrestrial laser scanning for a time period of three and a half hours after a rain event. This study showed that sand transport increased with the drying of the beach surface, with erosion taking place at the wet-dry surface boundary of sand strips and deposition taking place further downwind. As the duration of the field campaign was short, the study does not provide insights into how these sand strips behave under different conditions. The patterns were later described in a cellular automaton model (Nield, 2011), which computed sand strip emergence and evolution at different relative spatial scales, depending on surface properties and transport processes. This provided great insight on variables affecting sand strip appearance, but research based on a large field dataset, covering multiple years, has not been done yet. Argus, being able to observe sand strips, provides an excellent way of studying their characteristics for long periods of time. Chapter 2 covers research question 1.

2. *How do transport limiting factors affect aeolian sand transport on long time scales at a narrow beach?*
   When Argus imagery is combined with meteorological data, it can find moments of aeolian sediment transport with less intense transport than expected based on the wind velocity (in other words, the transport is limited), or with an expected transport intensity (unlimited transport). Studying the limited and unlimited events will help to identify the factors that limit aeolian transport, for example, rain, air temperature and wind direction. Research question 2 is answered in Chapter 3.

3. *Can a fetch model, building on the work of Delgado-Fernandez (2011), predict the timing of limited and unlimited aeolian sediment transport correctly?*
   Bauer and Davidson-Arnott (2002) proposed a set of explicit equations to improve aeolian sediment transport rates on a seasonal to yearly scale, which were used by Delgado-Fernandez (2011) to predict aeolian sediment transport rates measured during a 9-month field campaign at Greenwich Dunes, Canada. Delgado-Fernandez (2011) extended the model to exclude or reduce the potential aeolian transport rate during moments when aeolian transport would be impossible or limited. Video monitoring data were used to determine moments where aeolian transport would be impossible or limited, which restricts the general applicability of her model. Here, the Delgado-Fernandez approach is extended into a more general predictive framework by coupling a groundwater-surface moisture model to a fetch-based aeolian transport equation. This new model, called Aeolus, will be tested qualitatively by comparing the timing of its results to the moment signs of aeolian transport are visible on Argus imagery. Chapter 4 answers research question 3.

All questions focus on the same study site: Egmond aan Zee, the Netherlands. Chapter 2, 3, and 4 are based on journal articles and therefore show overlap in the description of the field site. Chapter 5 synthesises the results found in the previous chapters and offers an outlook to future research.

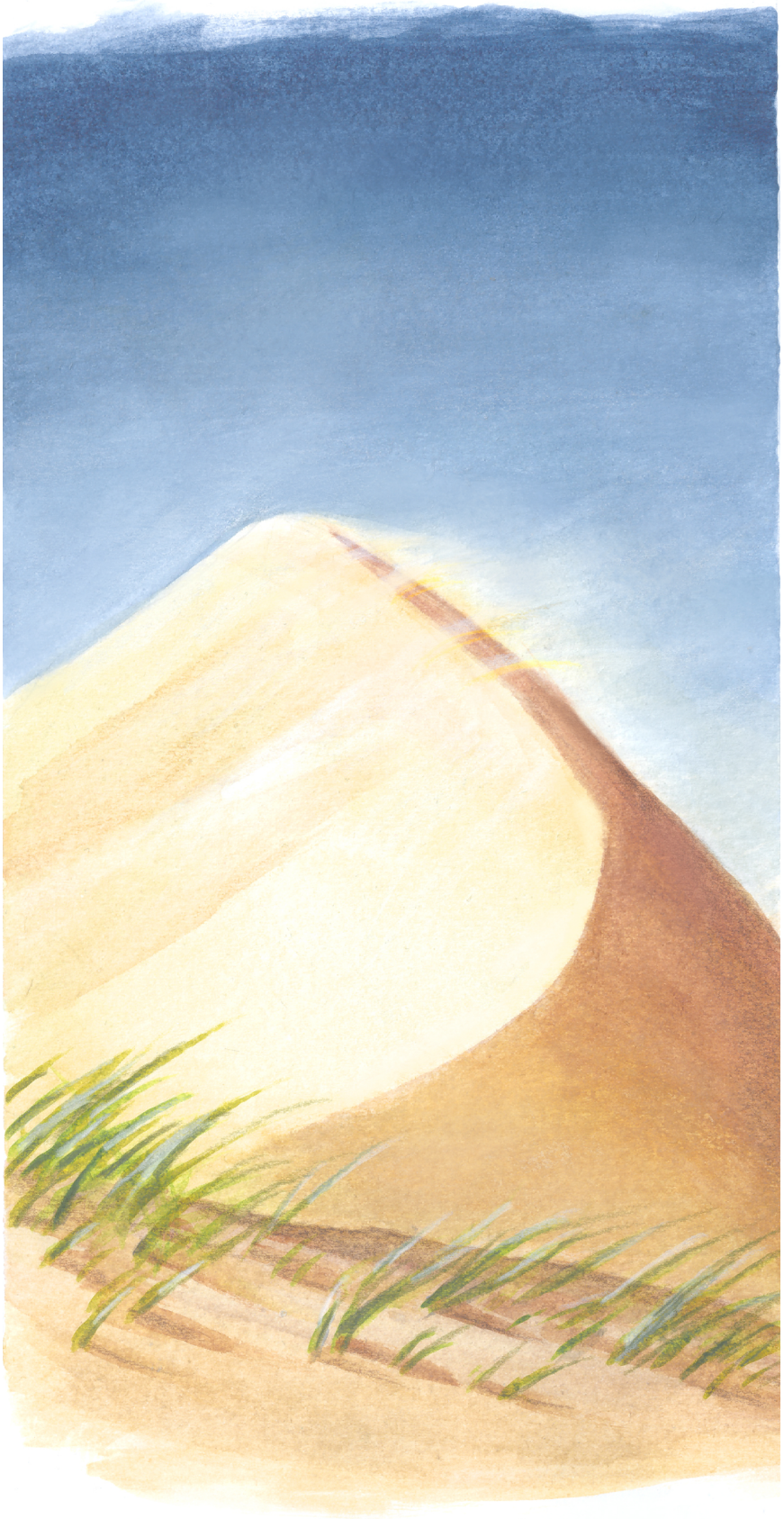

Chapter 2

Determining sand strip characteristics using Argus video monitoring

Based on: Hage, P.M., B.G. Ruessink, J.J.A. Donker (2018), Determining sand strip characteristics using Argus video monitoring. *Aeolian Research 33*, 1-11.
doi: https://doi.org/10.1016/j.aeolia.2018.03.007

Abstract

The wind transports sand from the beach to the dunes and is therefore important for dune growth and recovery after a storm. Identifying the conditions that favour aeolian sand transport is especially important for narrow beaches, where measured long-term (seasons to years) deposition volumes on the foredune are often substantially less than the potential input from the beach. One of the most visually distinct signs of aeolian transport can be seen when relatively dry sand moves over a wet beach and organises itself to form low, slipfaceless bedforms. These features are known as sand strips. Here, we investigate the presence and characteristics of sand strips and their dependence on regional wind conditions by using a multi-year data set of video images of the Argus tower at Egmond aan Zee, The Netherlands. The data set average wavelength and migration rate of the sand strips is 12.0 m and 1.24 m/h, respectively. Little to no relation was found between these two sand-strip characteristics and the wind velocity. The presence of these bedforms does not depend on wind velocity either, provided the wind velocity exceeds $\sim$ 8 m/s. Instead, the wind direction determines if fully-developed sand strips form, as they are seen during alongshore or almost alongshore winds only. Our observations are indicative of topographic steering of the wind by the 25-m high foredune into the alongshore direction, as sand strips move alongshore even under onshore-oblique, regional winds.

2.1 Introduction

The intertidal beach is the primary source of the wind-blown sand needed for dune growth and/or recovery after an erosive storm event (e.g. Hoonhout and de Vries, 2017). However, knowledge of aeolian sediment transport on beaches is limited (e.g. Delgado-Fernandez, 2010), and most existing models have a tendency to overestimate sand deposition on the foredune (Miot da Silva and Hesp, 2010; Keijsers et al., 2014; Davidson-Arnott and Law, 1996). These models relate time-averaged sediment transport to wind shear velocity (Davidson-Arnott and Law, 1996; Bauer and Davidson-Arnott, 2002) and grain size (Sherman et al., 2013a). While this is realistic for a steady wind blowing over an unobstructed, horizontal surface with a uniform grain size (Gares, 1988; Sherman and Hotta, 1990; Bauer et al., 2009; Sherman and Li, 2012), transport on a natural beach is affected by, for example, the moisture content of the sand, the beach slope and the bed roughness (e.g. Delgado-Fernandez and Davidson-Arnott, 2011; Edwards and Namikas, 2009; Wiggs et al., 2004; Nield et al., 2013; Nield et al., 2014; Bauer and Davidson-Arnott, 2002; Svasek and Terwindt, 1974; Davidson-Arnott and Law, 1996; Jackson and Nordstrom, 1998; Sherman et al., 1998). Therefore, the

moments with strong aeolian activity do not nessarily coincide with moments of high wind velocities (Delgado-Fernandez and Davidson-Arnott, 2011). Actual transport rates can be acquired through detailed field measurements (Sherman et al., 2011; Sherman et al., 2013b; Bauer et al., 2009; Davidson-Arnott and Bauer, 2009; Bauer and Davidson-Arnott, 2002; Udo et al., 2008; Davidson-Arnott et al., 2005; Jackson and Nordstrom, 1997; Baas and Sherman, 2006), however, most field campaigns on beaches concerning aeolian sediment transport are generally short in duration (ranging from minutes to weeks) and may therefore not contain the conditions that are most relevant to long-term (months to years) dune development (Delgado-Fernandez et al., 2009).

A suitable method for long-term measurements is video monitoring, which has already been used extensively to sample the wave-dominated part of the nearshore on timescales of years (van Enckevort et al., 2004; Ruessink et al., 2009; Pianca et al., 2015). Delgado-Fernandez et al. (2009) pioneered video monitoring to study aeolian transport. Their temporary camera system photographed the beach at Greenwich Dunes, Canada, at hourly intervals and occasionally picked up traces of aeolian sand transport during a nine-month period. Transported sand can be seen on video imagery because wind-blown sand usually is dryer and therefore lighter in colour than the moist bed, providing visual contrast. Additionally, the dry, transported sand can organise itself to form sand strips. These clearly visible, slipfaceless bedforms often form when a relatively moist bed is present (Bauer and Davidson-Arnott, 2002; Jackson et al., 2006; Davidson-Arnott et al., 2008; Bauer et al., 2009; Nield et al., 2011; Nield, 2011), especially when vegetation (Sherman and Hotta, 1990; Eamer and Walker, 2010), frozen material (Hesp and Arens, 1997), or other roughness elements are present as well. Sand strips can grow into ephemeral dunes, which have a slipface and a height in the range of decimetres to a metre (Guimarães et al., 2016; Kocurek et al., 1992; Elbelrhiti, 2012), but waves and tides often destroy sand strips before they can grow this far. Video monitoring has been used to study ephemeral dunes on a long-term timescale by Guimarães et al. (2016). Like the traces of aeolian transport in the work of Delgado-Fernandez et al. (2009), these features were visible on camera because of a difference in moisture content, and therefore colour, between the transported sand of the bedforms and the bed (McKenna Neuman and Langston, 2006).

The most extensive field research into sand strips has been conducted by Nield et al. (2011), who have measured sand strip patterns with terrestrial laser scanning for a period of three and a half hours after a rain event. During this field experiment, sand transport increased as the beach surface dried, with erosion taking place at wet/dry surface boundary, and deposition further downwind (Nield and Wiggs, 2011). The patterns were later described in a cellular automaton model (Nield, 2011). According to the model, sand strip development is related to bed roughness, saltation and moisture patterns. The results gave rise to a conceptual model where the feedback between the surface properties and transport processes results in the development of bedforms at different spatial scales. Despite sand strips being common features in wet aeolian systems (Bauer and Davidson-Arnott, 2002; Jackson et al., 2006; Davidson-Arnott and Bauer, 2009), their behaviour under a wide range of wind conditions is largely unknown.

The aim of this chapter is to quantify the presence, length and migration velocity of the sand strips found at the beach of Egmond aan Zee, the Netherlands, using long-term video imaging, and to determine how these characteristics depend on regional wind conditions.

2.2 Study area

The study site is located between the beach towns of Egmond aan Zee and Castricum, the Netherlands (Figure 2.1). The beach has a width varying between 30 and 100 m (depending on the tide) and is moderately sloping (1:30). The coastline is straight, with an orientation of 7° east of north. The sand has a median grain size of 240 μm. The intertidal beach typically contains one or two slipface bars (Masselink et al., 2006; Aagaard et al., 2005; Quartel and Grasmeijer, 2007). The foredune forms a uniform row parallel to the beach, with a height of 20-25 m. Its seaward front is steep (40-50°), due to occasional erosion events (de Winter et al., 2015). Most of the foredune is densely covered by European marram grass (*Ammophila arenaria*), especially at heights of 10 m and more above beach level.

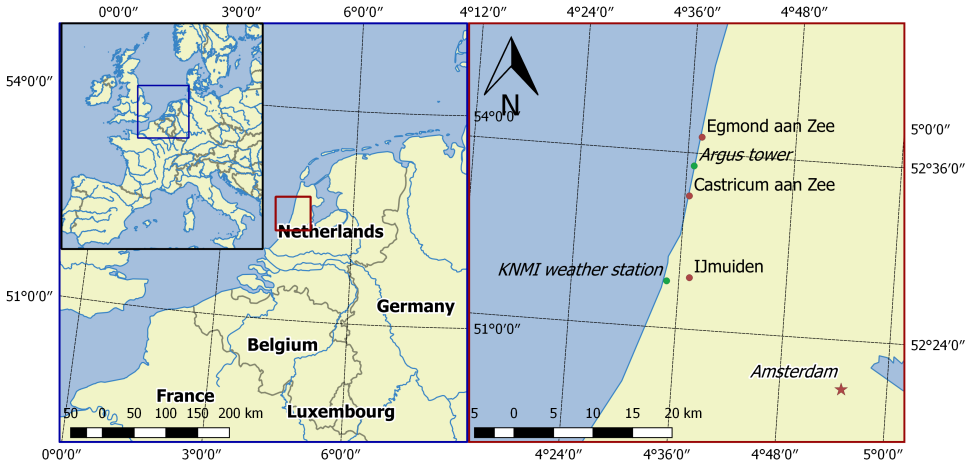

Figure 2.1: Location of the field site and weather station.

The site experiences a semidiurnal tide with a range of 1.4 and 1.8 m during neap and spring tide, respectively, and is exposed to waves with directions between southwest and north. The annual significant offshore wave height and period along the Dutch coast are 1.2 m and 5 s, respectively, and show small alongshore differences (Wijnberg and Terwindt, 1995). During storms the offshore wave height can be over 5 m. Especially storms from the northwest are associated with surges in excess of 1 m, which can flood the intertidal beach for several days (Quartel et al., 2007). The dominant wind direction at this beach is south-southwest (210-230° with respect to north, Figure 2.2), meaning the wind has a strong onshore-oblique character.

Egmond beach is monitored by an Argus video system (van Enckevort and Ruessink, 2001), an optical remote sensing system pioneered by Holman and Sallenger (1986) to sample the nearshore environment. An Argus system consists of a suite of cameras mounted on a high structure, which provides an unhindered view on the beach. A timing module ensures synchronous camera collections (Holman and Stanley, 2007). The Argus system at Egmond aan Zee has five RGB-colour cameras, mounted on a 45-m high tower standing on the upper beach (Figure 2.3). The cameras provide an 180° alongshore view, from south-southwest to north-northeast. The Argus system was installed in April 1998. The image resolution was 640×480 pixels from 1998 to February 2004, 1024×768 pixels from 2004 to August 2005 and 1392×1040 pixels since then. Three different, oblique images are produced by each camera

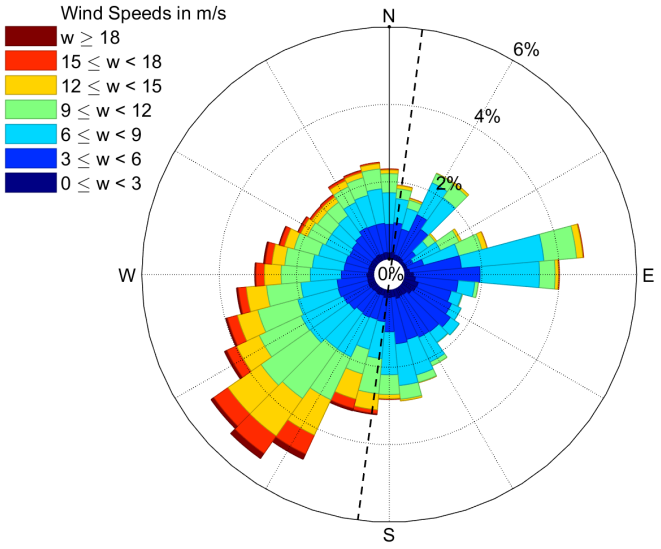

Figure 2.2: Windrose, based on hourly wind speed U and direction θ data collected between 2005 and 2012 at IJmuiden, approximately 15 km south of our study site. The dotted line represents the orientation of the coast.

every thirty minutes: a snapshot, a time-exposure (timex) and a variance image, where only the first two types are used here. The timex images are created by averaging snapshots that are taken with a frequency of 2 Hz over a 10-minute period. This blurs out movement that took place within those 10 minutes, such as individual waves breaking on the subtidal bars, people walking on the beach, and aeolian streamers.

The theoretical accuracy of the images is given by the footprint dimensions of individual pixels. The footprint, i.e. the projection of a square image pixel on the ground, is near-rectangular with a generally larger alongshore than cross-shore side. Here, for the post-2005 system, the cross-shore footprint dimension is less than 0.2 m, while the alongshore size increases from 0.2 m at 100 m from the tower alongshore, to ≈1.5 m at 400 m.
This research uses the hourly mean wind velocity U and wind direction θ collected by a weather station in IJmuiden, roughly 15 km south of the field site (Figure 4.1) as regional data. The weather data are made available by the Royal Netherlands Meteorological Institute (KNMI) with a resolution of 1 m/s for the U and 10° for θ. The anemometer is placed at a height of 10 m above ground level.

2.3 Methodology

The timex images from the Argus video system were used to study sand strip presence and occurrence. Finding images with sand strips manually is time-consuming, due to the vast size of the Argus database. Therefore, a first selection was made based on wind velocity. Sand transport can only take place when the wind velocity exceeds a certain threshold velocity. To this end, all Argus snapshots taken between October 2011 and March 2012 were

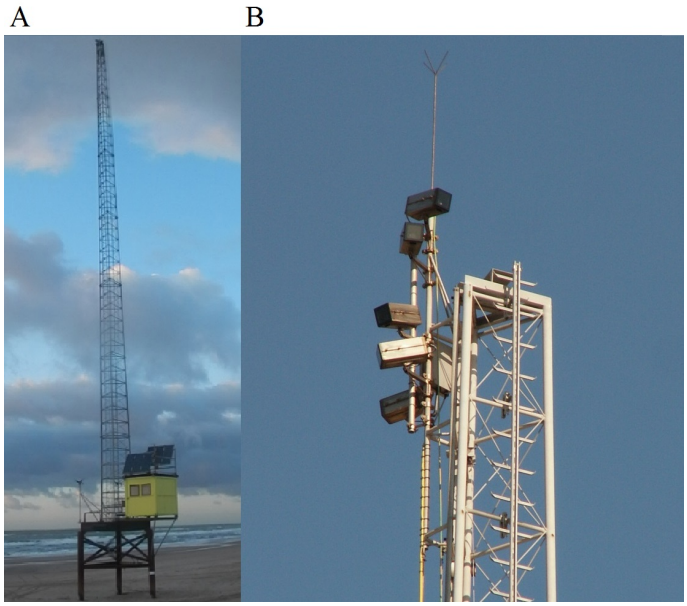

Figure 2.3: The Argus tower at Egmond aan Zee (A) and the cameras on top of the tower (B).

studied to determine this threshold wind velocity. Snapshots were classified as having no, weak, or strong aeolian activity, based on the strength and number of visual signs of aeolian transport. Clear examples for each class can be found in Figure 2.4. Aeolian activity was found predominantly for a wind speed in excess of 8 m/s, implying $U = 8$ m/s to be the threshold velocity. The images from 2005 to 2012 were filtered according to this threshold wind velocity, selecting only the days which had hourly mean wind velocities of 8 m/s or higher. Additionally, this threshold had to be surpassed for at least three hours to consider the wind transport event to be substantial for this site (Hage, 2014).

Spatial correlation was, as described below, used to study the wave length and migration velocity of sand strips, but the Argus images must meet a number of conditions in order to perform correlation calculations. Firstly, the sand strips must be well-developed and active for at least one hour, meaning their appearance should not be patchy and their movement must be visible in subsequent images. Furthermore, the area containing them must be substantial in size, i.e. it must be at least 50 m long in the direction of the wind. Lastly, the sand strips have to be clearly visible, meaning rain, poor light conditions, or other circumstances that reduce image quality must be avoided.
The selected timex images were rectified and merged to make a plan view image as described by Holland et al. (1997) and Holman and Stanley (2007) (Figure 2.5). The rectification involves the transformation from the two-dimensional (u, v) pixel coordinate scheme to the three-dimensional (x, y, z) real-world scheme, where x an y are horizontal coordinates and z is vertical elevation. Going from a 2D to a 3D coordinate system results in a system of equations that is underdetermined, but it can be solved by constaining z to a fixed value (Holland et al., 1997). In earlier Argus research that focussed on wave-breaking patterns, z was set to the tidal level (e.g. Lippmann and Holman (1989)). Because the sand strip patterns studied here were on the upper beach, z was set to 1 m above NAP (Amsterdam Ordnance Datum, with 0 m NAP corresponding to Mean Sea Level, MSL).

Figure 2.4: Examples of snapshots made by the north-facing camera classified according to their signs of aeolian activity: no visual aeolian transport (A), some signs of aeolian activity, with small patches of relatively dry sand on a moist surface (B), strong signs of aeolian activity, where almost the entire beach is covered with sand strips (C). The wind conditions were: (A) U = 9 m/s, θ = -7°; (B) U = 13 m/s, θ = 37°; (C) U = 16 m/s, θ = 77°; where θ = 0° is cross-shore, θ = -90° is the alongshore wind coming from the north, and θ = 90° is alongshore from the south.

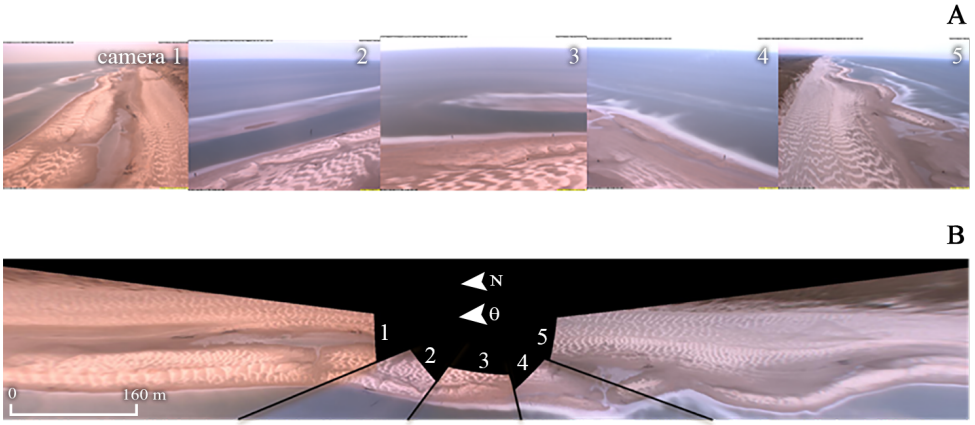

Figure 2.5: The five original oblique Argus images (top row) were rectified and merged to get a plan view image (bottom panel). Here, the plan view image has an alongshore and cross-shore length of 800 and 200 m. The example images were taken on 01-04-2008, The wind speed and direction were U = 9 m/s and θ = 97° (i.e. almost alongshore). The arrows indicate the direction of the wind (θ) and the north (N). θ = 0° is cross-shore, θ = -90° is the alongshore wind coming from the north, and θ = 90° is alongshore from the south.

As aforementioned, the oblique nature of the original timex images causes the quality of the plan view images to diminish with distance from the Argus tower. Sand strips at Egmond are therefore visible only if they are within a few hundred meters from the tower. For this study, the area transposed from oblique to plan view is 800 m alongshore (400 m at each side of the tower) and 300 m wide cross-shore (Figure 2.6A). These plan view images were set to have a resolution of 0.5×0.5 m per pixel, meaning that the sand strips must migrate with at least 0.5 m/h for their movement to be visible. The next step involved cutting out a small area

containing well-developed sand strips from the 800 by 300 m plan view images and turning it greyscale (Figure 2.6B) according to

$$Greyvalue = 0.2989 * R + 0.5870 * G + 0.1140 * B, \tag{2.1}$$

where R, G, and B are the pixelvalues for red, green, and blue, respectively (ITU-R, 2011). The cropped area had a size of approximately (cross-shore) 25 by (alongshore) 100 m and covered a part of the upper beach with distinctive, well-developed sand strips, preferably close to the tower where the image quality is best. The exact size and location of the cropped area differed per day, since sand strips did not always develop at the same parts of the beach. Based on visual observation, the greyscale images were manually rotated to align the sand strips vertically before cropping. Figure 2.6C shows examples of the pixel values of the same pixel row of the three consecutive hours shown in Figure 2.6A, after being detrended by computing the least-squares fit of a straight line and normalised to have a mean of 1. The pixel value increases with increasing pixel brightness. Because sand strips create a pattern of alternating dark (wet sand) and light (dry sand) colours, the pixel values of a horizontal pixel row give an approximately sinusoid signal.

Autocorrelation was used to calculate sand strip wave length in each pixel row. This technique compares two sequences to find their correlation at different lags, where one sequence is the original signal, and the other a copy of that original but with a lag. This was done with the pixel values for each horizontal pixel row of the cropped area according to

$$r(\tau) = E[(X_m - \mu)(X_{m+\tau} - \mu)]/\sigma^2, \tag{2.2}$$

where r is the correlation coefficient, τ is the lag, E is the expected value operator, X_m is the pixel value at a certain distance m, μ the mean and σ^2 is the variance. By definition, $r(0) = 1$. Positive peaks for r are found when the corresponding lag matches with the wavelength or multitude of wavelengths of sand strips. At the lag of the positive peak closest to $r(0)$, the pixel values of the sand strips of the original signal are compared with the pixel values of the neighbouring sand strips, giving the sand strips' wavelength in number of pixels. The lag corresponding to this peak was determined for each horizontal pixel row in each cropped image, as long as it surpassed a threshold of 0.3 for r. This threshold was chosen after comparing the lag of the first positive peak with its value for r for all pixelrows of all images used. Values for r below 0.3 result in a wide range of lags, which reflect highly irregular sand strips or may indicate a noisy signal. Meanwhile, an r above 0.3 gives lags focused around a central value that seems to be more realistic for the wavelength of sand strips. Results that seemed to be a multitude of this central value were ignored.

An example of the selected lags for each pixelrow of a single hour can be found in Figure 2.7, which shows that no lag was selected when a pixelrow did not have an r above the threshold of 0.3. The selected lags of the images part of the same sand strip event (subsequent hours during which sand strips are active) were averaged. This gives a mean wavelength in metres per sand strip event when multiplied with the 0.5 m pixel resolution.

The method for determining the migration velocity of the sand strips is similar to the one used for determining the wavelength. The same cropped area was used, but instead of using autocorrelation on the horizontal pixel rows, cross-correlation was used. Here, the pixel value signal of two subsequent hourly timex images were compared to each other. The lag with the first peak in the correlation represents the distance that the sand strips have moved, while the sign of the lag reflects migration direction. The minimal value for this correlation peak was 0.6, which was chosen in a similar manner as the 0.3 threshold for r for the sand strip wavelength calculations. At rare occasions, the highest correlation peak for a single pixelrow can be found at a lag that is upwind. As sand strips are not very likely to move

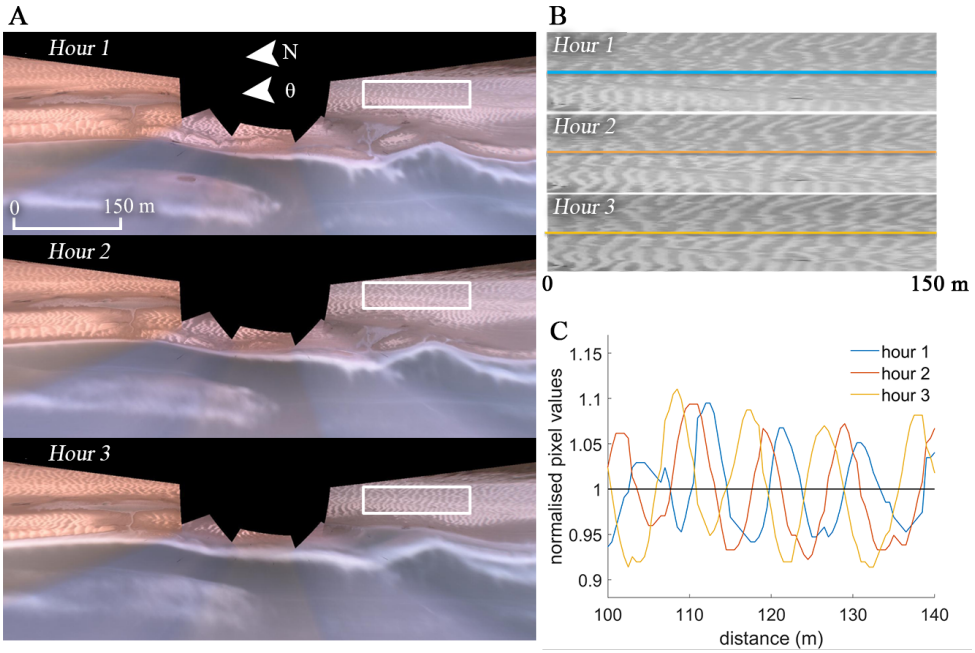

Figure 2.6: (A) shows three consecutive hours with well-developed sand strips. (B) shows the cropped, greyscale images (boxes in A). The lines in (B) highlight the same horizontal pixel row in subsequent hours, whose normalised pixel values are plotted against alongshore distance in (C). The normalised pixel values show a sinusoidal signal that shifts to the left with time, reflecting migration in northward direction. The example images were taken on 01-04-2008., The wind speed and direction were $U = 9$ m/s and $\theta = 97°$. $\theta = 0°$ is cross-shore, θ = -90° is the alongshore wind coming from the north, and θ = 90° is alongshore from the south.

in this direction, these outcomes were ignored. Unrealistically high lags, where the migration velocity was higher than its corresponding wavelength minus the standard deviation of the wavelength, were ignored as well, because these outcomes are more likely to represent the wavelength of the strips instead of their migration velocity. As with the wavelength of sand strips, the mean migration velocity per sand strip event was calculated by averaging over all rows and images.

2.4 Results

The conditions needed for visual traces of aeolian transport were investigated, using the Argus snapshot images taken between October 2011 and March 2012. Hours with any visual form of aeolian transport had, as aforementioned, wind velocities above $\approx$ 8 m/s and could be found for all wind directions, but showed a strong peak around south-westerly winds and a smaller one around north-westerly winds (Figure 2.8). This corresponds to the wind climate at the field site. Visually strong aeolian activity, which includes well-developed sand strips, was found predominantly when the wind blew (almost) alongshore. The wind velocity dur-

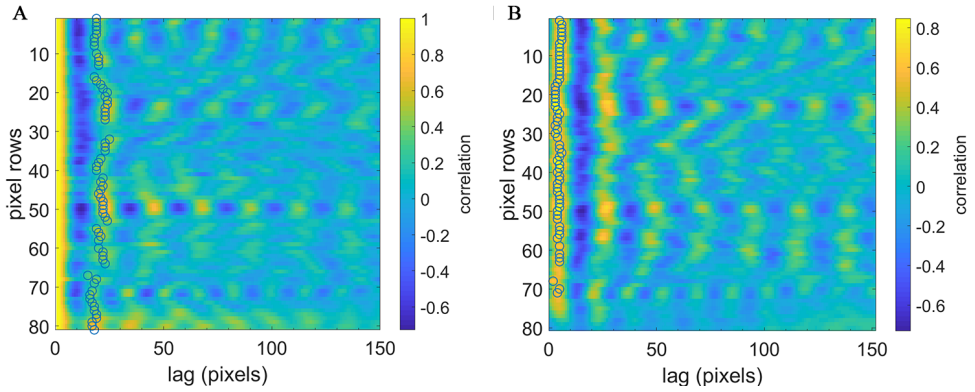

Figure 2.7: Example of the correlation coefficients for the sand strip wavelength (A) and migration velocity (B), calculated for different lags for each pixelrow of the cropped area in Figure 2.6. The pixelrows are orientated parallel to the migration direction of the sand strips. The circles indicate the lags that correspond with the sand strip wavelength in A or migration velocity in B. These lags are the first peak of the correlation signal of a pixel row and they have to surpass a threshold of 0.3 for the wavelength and 0.6 for the migration velocity. These examples were made by using auto-correlation for the Argus image taken at 9.00h on 01-04-2008 for A, while B used cross-correlation with the images taken at 9.00 and 10.00 h. One pixel corresponds to 0.5 m.

ing hours with strong signs of aeolian transport is not noticeably different from hours with weak signs. In other words, sand strips developed at all wind velocities above the threshold for aeolian transport to become visible in the Argus imagery and the observed intensity of the transport is strongly governed by the wind direction.

Visual observation of the Argus images provided insight into sand strip development. Firstly, sand strips usually formed at the dune foot and then spread towards the sea with falling tide (Figure 2.9). Their initial formation was only close to the waterline when the beach was wide and the wind had a seaward direction, but such conditions were rare. Secondly, sand strips often started out as patches of moving, dry sand that turned into thin strips over time (a few hours), which can also be seen in Kocurek et al. (1992). The length and the width of such a single sand strip grew larger (Figure 2.10), but the wavelength usually did not change during this process. Sometimes, when remnant sand strips of an earlier aeolian transport event were present, the new sand strips appeared to have the same shape, size and location of the remnant strips. This changed when the new sand strips began to move.

Several processes cause sand strips to become inactive. The first process takes place when the wind velocity drops below the threshold wind velocity. When this happens, the sand strips remain visible for some time, but they do not move or grow. The second process for sand strip disappearance is the most common: the rising tide stops sand strip activity and, obviously, destroys sand strips present on the intertidal beach (Figure 2.11). Sand strips also disappeared temporarily due to precipitation, but were observed to recover within an hour after a rain event as long as the wind remained above the threshold velocity. Rainfall was not measured at the field site, but the sudden appearance of water droplets on the camera lens and a drastic darkening of the beach indicated a rain event. A possible third process involves drying of the initially moist sand of the bed, which causes the moist, dark sand to acquire the same colour as the sand strips (Figure 2.12). The bedforms may still be there after this

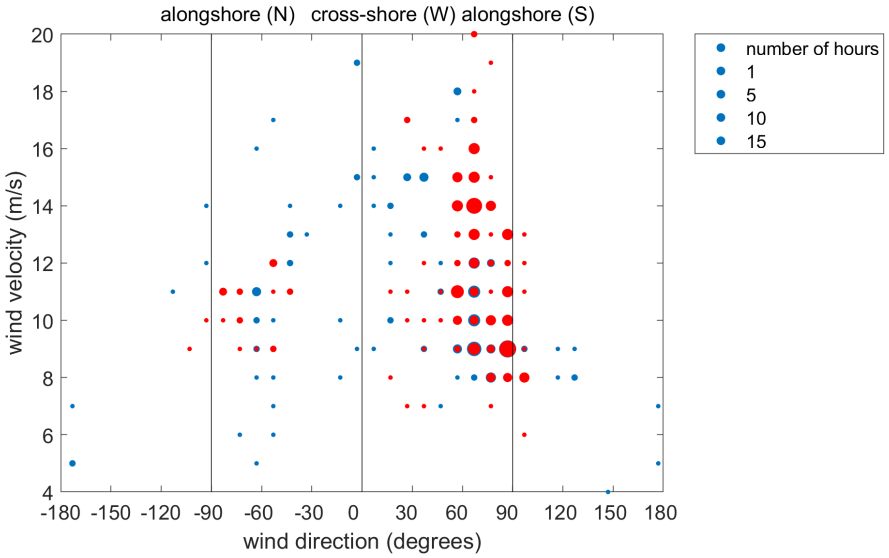

Figure 2.8: Wind velocity (m/s) against wind direction (degrees), where 0° is cross-shore from the west, 90° alongshore from the southern direction and -90° from the northern direction. The blue dots represent hours from October 2011 to March 2012 with any visible trace of aeolian transport. The red dots represent events with strong visual traces of aeolian transport. The total number of observations (hours) that showed signs of aeolian transport is 381, of which 77 were classified as having strong signs of aeolian activity.

drying process, but they are no longer distinguishable in the imagery. However, as one of the possible demands for sand strip development is wet sand (Nield et al., 2011), it is also feasible that the drying of the sand causes sand strips to decay. In that case, aeolian transport might continue through saltation or creep which cannot be seen by the cameras.

A total of 44 events with well-developed, active sand strips were selected from the 2005-2012 Argus dataset to study their wavelength and migration velocity. Low correlation coefficients (< 0.3) were found for 3 events during the auto-correlation calculations for the sand strip wavelengths. These events were excluded from the dataset and brought the number of events with well-developed, active sand strips down to 41 for determining the sand strip wavelength. There was 1 event in which the cross-correlation calculations for the sand strip migration velocity remained below 0.6, which resulted in 43 events for the sand strip migration velocity calculations. The analysed imagery resulted in an average sand strip wavelength of 12.0 m with a standard deviation of 2.8 m. A weak, yet statistically significant (at the 95% confidence interval) relationship could be found between the wavelength of the sand strips and the wind velocity ($r = 0.38$, see Figure 2.13).

Sand strips moved with an average velocity of 1.24 m/h with a standard deviation of 0.78 m/h. The relationship between the sand strip migration rate and the wind velocity is again weak ($r = 0.32$, $\alpha = 0.05$ Figure 2.14), yet statistically significant.

Furthermore, it was observed during the selection of the Argus images that sand strips did not necessarily migrate after their formation, or at least not fast enough to be seen by the cameras. Images where this was the case were not selected for further study. If the sand strips did move, their migration did not always happen immediately; the moment of migration

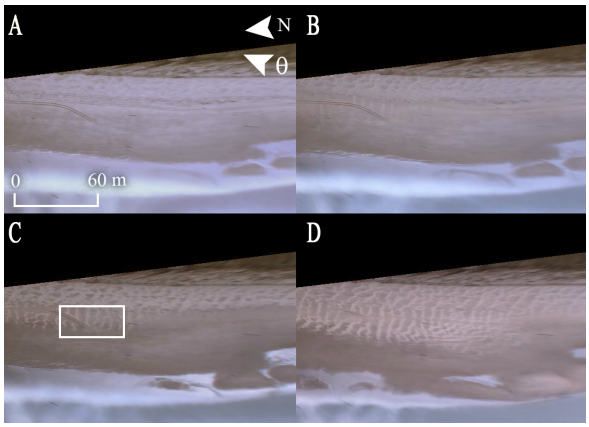

Figure 2.9: Development of sand strips. (A) shows a beach without sand strips, (B) shows faint traces of aeolian transport close to the dune, while (C) has well-developed sand strips. The bedforms spread towards the waterline in (D). The images were taken on 07-03-2008 at hourly intervals. The wind speed increased from 9 to 11 m/s and $\theta \approx 67°$. $\theta = 0°$ is cross-shore from the west, θ = -90° is the alongshore wind coming from the north, and $\theta = 90°$ is alongshore from the south. The dunes, visible by their vegetation, can be found in the east, while the east shows the sea, whose waves have been blurred out by the timex images.

ranged from minutes (i.e. the next Argus image) to several hours after sand strip formation. A section of a sand strip was sometimes observed to move faster than other sections. It then disconnected from the rest of the sand strip, only to reconnect to a sand strip in front of it. This is known as defect repulsion (Kocurek et al., 2010) and can be observed in dunefields (Ewing and Kocurek, 2010; Ewing et al., 2006). The Argus images also showed that sand strips have the tendency to move alongshore, even when the regional wind approached the shoreline at an oblique angle.

2.5 Discussion

The Egmond Argus video monitoring station has provided a multi-year data set of visual signatures of aeolian transport events. The imagery provides insight into the conditions needed to see visual traces of aeolian transport, even though there is no quantitative data on transport rates.

The average migration velocity for the sand strips was 1.24 m/h, which is larger than the sand strip migration velocities found by Nield (2011) (0.176 m/h for real-world beach measurements and 0.39 m/h for simulated bedforms) and for early-stage protodunes (0.32 m/h found by Baddock et al. (2017)). However, our results show a large variability and are based on multiple sand strip events, while Nield (2011) and Baddock et al. (2017)) focussed on a single moment of transport.

Not all sand strip development and migration can be seen on Argus images, mostly due to bad visibility, but also because not all transport events may result in sufficient colour contrast between transported and non-transported sand to be used in subsequent analyses. For example, aeolian sand transport over dry sand just in front of the foredune cannot be detected in the imagery.

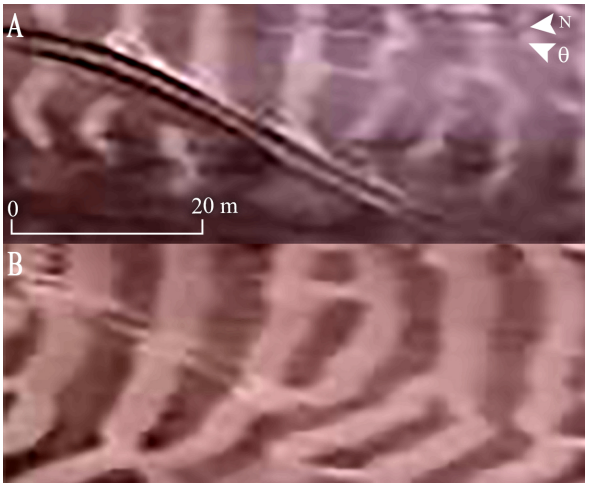

Figure 2.10: A section of the beach containing newly developed sand strips, which are relatively narrow and patchy in (A). The sand strips have thickened in (B), and the strips on the right have changed shape. The images were taken on 07-03-2008, 4 hours apart. The wind speed and direction were $U \approx 11$ m/s and $\theta \approx 67°$.

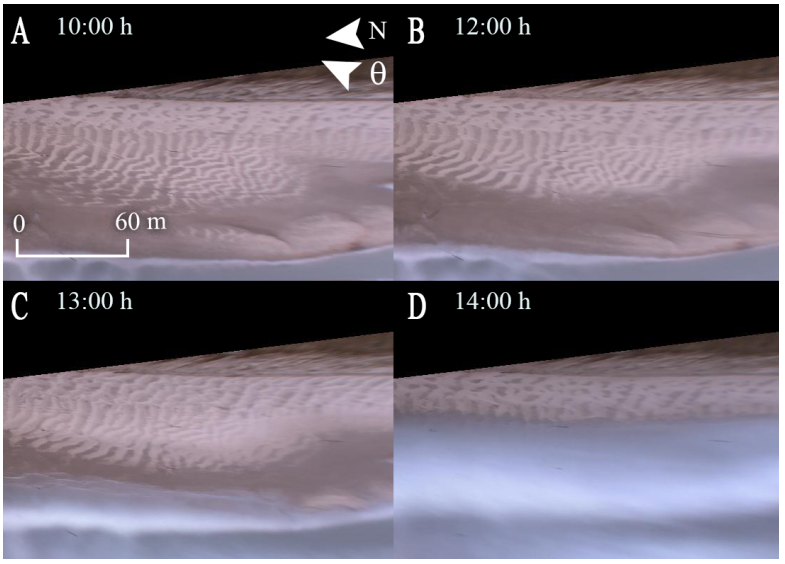

Figure 2.11: Sand strips getting washed away by the rising tide. The beach width did not become narrower at first (A to B), but the area with sand strips became smaller. The beach became narrower from (B) to (C), and then at a faster rate from (C) to (D). The images were taken on 07-03-2008 at an hourly interval, except between (A) and (B) which covers a two-hour time gap. The wind speed and direction were $U \approx 12$ m/s and $\theta \approx 67°$. $\theta = 0°$ is cross-shore from the west, θ = -90° is the alongshore wind coming from the north, and θ = 90° is alongshore from the south.

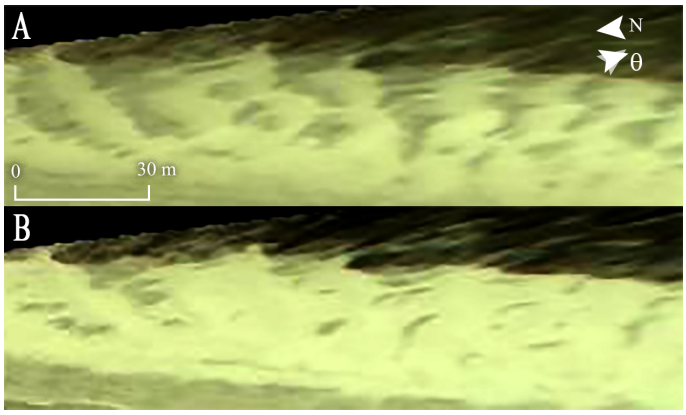

Figure 2.12: (A) shows a beach section with sand strips. The bedforms are less distinct in (B), probably due to drying of the moist, dark sand. The images were taken on 24-07-2007 and are 2 hours apart. The wind speed was $U \approx 15$ m/s and θ changed from -73° to -53°. θ = 0° is cross-shore from the west, θ = -90° is the alongshore wind coming from the north, and θ = 90° is alongshore from the south.

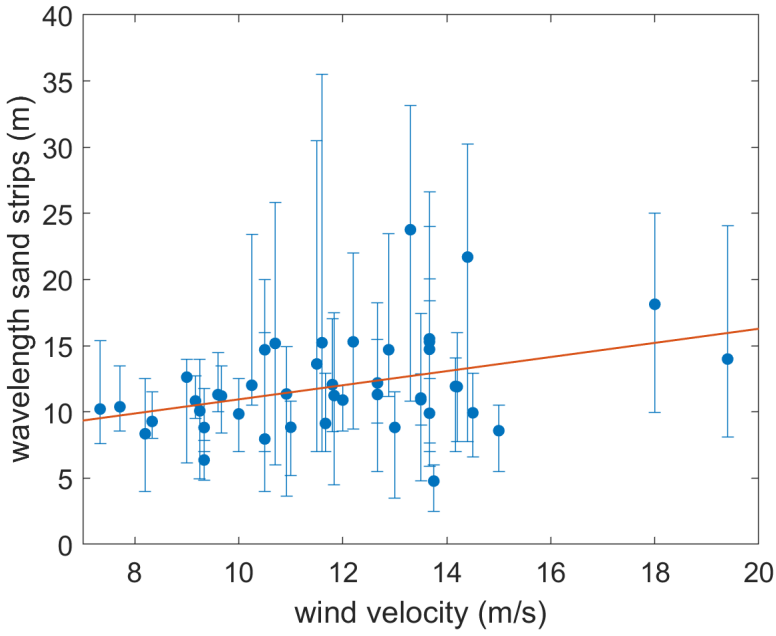

Figure 2.13: Sand strip wavelength (m) versus wind velocity (m/s). Each datapoint represents one sand strip event. The corresponding wind velocity has been obtained by averaging the hourly mean wind velocities that were measured at the time the sand strip event took place. The vertical lines represent the 2.5 and 97.5% percentile. The red line is the best fit linear line ($r = 0.38$).

Dune growth is the result of numerous aeolian events with different transport magnitudes occurrence frequencies. Events with strong winds may result in a high potential transport rate but because their infrequent occurrence may not contribute considerably to long-term aeolian input from the beach to the foredune (Wolman and Miller, 1960; Delgado-Fernandez and Davidson-Arnott, 2011). The results of this research indicate that the wind direction can reduce the impact of (visually) large transport events at this field site even further. Firstly, sand strips were observed when the regional wind was strongly shore-oblique. Therefore, it is possible that only a small fraction of the transported sand will be deposited at the dune foot as the input is proportional to the cosine of the angle of the wind approach from shore normal (Davidson-Arnott and Law, 1996), which is here usually above 60°. Secondly, the steep slope of the foredune is likely to cause the local (on the beach) wind direction to differ from the regional value (Walker et al., 2006; Bauer et al., 2009). The dunes can act as a wall, deflecting oblique winds alongshore. At our site, this is reflected by the alongshore migration of the sand strips, even though the regional wind direction is shore-oblique. This mismatch between the local and regional wind direction will further diminish aeolian input because of the above mentioned cosine effect. Wind velocity is also expected to differ from the regional value and to vary across the beach. In particular, the wind is stronger at the waterline (Walker et al., 2006), which may explain why sand strips move at different velocities along the width of the beach, sometimes resulting in sand strip overtaking (e.g. Figure 2.15). It should be noted that the difference in migration velocity was not included in our

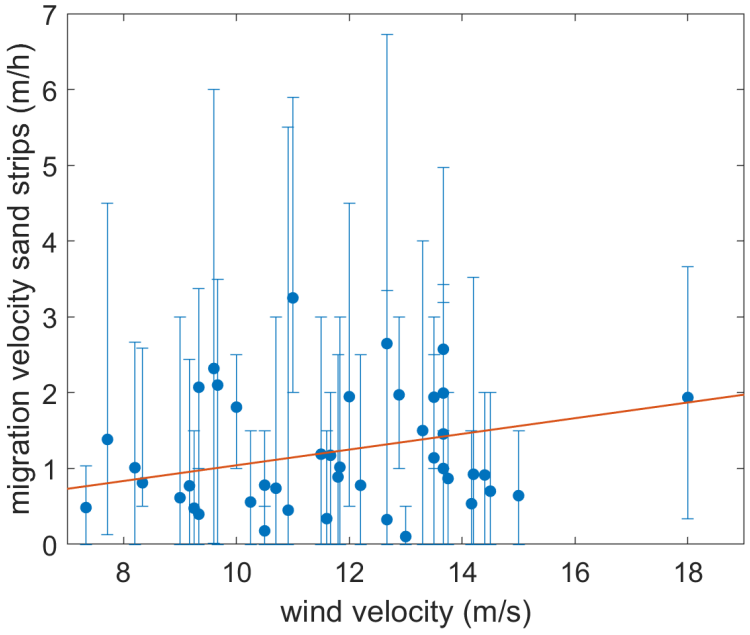

Figure 2.14: Sand strip migration velocity (m/h) versus wind velocity (m/s). Each datapoint represents one sand strip event. The corresponding wind velocity has been obtained by averaging the hourly mean wind velocities that were measured at the time the sand strip event took place. The vertical lines represent the 2.5 and 97.5% percentile. The red line is the best fit linear line ($r = 0.32$).

analysis as we focussed on sand strip characteristics on the upper beach. On the whole, our sand strip analysis is thus indicative of substantial differences between local and regional wind characteristics. The common use of regional rather than local wind data in the prediction of long-term sand deposition on the foredune may thus also contribute to the common overprediction of measured deposition volumes.

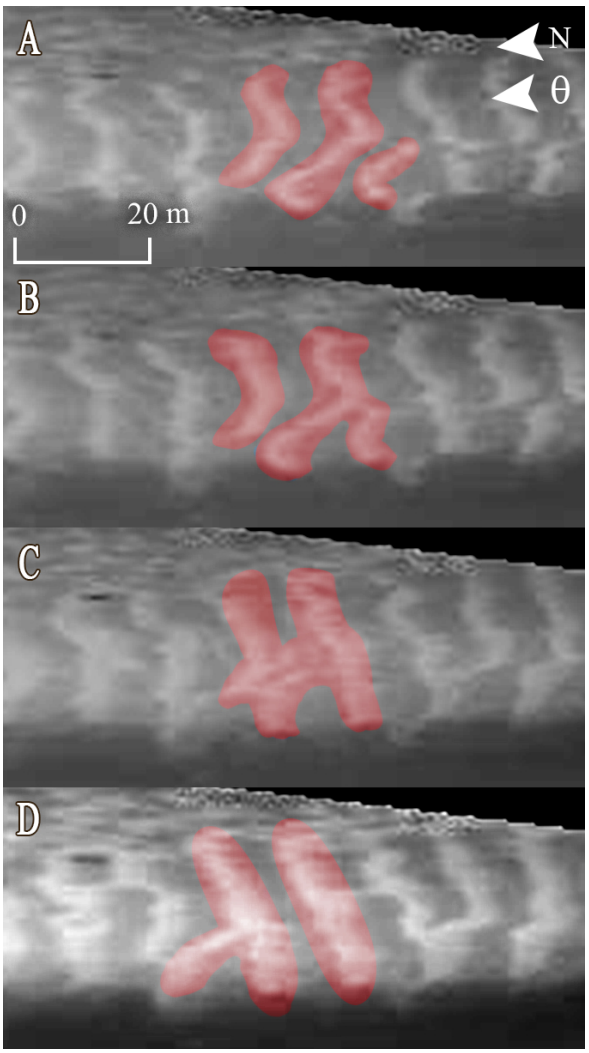

Figure 2.15: Rebranching sand strips. In (A), the sand strips marked with red are not connected to each other. (B) shows one strip connecting to the middle one. In (C), all sand strips have merged together, only to turn into separate sand strips again in (D). The images were taken on 29-11-2011 at an hourly interval. The wind speed and direction were $U \approx 9$ m/s and $\theta \approx 97°$. $\theta = 0°$ is cross-shore from the west, θ = -90° is the alongshore wind coming from the north, and $\theta = 90°$ is alongshore from the south.

2.6 Conclusions

An Argus video monitoring station has been used to study signs of aeolian sand transport on the beach of Egmond aan Zee, the Netherlands. The transported sand can create low, slipfaceless bedforms, known as sand strips, depending predominantly on the wind direction. Cross-shore winds result in poorly developed sand strips, consisting of only a few patchy stripes of sand. When the wind blows in an (almost) alongshore direction, sand strips form at the dune foot and then the area they cover spreads towards the intertidal area as the tide falls, beginning as patches of dry sand and growing into strips over time. Sand strips disappear when the bed dries or the rising tide washes them away. The average wavelength of sand strips is 12.0 m (with a standard deviation of 2.8 m), while their average migration velocity is 1.24 m/h (with a standard deviation of 0.78 m/h). The migration velocity and wavelength of sand strips are only weakly dependent on the wind velocity ($r = 0.38$ and 0.32, respectively). Sand strips are often oriented alongshore, even though the regional wind is onshore oblique. This suggests substantial wind steering by the steep, 25 m high foredune at the study site.

Chapter 3

Using Argus video monitoring to determine limiting factors of aeolian sand transport on a narrow beach

Based on: Hage, P.M., B.G. Ruessink, and J.J.A. Donker (2018), Using Argus Video Monitoring to Determine Limiting Factors of Aeolian Sand Transport on a Narrow Beach. *Journal of Marine Science and Engineering 6*, 4, 138. doi: https://doi.org/10.3390/jmse6040138

Abstract

Aeolian sediment transport on beaches is responsible for dune growth and/or recovery. Models predicting potential aeolian sediment transport rates often overpredict the amount of deposition on the foredune when applied to narrow (<100 m) beaches, pointing to supply limitations. Our goal is to better understand these limitations, especially in the long-term (>years) in order to improve predicted transport volumes and the timing of transport. Here, we used 8 years of Argus video images at Egmond aan Zee, The Netherlands, in combination with routine weather data to delineate 241 limited from 467 unlimited sand transport events to explore supply-limiting factors. Our research shows that the wind is more oriented to the west (shore normal) and is generally stronger for limited transport events. This indicates that the available fetch distance is often less than the critical fetch needed for unlimited transport. This is further confirmed by the timing of the transport events, as limited events often became unlimited during low tide when the beach was the widest and fetch potentially the longest. Our results help understanding the nature of aeolian sediment transport on narrow beaches, which will hopefully lead to better predictions of annual aeolian sediment transport rates.

3.1 Introduction

The sand needed for coastal dune growth primarily comes from the intertidal and supratidal beach. Aeolian sand transport on beaches is, however, poorly understood. While aeolian models relating time-averaged transport to grain size (Sherman et al., 2013a) and wind shear velocity (Davidson-Arnott and Law, 1996; Bauer and Davidson-Arnott, 2002) do well for steady winds blowing over a horizontal surface with a uniform grain size (Gares, 1988; Sherman and Hotta, 1990; Bauer et al., 2009; Sherman and Li, 2012), they often overestimate the amount of sand deposited on the foredune fronting beaches in more complicated settings (Davidson-Arnott and Law, 1996; Miot da Silva and Hesp, 2010; Keijsers et al., 2014).

Transport on a natural beach is affected by, for example, the moisture content of the sand, the beach slope and the bed roughness (e.g., Svasek and Terwindt, 1974; Davidson-Arnott and Law, 1996; Jackson and Nordstrom, 1998; Sherman et al., 1998; Bauer and Davidson-Arnott, 2002; Wiggs et al., 2004; Edwards and Namikas, 2009; Delgado-Fernandez and Davidson-Arnott, 2011; Nield et al., 2013; Nield et al., 2014). These factors cause moments of strong aeolian activity to not always coincide with moments of high wind velocities,

and the other way around; moments of high potential transport based on wind velocity do not necessarily lead to high actual transport, which was found by Delgado-Fernandez and Davidson-Arnott (2011) and in Chapter 2. Detailed field measurements concerning aeolian sediment transport on beaches have identified these influences (Jackson and Nordstrom, 1997; Bauer and Davidson-Arnott, 2002; Davidson-Arnott et al., 2005; Baas and Sherman, 2006; Udo et al., 2008; Bauer et al., 2009; Davidson-Arnott and Bauer, 2009; Sherman et al., 2011; Sherman et al., 2013b), but tend to be short in duration, ranging from minutes to weeks. Therefore, the effect of limiting factors on long-term (months to years) transport and dune development is unknown (Delgado-Fernandez et al., 2009) and not properly quantified. This would require long-term observations with high (hourly) temporal resolution to determine which wind events do induce high aeolian activity and which factors determine this.

Video monitoring with high temporal resolution can be used to observe the coast on long time scales. The method has successfully been used to research the nearshore on time periods of years (van Enckevort et al., 2004; Ruessink et al., 2009; Pianca et al., 2015), and has been used by Delgado-Fernandez et al. (2009) and Guimarães et al. (2016) and in Chapter 2 to study signs of aeolian sand transport on the beach. Aeolian sediment transport can be seen on video imagery as saltation streamers and sand strips. Streamers are elongated features of saltating grains with a strong spatial and temporal variability (Baas and Sherman, 2005; Sherman and Li, 2012). Sand strips are slipfaceless bedforms, and often appear when sand is blown over relatively moist beds (Jackson et al., 2006; Davidson-Arnott et al., 2008; Bauer et al., 2009; Nield et al., 2011; Nield, 2011), especially when roughness elements like vegetation (Sherman and Hotta, 1990; Eamer and Walker, 2010) and frozen material (Hesp and Arens, 1997) are present as well.

Delgado-Fernandez et al. (2009)'s temporary camera system at Greenwich Dunes, Canada, could pick up these traces of aeolian transport, as wind-blown sand usually is dryer and therefore lighter in colour than the moist bed, providing visual contrast. When undisturbed, sand strips can grow into ephemeral dunes, which have a slipface and a height in the range of decimetres to a metre (Kocurek et al., 1992; Elbelrhiti, 2012; Guimarães et al., 2016). Like the traces of aeolian transport in the work of Delgado-Fernandez et al. (2009), these features were visible on camera because of a difference in moisture content, and therefore colour, between the transported sand of the bedforms and the bed (McKenna Neuman and Langston, 2006).

Delgado-Fernandez et al. (2009)'s study further showed that video monitoring can be used to provide information about vegetation cover, the position of the shoreline, fetch distances, and surface moisture content. After monitoring the beach at Greenwich Dunes for 9 months, they found that the angle of the approaching wind, which affects the maximum fetch distance, might be more important than a strong wind. Very strong winds, onshore as well as oblique, even led to wave scarping and a loss of sediment. Other limitations that stopped or hindered aeolian transport were the duration of the event and, in winter, snow and ice cover.

The aim of this paper is to find how limiting factors affect transport on long time scales at the narrow beach of Egmond aan Zee, The Netherlands, with the use of long-term (>years) video monitoring data, together with concurrent meteorological data station operated by the Royal Dutch Meteorological Institute (KNMI). The methodology will be introduced in Section 3.2, including a description of the field site, the used video monitoring system and the weather station. Section 3.3 describes our results, which is followed by our discussion, and conclusions in Sections 3.4–3.5, respectively.

3.2 Methodology

3.2.1 Study site

The study site lies between the towns of Egmond aan Zee and Castricum, The Netherlands (Figure 3.1). The coastline is straight, with an orientation of 7° east of north, and has a beach with moderate slope (1:30) containing sand with a median grain size of 240 μm. The beach width depends on the tide and varies between 30 and 100 m. Usually, one or two slipface bars are present on the intertidal beach (Masselink et al., 2006; Aagaard et al., 2005; Quartel and Grasmeijer, 2007). The established foredune has a height of 20 to 25 m and forms a uniform row parallel to the beach. Occasional erosion events have made its seaward front steep (40–50°) (de Winter et al., 2015). European marram grass (*Ammophila arenaria*) grows on most parts of the foredune, especially at heights exceeding 10 m above beach level. Occassionally, embryo dunes develop at the transition between beach and foredune (e.g., de Winter et al. (2015)), typically at 3 to 5 m above mean sea level.

The site experiences a semidiurnal tide, which ranges from 1.4 m (neap tide) to 1.8 m (spring tide). The significant offshore (in 20 m depth) wave period and height for the Dutch coast are 5 s and 1.2 m, respectively, and do not show strong alongshore differences. The beach is exposed to waves from the southwest to the north (Wijnberg and Terwindt, 1995). The south-southwest (210–230° with respect to north, Figure 3.2) is the dominant wind direction at this beach. The offshore wave height can increase to over 5 m during storms. Especially storms from the northwest are associated with surges in excess of 1 m. As a result, the intertidal beach can be flooded for several days (Quartel et al., 2007), which can destroy the intertidal bars and embryo dunes. On average, the foredune along this part of the coast gains 10 to 15 m^3/m/year, see de Winter et al. (2015) and de Vries et al. (2014). The potential volume of sand transported towards the dunes based on hourly mean wind velocity from the weather station described below, as calculated with the equation based on Hsu (1974), is substantially higher at 29 m^3/m/year.

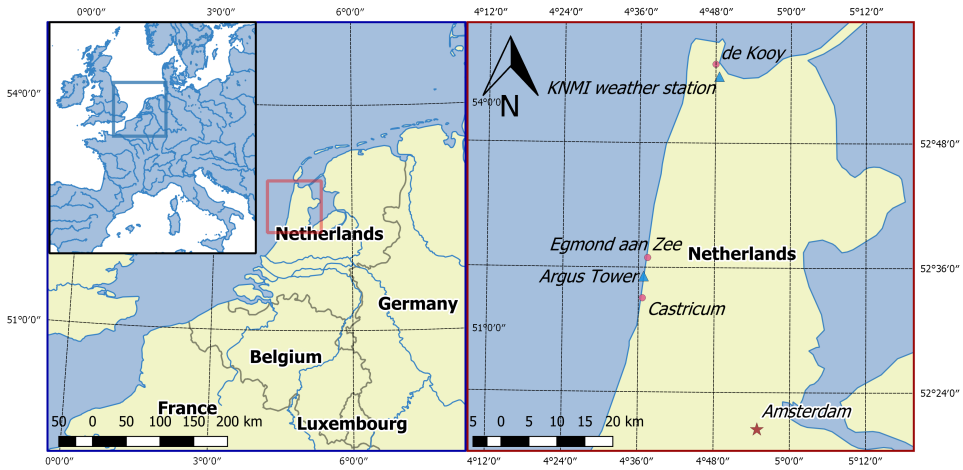

Figure 3.1: Map of the field site and weather station.

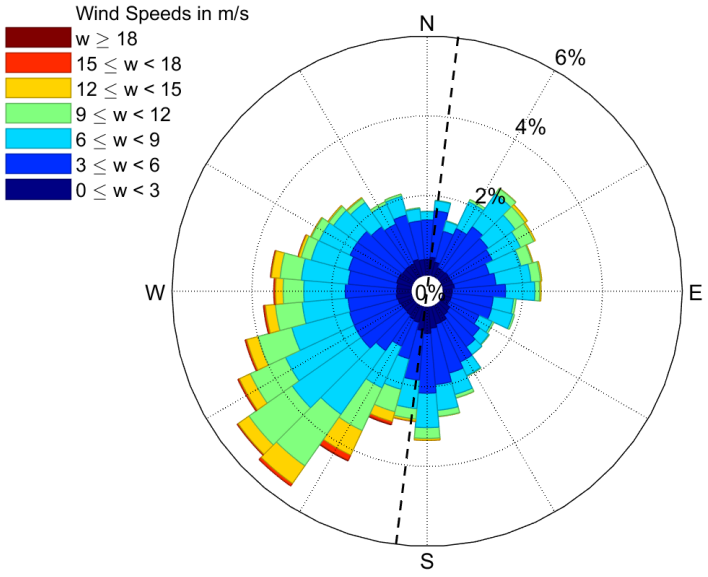

Figure 3.2: Wind rose based on hourly wind speed U and direction θ data collected between 2005 and 2012 at de Kooy, approximately 40 km north of our study site. The dashed line indicates the orientation of the coast. The data are made available with a resolution of 1 m/s for U and 10° for θ. The anemometer and wind vane are located at a height of 10 m above ground level.

3.2.2 Used data

The study area lies in the field of view of an Argus video system (van Enckevort and Ruessink, 2001), which is an optical remote sensing system pioneered by Holman and Sallenger (1986) for sampling the nearshore environment. An Argus system consists of a suite of cameras at the top of a high structure in order to gain an unhindered view of the beach. A timing module is installed to ensure a synchronised collection of the images (Holman and Stanley, 2007). The Argus system at Egmond aan Zee consists of five RGB-colour cameras, which were mounted on a 45-m high tower on the supratidal beach. The Argus system was installed in April 1998 and removed in June 2017, although data collection already ceased in October 2015. The cameras provided a 180° view, from south-southwest to north-northeast with a resolution of 640 × 480 pixels from 1998 to February 2004, 1024 × 768 pixels from 2004 to August 2005 and 1392 × 1040 pixels since then. Three different oblique images were produced by each camera every 30 min: a snapshot, a time-exposure (timex) and a variance image. Only the first two types of images are used in this research. The timex images were created by averaging the snapshots that were taken with a frequency of 2 Hz over a 10-minute period. This procedure blurs out all movement that occurred in that 10-minute time frame, which includes individual waves breaking on the subtidal bars, people walking on the beach, and aeolian streamers. In the timex images aeolian activity is thus seen through sand strips (e.g., Chapter 2). In order to make our research comparable to our previous study, we focus on the imagery available from January 2005 to December 2012.

The footprint dimensions of individual pixels give the theoretical accuracy of the images. This footprint is the projection of a square image pixel on the ground, which is close to rectangular with a larger alongshore than cross-shore side. The cross-shore footprint dimension is less than 0.2 m for the post-2005 system at this site, while the alongshore size increases from 0.2 m at 100 m from the tower alongshore to $\approx$1.5 m at 400 m.

This study used various meteorological characteristics collected by a weather station in the Kooy, roughly 40 km north of the field site (Figure 3.1). The weather data were made available by the Royal Netherlands Meteorological Institute (KNMI) and include the wind direction θ, hourly mean wind velocity U, ten-minute mean wind velocity, maximum wind gust per hour, temperature at the time of observation, minimum temperature in the preceding 6-h period, dew point temperature at the time of observation, sunshine duration, precipitation duration, hourly precipitation amount, air pressure, atmospheric humidity, cloud cover, and the presence of fog, snow, ice, and thunder. The time resolution for all meteorological variables is 1 h. The anemometer and wind vane are located at a height of 10 m above ground level.

3.2.3 Classification of limited and unlimited events

Both the snapshot and timex images from the Argus monitoring system were used to find traces of aeolian sediment transport. A first selection of images was made based on U, as sand transport can only take place when the wind exceeds a certain threshold. In a previous study, we showed that this threshold was 8 m/s (Chapter 2). Furthermore, the threshold had to be surpassed for at least three hours to ignore short events that contribute little to the total potential transport, but which would otherwise strongly increase analysis time (Hage, 2014). Part of this $>$3 h time period has to fall within daylight hours, which ranged from 8:00 to 16:00 (GMT) for January and December, 7:00 to 16:00 for February and November, 6:00 to 17:00 for March and October, 5:00 to 18:00 for April and September, 4:00 to 19:00 for May and August, and 6:00 to 17:00 for June and July. This resulted in 709 wind events between January 2005 and December 2012. Of those events, the hour with the highest hourly mean wind velocity during daylight hours was selected.

The Argus image corresponding to the hour with the highest hourly mean wind velocity of the event was visually inspected for traces of aeolian transport, for which both the snapshot and timex images were used. Active streamers cannot always be distinguished from remnant streamers or small patches of immobile sand on snapshot images, as they all appear as elongated streaks of dry sand. Since active streamers move quickly, they get blurred out in the timex images while the inactive ones remain visible, making it possible to distinguish the active ones when both image types are compared (Figure 3.3). Sand strips appear the same in snapshot and timex images because they move with only a few metres per hour, which is too slow for the timex images to pick up and blur out their movement. Images taken at subsequent hours were therefore checked to spot sand strip movement.

As no quantitative data concerning transport rates are available or can be assessed from the imagery, it is assumed that the presence and state of streamers and sand strips visible on the Argus images indicate how well developed aeolian sediment transport is. A transport event is considered to be unlimited when the beach is covered with sand strips, which are strong visual signs of transport. Likewise, an event that shows no signs of aeolian transport is considered limited, as the wind velocity was above the threshold for transport and should result in visible signs of transported sand. That, however, leaves situations where only small signs of aeolian sediment transport, like moving patches of sand or underdeveloped sand strips, are visible. Whether these situations are limited is presumably related to the duration of the wind event. Seppälä and Lindé (1978) found in their wind tunnel experiment that the time needed for aeolian ripples to form is inversely related to the wind velocity. Similar results were found in other environments, such as for current ripples in a flume (Baas et al., 1993;

Figure 3.3: Example of a snapshot (**A**) and timex image (**B**). Streamers and waves are visible in the snapshot, but they are blurred out in the timex image. The images were taken on 25-09-2012 around 6.00 h (GMT). The hourly mean wind velocity U was 8 m/s and the wind direction θ was 97°. θ = 0° is cross-shore from the west, θ = -90° is the alongshore wind coming from the north, and θ = 90° is alongshore from the south.

Baas, 1994). Therefore, it is more likely to see better-developed bedforms after a wind event of a certain length when winds are strong. Bagnold (1941) found that wind ripples disappear with high wind velocities, and that transport may turn to sheetflow. However, such a wipeout of sand strips has not been observed in a previous study using the present Argus images (Chapter 2), even for $U \approx 20$ m/s.

The focus of this paper is on instantaneous limiting factors. To do so, the events were sorted into four different classes based on their maximum hourly mean wind velocity (Table 3.1) and five different classes according to their visual signs of transport (Figure 3.4). Class 0 of the visual classification shows no signs of transport (Figure 3.4A). Class 1 shows very small signs of transport (Figure 3.4B), like single moving patches of sand or a handful of streamers. Class 2 shows more of these sand patches, but they have not formed rows of sand strips (Figure 3.4C). This happens in class 3, but the beach area that the sand strips cover is patchy (Figure 3.4D). Class 4 is for images where most of the beach is covered by active sand strips, often in combination with high streamer activity (Figure 3.4E). Chapter 2 has shown that the wavelength of the sand strips in this class is ≈12 m and their migration velocity is around a metre per hour. Neither sand strip length nor migration speed depends convincingly on wind speed.

Table 3.1: Wind classes.

Wind Class	Wind Velocity (m/s)
1	8
2	9–11
3	12
4	≥13

All events that show strong signs of transport, i.e., fully developed, active sand strips (class 4 in Figure 3.4) are unlimited, no matter their wind velocity class. Likewise, events that show no visual signs of transport were considered limited. That leaves events with little to medium signs of aeolian transport (class 1 to 3 in Figure 3.4), of which it is harder to determine whether their bedform development is hindered by factors that limit aeolian transport or is still in the process of developing. For these events, the combination of classes

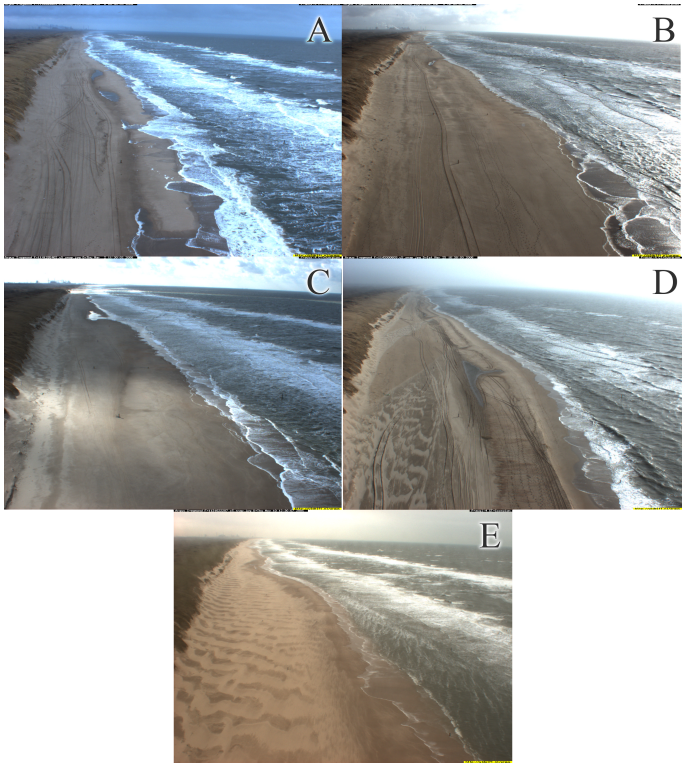

Figure 3.4: Examples of snapshots made by the south-facing camera and classified according to their visual signs of aeolian activity, where class 0 shows no signs of transport (**A**); class 1 shows very small signs of transport, like single moving patches of sand or a handful of streamers (**B**); class 2 has more of these sand patches, but they have not formed rows of sand strips; class 3 does have rows of sand strips, but they cover a patchy area; and class 4 features sand strips that cover most of the beach, often in combination with high streamer activity The date of the image and wind conditions were: 08-02-2006, $U = 7$ m/s, $\theta = -23°$ (**A**); 05-03-2006, $U = 8$ m/s, $\theta = -23°$ (**B**); 02-03-2006, $U = 9$ m/s, $\theta = 17°$ (**C**); 25-03-2006, $U = 10$ m/s, $\theta = 47°$ (**D**); 10-11-2005, $U = 12$ m/s, $\theta = 57°$ (**E**); where $\theta = 0°$ is cross-shore, $\theta = -90°$ is the alongshore wind coming from the north, and $\theta = 90°$ is alongshore from the south.

based on wind velocity and visual transport determined whether or not a certain class combination was considered to be limited or unlimited, as the lag in bedform development will be more prominent for events with low wind velocities. The events with little to medium signs of aeolian transport were seen as unlimited when the class based on their wind velocity was lower than their class based on visual transport. It differs per transport class how much lower the wind velocity class has to be. For transport class 1, for example, both wind class 3 and 4 are considered limited. This is the same for transport class 2, even though it ranks higher. This difference is based on how often a higher transport class was encountered when studying other Argus images of the same day of a certain event. If more than 75% of the events of a certain wind and transport class combination contained a moment with stronger

visual signs of aeolian transport a couple of hours before the hour with the maximum mean wind velocity, the class combination was considered limited, and not merely lagging behind with bedform development. This resulted in 241 limited and 467 unlimited transport events (Table 3.2). All meteorological characteristics measured by the weather station in de Kooy were studied for differences between the limited and unlimited events.

Table 3.2: Number of events sorted according to their wind class (Table 3.1) and transport class (Figure 3.4). The limited events are coloured in grey.

	Transport Class				
Wind Class	**0**	**1**	**2**	**3**	**4**
1	82	99	32	27	21
2	46	87	27	38	53
3	9	23	16	11	23
4	18	25	17	5	49

When studying the Argus images, it was noticed that 129 of the 241 limited events showed unlimited transport later or earlier on the same day. The conditions during the limited part of the day were compared to the unlimited part. This was done for the weather characteristics mentioned above, but also for the relative beach width as a proxy for the relevance of fetch effects. The cross-shore distance between the tower and the waterline was determined with the Intertidal Beach Mapper (IBM), an application that uses Argus timex images to determine the intertidal bathymetry of a beach with the help of the shoreline. For this research, only the location of the shoreline was needed. IBM determines this location relative to the position of the Argus tower. A Region Of Interest (ROI) was defined in which the shoreline could be found, then the IBM identified the location of the shoreline by automated clustering of land and water pixels in Hue-Saturation-Value (HSV) colour space. The land and water pixels form two peaks in a histogram plot and are separated by a discriminator function. The pixels that correspond with the line of the function are exactly between water and land, i.e., the shoreline. A more detailed description of the IBM application can be found in Aarninkhof et al. (2003). IBM was applied to the shoreline 90 to 470 m south of the Argus tower, though the exact alongshore location of the waterline varied for each image, as the location with the optimal contrast between sand and water was chosen to determine the waterline. The results for each Argus image were averaged alongshore.

3.3 Results

An overview of the studied variables and significance between limited and unlimited transport events can be found in Table 3.3. More specifically, this table shows the result from two-sample Kolmogorov-Smirnov tests. The null hypothesis states that the data for limited and unlimited events are from the same continuous distribution, while the alternative hypothesis is that limited and unlimited events are from different continuous distributions. For many variables, the frequency distribution between limited and unlimited events did not differ as marked with 0 for (almost) all α. Only the wind velocity and direction, monthly frequency, and temperature showed significantly different results at $\alpha = 0.05$. We focus on these variables in the remainder of this section. The wind rose for the unlimited transport events (Figure 3.5A) features a narrow peak for winds coming from the southwest. Other wind directions are far less prominent. It must be noted that Argus observations of unlimited events then show aeolian transport in the alongshore direction, which was also observed in Chapter 2. Westerly (onshore) winds were more prominent in the wind rose for limited transport

Table 3.3: Two-sample Kolmogorov-Smirnov test between limited and unlimited data for various variables and alpha values. Acceptance of the null hypothesis are marked with 0, a rejection (i.e., the data comes from different distributions) it with 1.

	α						
	0.001	0.005	0.01	0.02	0.05	0.1	0.15
hour of occurence	0	0	0	0	0	0	1
month of occurence	1	1	1	1	1	1	1
wind direction	1	1	1	1	1	1	1
wind velocity (mean)	1	1	1	1	1	1	1
wind velocity (last 10 min of each hour)	1	1	1	1	1	1	1
wind velocity (highest gust of each hour)	1	1	1	1	1	1	1
temperature (at time of observation at 1.5 m)	1	1	1	1	1	1	1
temperature (minimum for preceding 6 h at 0.1 m)	0	0	0	0	0	0	0
temperature (dew point at 1.5 m)	1	1	1	1	1	1	1
sunshine duration	0	0	0	0	0	0	0
global radiation	0	0	0	0	0	1	1
precipitation duration	0	0	0	0	0	0	0
hourly precipitation amount	0	0	0	0	0	0	0
air pressure	0	0	0	0	0	1	1
cloud cover	0	0	0	0	0	0	0
relative atmospheric humidity (at time of observation at 1.5 m)	0	0	0	0	0	0	0
fog occurence	0	0	0	0	0	0	0
rain occurence	0	0	0	0	0	0	0
snow occurence	0	0	0	0	0	0	0
thunder occurence	0	0	0	0	0	0	0
ice occurence	0	0	0	0	0	0	0

events (Figure 3.5B). There no longer is a distinct peak, as the results cover all wind directions between the southwest and the west-northwest. It also has relatively more events with high wind velocities. The video imagery further showed that strong winds from the west to northwest could cause a surge high enough to flood parts of or even the entire beach. This was common for events with high wind classes (class 3 and 4), but with little to no visible traces of aeolian transport (class 0 or 1).

The wind roses also show that both limited and unlimited events happen under a wide range of wind velocities, though high wind velocities (>11 m/s) are more common for limited events. This is better illustrated in Figure 3.6. The wind velocity shows a peak at 8 m/s for both limited and unlimited events, which makes up 28% of all events. There is a second, smaller peak at 12 m/s for the limited events, and high wind velocities are relatively more common. The mean wind velocity for unlimited transport events is 10.3 m/s (standard deviation of 1.9 m/s) and 11.1 m/s (standard deviation of 2.3 m/s) for limited transport events.

All events with high visual transport classes resulted, as aforementioned, from shore-oblique winds. Precipitation sometimes interrupted transport during these events, which was visible as a darkening of the beach and rain drops on the camera lens. Sand strips often disappeared during precipitation, but streamers sometimes remained visible when relatively strong winds (>10 m/s, depending on the amount of rain drops visible on the camera lens) were present. Strong winds could also cause streamers and sand strips to reappear quickly (i.e., an hour later) when the precipitation stopped. Limited and unlimited events did not differ in the presence, duration, and amount of precipitation.

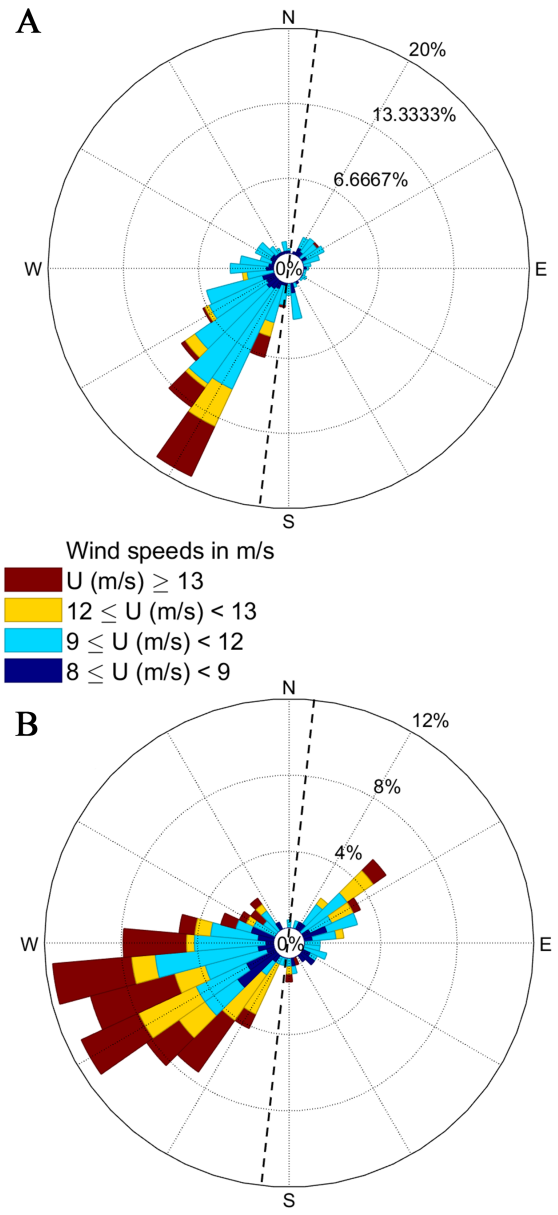

Figure 3.5: Wind rose for (**A**) unlimited and (**B**) limited transport events. Mind the different scales of the two wind roses. The dashed line indicates the orientation of the coast.

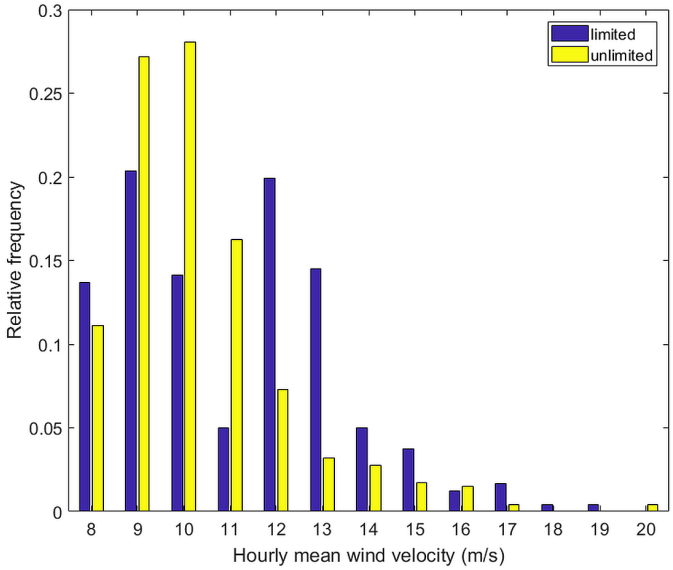

Figure 3.6: Relative frequency of the wind velocity for limited and unlimited events. The mean wind velocity for unlimited events is 10.3 m/s (standard deviation of 1.9 m/s) and 11.1 m/s (standard deviation of 2.3 m/s) for limited transport events.

The frequency distribution of temperature differs between limited and unlimited events (Figure 3.7). The mean temperature for unlimited and limited events was 12.4 °C (with a standard deviation of 5.1 °C) and 10.5 °C (with a standard deviation of 5.9 °C), respectively. The difference in mean temperature and temperature distributions were not caused by a daily pattern, as unlimited events did not occur more often around the warmest part of the day than limited events did. Instead, there is a seasonal trend, with the amount of limited transport events being relatively low from May to September (Northern Hemisphere summer) compared to other times of the year (Figure 3.8). Furthermore, unlimited events in May, June and July, have relatively few class 4 events, unlike October, November, December, and January. Small unlimited events therefore seem to be common during summer conditions, while the winter features large unlimited events, but also numerous limited events.

Some limited events show unlimited transport at an earlier/later moment of the day. There are no significant differences in weather between the hour with limited transport and the one with unlimited transport. However, the moment with unlimited transport has a much wider beach. Figure 3.9 shows the difference in beach width between the hour with limited transport and the hour earlier/later with unlimited transport. A positive value implies a broader beach during the moment with unlimited transport. Figure 3.9 shows the difference in beach width has a tendency to be positive, with a peak around 20 and 50 m and an average value of 19.6 m. In other words, the beach is usually broader during the moment of unlimited transport than at the hour with the highest hourly mean wind velocity of the transport event.

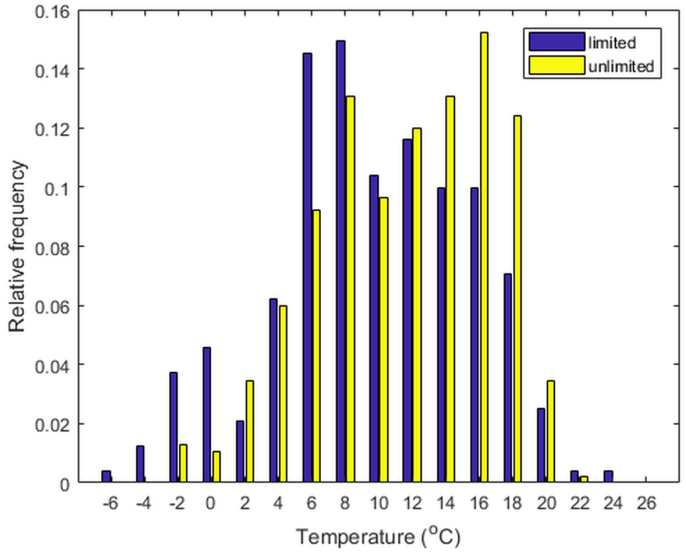

Figure 3.7: Relative frequency of the temperature at the time of observation (1 observation per hour) during the limited and unlimited transport events. The mean temperature for unlimited and limited events was 12.4 °C (with a standard deviation of 5.1 °C) and 10.5 °C (with a standard deviation of 5.9 °C), respectively.

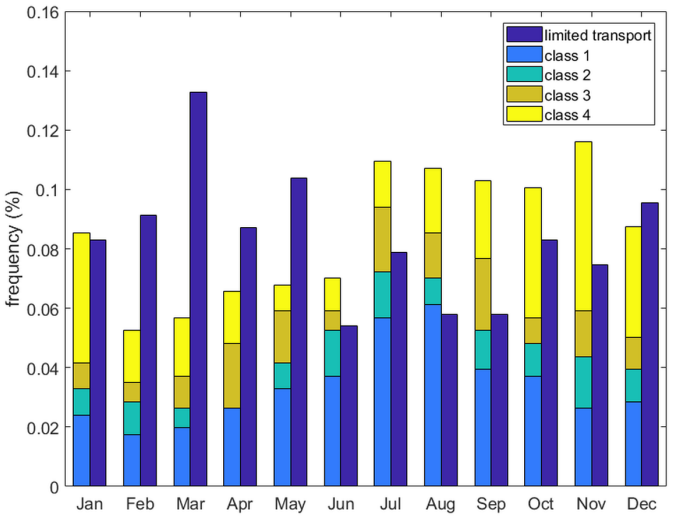

Figure 3.8: Relative monthly occurrence of limited and unlimited events. The unlimited events shown are separated in the visible transport classes given in Figure 3.4.

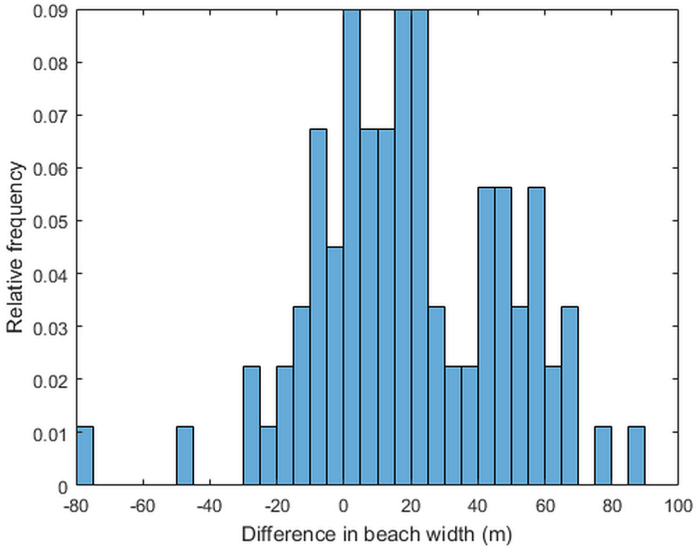

Figure 3.9: The difference in beach width during the part of the day with limited and unlimited transport. A positive difference implies a larger width during unlimited transport than during limited transport.

3.4 Discussion

The multi-year data set of the Egmond Argus video monitoring station gives visual signatures of aeolian transport events, which were employed here to investigate which factors affect aeolian sediment transport on long time scales (>years). The limited and unlimited events differed in dominant wind direction and velocity, temperature, and beach width, as well as in the frequency distribution of velocity, and temperature. Shore-perpendicular wind directions, higher wind speeds and lower temperatures all increase the likelihood of a limited transport event. The limited transport events occurred under a higher mean wind velocity (with a secondary peak around 12 m/s) and were relatively more common for even larger wind velocities than unlimited events (Figure 3.6). High wind velocities increase aeolian transport volumes according to models like Hsu (1974), but high wind velocities cause a longer critical fetch distance as well, which can limit transport on a narrow beach. The critical fetch (that is, the fetch at which aeolian transport has saturated at its potential value) cannot be determined with the Argus images, but an equation based on field results by Davidson-Arnott and Law (1990) exists, and even though its general application is not proven, it can give an indication of typical critical fetch distances F_c for dry, sandy surfaces with a mean grain size of 200–300 μm (see also Delgado-Fernandez (2011)):

$$F_c = 4.38 * U - 8.23$$

For our study site, where typical wind velocities for transport events are 8 to 15 m/s, the critical fetch distance will be 27 to 57 m under optimal circumstances; moist sand can increase the critical fetch distance with >50% or more. This would make the maximum fetch distance highly important for the study site, as the beach width is ≈100 m at most at low tide, but is more often substantially less wide. The maximum fetch will be less, as most

parts of the beach remain too wet for sands to be picked up by the wind (Smit et al., 2018; Brakenhoff et al., 2019). The importance of the maximum fetch distance disagrees with the findings of Lynch et al. (2016). They found a decay in aeolian sediment transport after having reached the critical fetch distance, which strongly affected an accurate prediction of aeolian sediment transport rates. The critical fetch distance was short (just a few metres), making it relatively unimportant for fine sandy beaches (Lynch et al., 2016). The sand at Egmond aan Zee, however, is medium fine. The Egmond beach is therefore more likely to have a critical fetch distance of a few tens of metres, as was found in various experiments with medium grain sizes (Delgado-Fernandez, 2010).

Winds from the southwest, which might rotate to a more alongshore direction due to topographic steering by the high and steep foredune, as was found by Walker et al. (2006) and Bauer et al. (2009) and in Chapter 2, lead to an increase in maximum fetch distances. During onshore westerly winds, the maximum fetch might be smaller than the critical fetch, so no full transport is reached. This is qualitatively consistent with findings in Nordstrom and Jackson (1993), who, for similar wind velocities, observed smaller aeolian transports under onshore rather than alongshore winds. Strong, stormy winds from the northwest can cause a storm surge which (partially) floods the beach, causing the beach to become very narrow. No significant difference could be found for the wind velocity and direction for different quarters of the year (divided as: December, January, February; March, April, May; June, July, August; and September, October, November), with the exception of the wind velocity in December, January, and February versus June, July, and August. A circular Kuiper test was used here to test if the wind directions were significantly different for the quarters of the year, while a Kolmogorov-Smirnov test was used to do the same for the quarters' wind velocities ($\alpha = 0.05$ for both tests). The wind velocity was higher during the Northern Hemisphere winter months than summer months (e.g. 11.1 m/s in January and 10.3 m/s in July). Lower wind velocities give shorter critical fetch distances, which favours unlimited transport.

High evaporation keeps the moisture content of the sand low, which favours transport (Wiggs et al., 2004; Davidson-Arnott et al., 2005). Winter months generally have lower evaporation rates. This, together with the seasonal difference in velocity, might explain the relatively more numerous unlimited events in July. The role of evaporation on surface moisture dynamics is, however, unclear (Namikas et al., 2010) and is mostly assumed small (e.g., Brakenhoff et al. (2019)). A closer inspection reveals that the beach in July is narrower than in January for unlimited events (22.2 m and 27.9 m seawards of the Argus tower, respectively), which agrees with the results of Quartel and Grasmeijer (2007), but contradicts the relatively more numerous unlimited events in July. The shorter critical fetch and/or higher evaporation therefore seem to exceed the effect of a narrower beach.

The maximum fetch distance, at least during rising tide, seems more important for aeolian transport than moisture content. During falling tide, sand from the intertidal beach becomes available for aeolian transport as the sand dries here below the moisture threshold that inhibits aeolian transport (Smit et al., 2018). Nordstrom and Jackson (1992) and de Vries et al. (2014) also pointed to the role of beach width in limiting aeolian supply to the dry upper beach. During rising tide the beach continues to dry until it inundates (Smit et al., 2018), but this does not seem to outweigh the effect of reducing beach width on aeolian transport.

It is possible that our results would have been slightly different when another nearby weather station had been used, as the local weather characteristics can differ from the regional characteristics (Chapter 2). The weather station at de Kooy is an inland station, which results in weaker onshore winds compared to a coastal station. Our research, however, mainly focused on patterns and relative differences between limited and unlimited events, so our main findings are not likely to be considerably different. Only weather characteristics

that vary strongly within a distance of 40 km might have a different outcome, which can be the case for precipitation when the weather is characterised by local showers.

Most existing models to predict annual sand supply to the foredune rely on hourly mean wind characteristics alone, while this study shows that beach width should be incorporated as well. Following the work of Delgado-Fernandez (2011), our next research step will be to extend the fetch model of Bauer and Davidson-Arnott (2002) into a predictive model that will check whether the timing of the predicted transport moments agrees with the visual signs of transport on Argus imagery. In other words, whether unlimited and limited events examined here are also predicted to be unlimited and limited.

3.5 Conclusions

This research focussed on the limitations of aeolian sediment transport on a narrow beach by studying the weather characteristics of limited and unlimited aeolian transport events. The limited and unlimited events were found after comparing wind velocities measured by a KNMI weather station with traces of aeolian transport on corresponding Argus images. Wind speed, direction and temperature were the most prominent weather characteristics that could explain the discrimination between limited (241) and unlimited (467) events. The wind had more often a cross-shore (westerly) direction and was generally stronger for limited transport events, while oblique winds (south westerly direction) were more common for unlimited transport events. Some limited events that took place during high tide showed unlimited transport during low tide. Furthermore, it was observed that strong westerly winds often caused a high surge, which flooded large parts of the beach. These results indicate that the maximum fetch distance strongly influences aeolian transport on a narrow beach. Finally, the unlimited events were relatively more common in the warmer summer months. It is unclear whether this points to evaporation as an important meteorological factor that determines annual onshore sand supply to the foredune.

Chapter 4

Using video monitoring to test a fetch-based aeolian sand transport model

Based on: Hage, P.M., B.G. Ruessink, Z.E.M. van Aartrijk and J.J.A. Donker (2020), Using Video Monitoring to Test a Fetch-Based Aeolian Sand Transport Model. *Journal of Marine Science and Engineering 8*, 2, 110. doi: https://doi.org/10.3390/jmse8020110

Abstract

Transport of beach sand to the foredune by wind is essential for dunes to grow. The aeolian sand transport rate is related to wind velocity, but wind-based models often overpredict this transport for narrow beaches (<100 m). To better predict aeolian sand transport, the fetch-based Aeolus model was developed. Here, we qualitatively test this model by comparing its transport-rate output to visual signs of aeolian transport on video imagery collected at Egmond aan Zee, the Netherlands, during a six-month winter period. The Aeolus model and the Argus images often agree on the timing of aeolian transport days, except when transport is small; that is not always visible on the Argus images. Consistent with the imagery (minimal signs of aeolian activity in strong winds), the Aeolus model sometimes predicts the actual transport to be smaller than the potential transport. This difference is largest when wind velocity is large, and its direction is cross-shore. Although transport limitations are not predicted to be common, the results suggest that their effect on the total transport in the study period was substantial. This indicates that the fetch distance should be taken into account when calculating aeolian transport for narrow beaches on longer timescales (>weeks).

4.1 Introduction

Coastal dunes are dynamic systems whose evolution is determined by aeolian and marine processes, the presence of vegetation, and human activities. Storms are responsible for dune erosion, a process lasting a few hours or days, while dune recovery and growth are driven primarily by the wind, a process that can take months to years. Time-averaged aeolian transport models often use only grain size and wind shear velocity (Hsu, 1974; Davidson-Arnott and Law, 1996; Bauer and Davidson-Arnott, 2002; Sherman et al., 2013a). This provides good results under controlled conditions, with a dry, horizontal surface, uniform grain size and steady wind, but transport on a natural beach is also affected by, for example, the moisture content of the sand, the beach slope, the bed roughness, and wind deflection by the foredune (e.g., Delgado-Fernandez and Davidson-Arnott, 2011; Edwards and Namikas, 2009; Wiggs et al., 2004; Nield et al., 2013; Nield et al., 2014; Bauer and Davidson-Arnott, 2002; Svasek and Terwindt, 1974; Davidson-Arnott and Law, 1996; Jackson and Nordstrom, 1998; Sherman et al., 1998; de Winter et al., 2020). The computed volume of wind-blown sand often exceeds the volume deposited on the foredune, with the latest reaching values as small as 15% of the former when the beach is narrow (Svasek and Terwindt, 1974; Bauer et al., 1996;

Davidson-Arnott and Law, 1996; Jackson and Nordstrom, 1998; Sherman et al., 1998; Bauer et al., 2009).

Aeolian sand transport has a clear visual signal, as the transported sand organizes itself as streamers, which are elongated features of saltating grains with a strong spatial and temporal variability (Baas and Sherman, 2005; Sherman and Li, 2012), and sand strips, which are slip-faceless bedforms (Montreuil et al., 2018; Nield et al., 2011; Nield, 2011) with a wavelength of around 10 m and a migration velocity of a few meters per hour as was found in Chapter 2. Delgado-Fernandez et al. (2009) observed that strong winds do not necessarily result in large amounts of aeolian transport and/or the presence of aeolian bedforms. A similar mismatch was also observed in Chapter 3, where it was found that small wind velocities ($\approx$8 m/s), and therefore small potential aeolian transport rates, can nonetheless cause sand strips to cover the beach. According to these studies, a short fetch, i.e., the distance over which the wind blows over the beach, and a large surface moisture content form important limitations for aeolian sand transport. For arctic beaches, ice and snow cover form limiting factors as well (Delgado-Fernandez et al., 2009), while nourished beaches may have reduced aeolian transport because of shell lag deposits (Van der Wal, 1998).

To improve the prediction of aeolian sand transport on narrow beaches, Bauer and Davidson-Arnott (2002) proposed a series of spatially explicit equations that include fetch distances. In addition to the fetch itself, they considered the maximum possible fetch and a critical fetch, which is the downwind distance needed for aeolian sand transport to reach its (potential) maximum. When the critical fetch is longer than the maximum fetch, the maximum transport rate cannot be reached, and transport will be limited. The modelling framework does not predict a quantitative transport rate, but it is a conceptual model capable of calculating the spatial distribution of a relative sand transport rate as a function of the critical fetch distance, beach geometry, and wind angle. The model was tested with data from a 9-month field campaign at Greenwich Dunes, Canada, by Delgado-Fernandez (2011) and further extended to be able to calculate sand transport for limited transport conditions. The model of Delgado-Fernandez (2011) forms the basis of this research and extracts a beach width and uniform moisture content for the beach from video imagery. The model applies several filter steps to select events likely to have transport. All events where no transport to the dunes is expected are ignored: the wind must be above the threshold of sand entrainment and have an onshore component, the gravimetric moisture content of the beach must be below 10%, the beach should not be fully inundated, and ice and snow should not cover more than half the beach. Then the critical fetch distance is determined from the wind velocity and increased with moisture content, making it more likely that it will exceed the maximum fetch (causing limited transport) when the beach is moist. Limited transport events will have a smaller transport rate, depending on the ratio between the critical and maximum fetch. It was found that for the studied period at Greenwich Dunes, the total transport rate was almost 29 times larger than the measured transport amount when only wind direction and entrainment threshold were used as a filter. This diminished to a factor 11.8 when the filter for snow cover, $>$10% moisture content, and an inundated beach were used. Including the effect of fetch diminished it further to a factor 8.2, and when the full model was used, this became to 6.2 times the measured transport amount. The improved predictions for transport show the feasibility of the fetch-approach, but the strong dependence on video data makes this model hard to apply to unmonitored coastal sites.

In this Chapter, we extend Delgado-Fernandez (2011)'s work with a new fetch-based model, called Aeolus, which uses time series of seawater elevation to determine groundwater cross-shore variability depth, which in turn determines a spatially and temporally varying surface moisture content. Furthermore, the Aeolus model determines the width of the beach, which is needed for calculating fetch distances, from a given bed profile, wind, water

level, and wave data. Here, we aim to qualitatively test the Aeolus model for long time scales (months) by comparing its results to visual signs of aeolian sand transport at the narrow beach of Egmond aan Zee, the Netherlands, previously explored in Chapter 2 and 3. The predicted transport will be compared with visual signs of aeolian transport, as determined from video monitoring. In particular, we are interested to see if the model can provide a better match between predicted and visually observed transport than a wind-alone model. The methodology is introduced in Section 4.2, including a description of the Aeolus model, field site, video monitoring data, model set-up and synthetic runs. Section 4.3 describes our results. The discussion and conclusion can be found in Sections 4.4 and 4.5, respectively.

4.2 Methodology

4.2.1 Model description

The Aeolus model consists of three modules. The first module is a groundwater model that uses the non-linear Boussinesq equation for finite-amplitude water table fluctuations (e.g., Raubenheimer et al. (1999)) with a spatially constant aquifer thickness D. The Boussinesq equations follows from the substitution of Darcy's Law into the continuity equation (Nielsen, 1990). Here, the Boussinesq equation is extended to include infiltration by wave run-up, as proposed by Nielsen et al. (1998) and Kang et al. (1994). The groundwater model assumes that the sand is homogeneous and isotropic, and that groundwater flow is essentially horizontal, which is common for sandy beaches (Raubenheimer et al., 1999). The cross-shore (x) and temporal (t) evolution of the water table height η (m) with respect to Mean Sea Level (MSL) is then

$$\frac{\partial \eta(x,t)}{\partial t} = \frac{K}{n_e}\frac{\partial}{\partial x}\{[D+\eta(x,t)]\frac{\partial \eta(x,t)}{\partial x}\} + \frac{U_l}{n_e} \tag{4.1}$$

where K is the hydraulic conductivity of the beach (m/s), n_e is the effective porosity (-), and U_l is the run-up infiltration flow rate (m/s). U_l can be written as (Nielsen et al., 1998; Brakenhoff et al., 2019)

$$U_l = \begin{cases} C_l K f(x), & \text{if } x_{cf} \leq x \leq x_{ru} \\ 0, & \text{otherwise} \end{cases} \tag{4.2}$$

where C_l is an infiltration coefficient (-) and $f(x)$ is a function of x (-). x_{cf} is the location where the depth of the water table equals the thickness of the capillary fringe, and x_{ru} is the maximum run-up location. Following Brakenhoff et al. (2019), we let $f(x)$ increase linearly from 0 at x_{cf} to 1 at x_{ru}. The typical thickness for the capillary fringe on a sandy beach is 0.1 to 0.2 m (Turner and Nielsen, 1997). The parametrization by Stockdon et al. (2006) was adopted to compute x_{ru}. Huizer et al. (2017) and Brakenhoff et al. (2019) mention the importance of wave run-up for accurately predicting $\eta(x,t)$ above the high-tide level, especially when waves are energetic.

Equation (4.1) was solved numerically, as described by Brakenhoff et al. (2019), with a centered finite difference method in space and a fourth-order Runge–Kutta integration technique in time. The seaward boundary condition is a moving shoreline at location $x_{sh}(t)$ with elevation $\eta_{sh}(t)$

$$\eta_{sh}(x_{sh},t) = \zeta_0(t) + \xi_{sh}(t) \tag{4.3}$$

It consists of the offshore water level $\zeta_0(t)$ and the wave set-up $\xi_{sh}(t)$, estimated with offshore wave data and the parametrization of Stockdon et al. (2006). The imposed landward boundary is $\partial\eta/\partial x = 0$. The beach profile must be monotonically increasing to apply Equation (4.1), meaning that intertidal sandbars and troughs cannot be present. This part of the model needs a spin up time of approximately a month to ensure that the predictions are no longer

affected by the model initialisation. The second part of the model determines the surface soil moisture of the beach. It is assumed that the moisture profile above the water table is in hydrostatic equilibrium, meaning that the rising and falling of the water table with time do not change the profile shape. The surface moisture thus responds immediately to changes in the groundwater level. These assumptions are discussed in, for example, Brakenhoff et al. (2019) and Smit et al. (2019), who argued that these assumptions are realistic unless the beach sand is rather fine (≈150 μm). By adopting the water retention curve by Van Genuchten (1980), the gravimetric surface moisture content w_s can be related to the groundwater depth h as

$$w_s = w_{res} + \frac{w_{sat} - w_{res}}{\left[1 + (\alpha|h|)^n\right]^{1-1/n}} \tag{4.4}$$

where w_{sat} is the saturated water content (-), w_{res} is the residual water content (-), and n is a measure of the pore-size distribution (-). α (m^{-1}) is related to the inverse of the air entry suction and affects the thickness of the capillary fringe.

The third module is based on the conceptual aeolian fetch model of Bauer and Davidson-Arnott (2002), as extended by Delgado-Fernandez (2011). Bauer and Davidson-Arnott (2002) proposed a parametrization of the increase in the aeolian transport rate q with downwind fetch distance F, with q the product of the potential transport rate q_p and a trigonometric function. According to Delgado-Fernandez (2010), the following function fits best with observations from agricultural fields

$$q(F) = min\left[q_p, q_p \times \sin\left(\frac{\pi}{2}\frac{F}{F_c}\right)\right] \tag{4.5}$$

In Delgado-Fernandez (2010), F_c depends positively on wind speed U as F_c = 4.38 U − 8.23, and the computed value of F_c is then modified based on w_s. In Delgado-Fernandez (2010), w_s and the F_c modification are spatially constant. If w_s is less than 4%, F_c remains unchanged. If w_s is between 4% and 6%, F_c increases with a factor 1.5, and if w_s is between 6 and 10%, F_c is 1.75 times as large compared to the dry-sand F_c. No transport is calculated if w_s is above 10%. In the Aeolus model, w_s varies in the cross-shore direction, which implies that F_c is spatially varying too. Therefore, Equation (4.5) was adapted into a spatially forward-stepping equation

$$q(i) = \begin{cases} min\left[q_p, q(i_1 - 1) + q_p \times \sin\left(\frac{\pi}{2}\frac{F(i)}{F_c(i)}\right)\right], & \text{if } w_s(i) \leq w_{s,max} \\ 0, & \text{otherwise} \end{cases} \tag{4.6}$$

where i are spatial indices. When the most seaward gridpoint has a value less than the threshold value $w_{s,max}$ set by the user, the computation of q starts. The remaining values for $w_s(x)$ are rounded to multiples of 0.5% (now referred to as w_s'). The fetch is the downwind distance over which the surface moisture is constant, starting one spatial gridpoint upwind of the most upwind gridpoint of a group of gridpoints with equal w_s'. This is indicated in Equation (4.5) with the $i_1 - 1$ index. i thus refers to all locations with constant w_s'. This approach causes F to reset to 0 with every change in w_s'. To avoid F resetting for even tiny changes in w_s, w_s was rounded to multiples of 0.5%.

The critical fetch in Aeolus is computed at each grid point as

$$F_c(i) = p(w_s') * [4.38U - 8.23] \tag{4.7}$$

Based on the work of Delgado-Fernandez and Davidson-Arnott (2011), p = 1 for $w_s' \leq 4\%$ and a 0.125 increase in p per 1% increase in moisture. q in Equation (4.6) is computed up and

including the transition from beach to dune, which occurs at elevation z_{up}, a user-specified value. We refer to q at z_{up} as the actual aeolian transport rate q_a.

The potential transport rate q_p (kg m^{-1} s^{-1}) is here computed following Hsu (1971) and Davidson-Arnott and Law (1996) as

$$q_p = 0.1 \times [-0.47 + 4.97 D_{mm}] \times 10^{-4} \left(\frac{\alpha_{Hsu} U}{\sqrt{g D_{cm}}} \right)^3 \tag{4.8}$$

where U is the time-averaged (over 10 to 60 min) wind velocity measured at a height of 2 to 10 m. As in Hsu (1974), the grain size has to be specified in mm for D_{mm} and cm for D_{cm} and $g = 981$ cm/s^2. The parameter α_{Hsu} relates U to the shear velocity U_* in cm/s can be determined with

$$\alpha_{Hsu} = \frac{100\kappa}{\log\left(\frac{z}{z_0}\right)} \tag{4.9}$$

where $\kappa = 0.41$ is Von Karman's constant, z is the height above the bed where the wind velocity is measured, and z_0 is the roughness length. Based on extensive measurements, Hsu (1974) proposed $\alpha_{Hsu} = 4$.

4.2.2 Observations

Field site

The study site is located south of Egmond aan Zee, the Netherlands (Figure 4.1). The straight coastline has an orientation of 7° east of north and consists of medium-fine sand with a median grain size of about 240 μm. The beach is exposed to waves from the southwest to the north (Wijnberg and Terwindt, 1995). The Dutch coast has a significant offshore wave period and height of 5 s and 1.2 m, respectively, which do not show strong alongshore differences. During storms, the significant offshore wave height can increase to over 5 m. Especially storms from the northwest are responsible for surges more than 1 m. As a result, the intertidal beach can be flooded for several days (Quartel et al., 2007). The mean wind speed is 5.8 m/s, based on wind data from 1981 to 2010 measured at de Kooy, 40 km north of the field site (Sluijter et al., 2011). During storms, U can attain values up to 30 m/s. The dominant wind direction at the site is south-southwest (210°–230° with respect to north).

The semi-diurnal tide ranges from 1.4 m (neap tide) to 1.8 m (spring tide) and affects the width of the beach, which usually varies between 30 and 100 m. The intertidal beach usually has one or two slipface bars (Masselink et al., 2006; Aagaard et al., 2005; Quartel and Grasmeijer, 2007). The high foredune (20 to 25 m) has a steep seaward front (40°–50°) due to occasional erosion events (de Winter et al., 2015). Large parts of the dune are covered in European marram grass (*Ammophila arenaria*), especially at heights exceeding 10 to 15 m above beach level. During prolonged periods of time without surges, embryo dunes can develop at the base of the foredune (Ruessink et al., 2019).

Video monitoring

The beach south of Egmond aan Zee was monitored with an Argus video system (van Enckevort and Ruessink, 2001) between April 1998 and October 2015. Argus is an optical remote sensing system pioneered by Holman and Sallenger (1986) for sampling the nearshore environment. An Argus system consists of a suite of cameras at the top of a high structure to gain an unhindered view of the beach. A timing module is installed to ensure a synchronized collection of the images (Holman and Stanley, 2007). The Argus system at Egmond aan Zee consisted of five RGB-color cameras, which were mounted on a 45-m high tower on the upper beach. The cameras provided an 180° view, from south-southwest to north-northeast

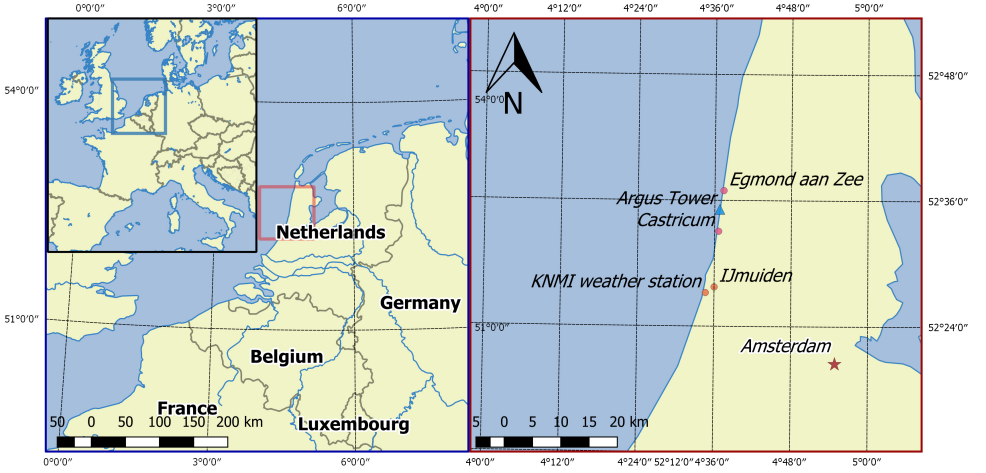

Figure 4.1: Map of the field site and weather station.

with a resolution of 640 × 480 pixels from 1998 to February 2004, 1024 × 768 pixels from 2004 to August 2005 and 1392 × 1040 pixels until 2015. Every 30 min, each camera produced three different oblique images: a snapshot, a time-exposure (timex) and a variance image. Only the first two types of images are used in this research. The timex images were created by images taken with a frequency of 2 Hz over a 10-min period. This procedure blurs out all movement in the 10-min time frame, such as individual waves breaking on the subtidal bars and aeolian streamers on the beach. The movement of streamers is thus best noticeable when a snapshot and timex of the same hour are compared: an active streamer can be seen on a snapshot image, but not on a timex image (Figure 4.2). This makes them stand out from immobile, small, irregular patches of dry sand that look like streamers on a snapshot image. Both snapshot and timex image can be used to determine the movement of aeolian bedforms called sand strips (Figure 4.2), but as sand strips move relatively slowly (a few meters per hour), subsequent hourly images must be studied to see their movement. The footprint dimensions of individual pixels (the projection of a square image pixel on the ground) give the theoretical accuracy of the images, which is close to rectangular (with the alongshore side being larger). For the post-2005 data, the cross-shore footprint dimension is less than 0.2 m, while the alongshore size increases from 0.2 m at 100 m from the tower alongshore to ≈1.5 m at 400 m.

For each day in October 2011 to March 2012, the Argus image that showed the strongest signs of aeolian sand transport was selected. The aeolian transport visible on the image was then classified according to Figure 4.3. A second classification used the strongest 10-min-averaged wind velocity of each day (Table 4.1), for which only daylight hours were used. The number of daylight hours is 11 h for October and March, 9 h for November and February, and 8 h for December and January. These hours were determined by observing the amount of light in Argus imagery.

Please note that the time intervals with the largest visual transport intensity is not necessarily the same as the moment with the largest wind speed. Additionally, wind directions (θ) are reported relative to shore normal in this Chapter, where $\theta = 0°$ is cross-shore and $\theta = 90°$ ($-90°$) alongshore from the north (south). The wind data were measured by the Royal Netherlands Meteorological Institute (KNMI) in IJmuiden, roughly 15 km south of the field site (Figure 4.1).

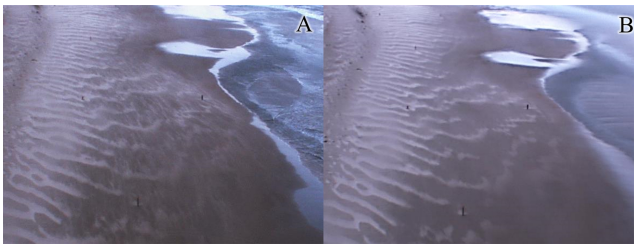

Figure 4.2: An example of (**A**) a snapshot image and (**B**) a timex image. Streamers are visible on the snapshot image (especially between sand strips), as a timex image blurs them out and shows the dark, moist sand instead. Sand strips, on the other hand, move so slowly that they appear almost the same in both images. The regional hourly mean wind velocity $U_{regional}$ was 8 m/s and the wind direction θ was -97°.

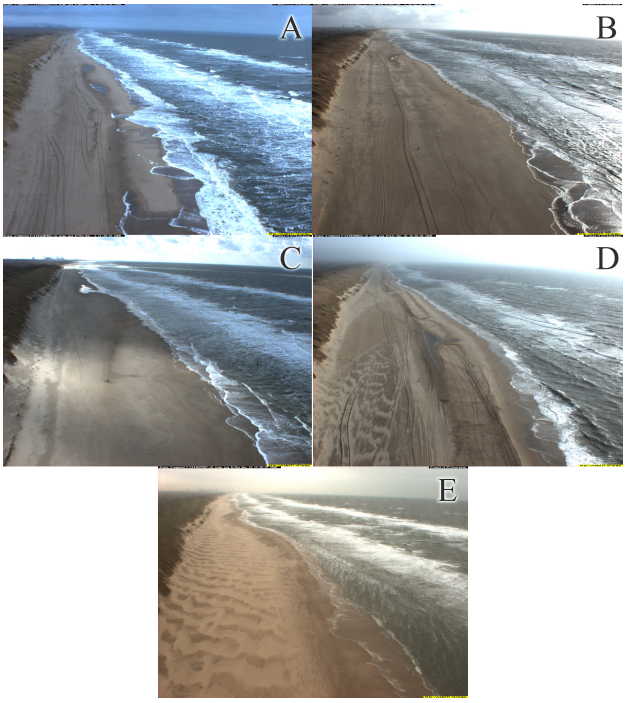

Figure 4.3: Snapshot images classified according to their visual signs of aeolian activity. (**A**) Class 0 shows no signs of transport; (**B**) class 1 shows very small signs of transport, like single moving patches of sand or a handful of streamers; (**C**) class 2 has more of these sand patches, but they have not formed rows of sand strips; (**D**) class 3 does have rows of sand strips, but the area they cover is patchy; and (**E**) class 4 features sand strips that cover most of the beach, often in combination with strong streamer activity. The date of the image and wind conditions were: (**A**) 08-02-2006, $U = 7$ m/s, $\theta = 23°$; (**B**) 05-03-2006, $U = 8$ m/s, $\theta = 23°$; (**C**) 02-03-2006, $U = 9$ m/s, $\theta = -17°$; (**D**) 25-03-2006, $U = 10$ m/s, $\theta = -47°$; (**E**) 10-11-2005, $U = 12$ m/s, $\theta = -57°$.

Table 4.1: Wind classes. The classification is based on the strongest hourly mean wind velocity measured regionally during daylight hours.

Wind Class	Wind Velocity (m/s)
1	<8.5
2	8.5–10.5
3	10.5–13.5
4	≥13.5

4.2.3 Model set-up

The model has been set up to fit the conditions found at Egmond aan Zee (Table 4.2). The chosen hydraulic conductivity K and infiltration coefficient C_l were obtained by minimizing the error between modelled groundwater values and observations at 5 cross-shore locations collected at the study site in October 2017 (Tuijnman, 2019; Smit, 2019). The settings for the Van Genuchten curve are taken from Smit et al. (2019) and are also based on Egmond observations. The applied cross-shore profile is given in Figure 4.4. It is nearly planar with a 1:55 slope. The bed profile was made by averaging three beach profiles that crossed or were near the study site. The profiles were taken from the JARKUS dataset, annual bathymetrical and topographical measurements that provide cross-shore beach profiles along the entire Dutch coast at an interval of 200 to 250 m. For this study, the profiles closest to our study site (# 41.250, 41.500, and 41.750) measured in January 2012 have been used. The resulting alongshore-averaged bed profile, which runs from -3 m to almost +4 m with respect to MSL, was smoothed to create a monotonically increasing profile. The smoothed profile was extended with $z = 4$ m for another $\approx$150 m, where we expect oscillations in η to have dampened completely. Finally, offshore wave heights and periods, as well as water levels were measured near the harbor of IJmuiden at ten-minute intervals. The wave conditions were used to compute wave set-up and the run-up location x_{ru} in Equation (4.2).

The regional wind velocity U are available with a 10-min resolution. The anemometer sits at a height of 10 m above ground level. The wind must surpass a certain threshold to start sand entrainment. This was found to be $\approx$8 m/s for the study site, based on visual observations (Chapter 2). However, this study used regional wind data, and according to a field campaign at the study site in 2017, the local wind (i.e., on the beach) is often weaker than the regional one because of the presence of the high foredune with a steep seaward side. Ruessink et al. (2018b) and de Winter et al. (2020) illustrated with detailed wind measurements at the study site that the regional (IJmuiden) wind speed generally overestimates local wind speed, especially when the wind is blowing onshore. Here, we adapt the wind direction (θ) dependent correction factors proposed by Ruessink et al. (2018b) to translate regional into local wind speeds and use these local wind speeds to calculate the critical fetch and the potential transport. The ratio of regional to local wind is smallest at $\approx$0.60 for onshore winds and increases to $\approx$1 for alongshore wind (Figure 4.5). The data also showed that the airflow over local topography could lead to differences between regional and local wind directions close to the dune toe, as was also found by Bauer et al. (2012). This difference is almost non-existent for the wind direction on the beach at this site. However, it has been observed that sand strips on the beach (especially when close to the dunes) can migrate in a different direction than the regional wind under almost alongshore to oblique winds (Chapter 2), which indicates some wind deflection and steering.

The fetch model of Aeolus can only be run for aeolian transport towards the foredune, meaning that any aeolian transport in the alongshore or offshore directions are set to zero. Sand transport with offshore winds is rare at Egmond aan Zee, and when it happens, only

Table 4.2: Used settings for the Aeolus model to represent the Egmond beach.

Spatial and temporal settings	
Start (dd-mm-yyyy)	01-10-2011
End (dd-mm-yyyy)	31-03-2012
Model output time step Δt	10 min
Spatial grid size Δx	0.5 m
Groundwater settings	
Calculation time step Δt_{gw}	2 s
Grid size	0.5 m
Aquifer depth D	11 m
Hydraulic conductivity K	4.63×10^{-4} m/s
Effective porosity n_e	0.3
Infiltration coefficient C_l	0.5
Minimum water table depth in run-up infiltration	0.2 m
Settings Van Genuchten curve	
Saturated water content w_{sat}	20.51 %
Residual water content w_{res}	2.92 %
α	$5.59\ \mathrm{m}^{-1}$
n	3.69
Aeolian transport settings	
α_{Hsu}	4
Grain size D_{50}	240×10^{-6} m
Maximum surface moisture content $w_{s,max}$	10%
Dunefoot elevation z_{up}	2.5 m
Minimum regional wind speed at which transport is possible U_{min}	8 m/s

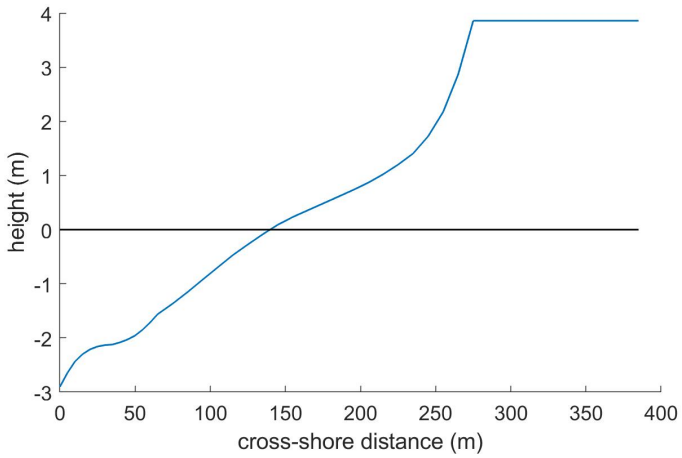

Figure 4.4: Smoothed Jarkus profile.

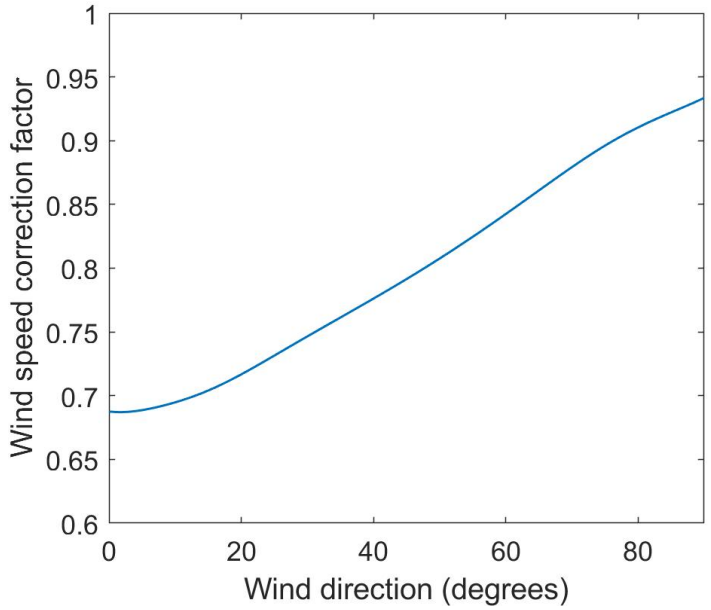

Figure 4.5: The correction factor needed when computing the local from regional wind velocities as a direction of regional wind direction. 0° is cross-shore (onshore).

small visual amounts of aeolian transport are visible (Chapter 3). (Nearly) alongshore winds with a slight offshore direction, however, are responsible for the strongest visual signs of aeolian transport (Bauer et al., 2012; Chapter 2). Therefore, alongshore winds between (-)90° and (-)100° (with 0° being cross-shore) were set to (-)90° to include these alongshore winds in the calculations. This filter was not applied to the Argus imagery, as we were interested in the occurrence of sand transport under offshore winds and, therefore, when the wind direction is limiting the model. The cosine effect (Davidson-Arnott and Dawson, 2001; Bauer and Davidson-Arnott, 2002; Delgado-Fernandez, 2010) is not included, as the focus of this study is on the timing of days with aeolian transport, not the amount of sand that will be deposited at the dune foot. The dune foot elevation z_{up} was set to 2.5 m, which is based on the beach profile at Egmond aan Zee (Figure 4.4). This is a little larger than the 2% exceedance value of the wave run-up maxima at the field site, which was 2.23 m in the studied period.

4.2.4 Synthetic runs

Several synthetic simulations were run to illustrate the output of the model and to aid in the interpretation of the Egmond simulations. We focus here on moisture and, in particular, aeolian transport rates, as output from the groundwater model has already been discussed extensively in Brakenhoff et al. (2019) and Smit et al. (2019). The imposed conditions were a semi-diurnal tide of 12 h and 25 min with an amplitude of 1.5 m and a wave period and height of 5 s and 1.2 m, respectively. The regional wind direction θ varied from 0° to $\pm$90° (with 0° being onshore) with a 15° step size and the regional wind speed was varied from 8 to 23 m/s with intervals of 5 m/s for each direction. To mimic the Egmond situation, the regional wind speed was transformed to the local wind. All other variables and parameters

were set to fit the Egmond site (see Section 4.2.3). Each simulation was run for 30 days to account for the model's spin up time. The results below focus on the 30th day.

Figure 4.6 shows the output of the surface moisture model. The upper part of the intertidal zone (between 220 and 240 m) slowly dries during low tide, and inundates quickly with rising tide. Please note that most of the intertidal beach remains too wet to sustain aeolian transport ($w_s > 10\%$). Figure 4.7 shows nine examples of the synthetic runs, displaying the actual transport rate q_a at z_{up} = 2.5 m (at $x \approx 260$ m in Figure 4.6), the potential transport rate q_p based on Hsu (1974), and the imposed offshore tide. Obviously, q_p does not depend on time, but because of the imposed wind speed correction it does depend on θ. In contrast, q_a can vary with time, as it does, for example, when $\theta = 15^\circ$ and $U_{regional}$ = 18 or 23 m/s (Figure 4.7A). The largest values for q_a were not reached at low tide when the beach is at its widest, but approximately 2 h before high tide, when the surface moisture at the upper intertidal zone is smallest, hence providing the largest surface of dry sand (Figure 4.6). The groundwater level keeps on falling until the beach is inundated by the tide. The groundwater level and surface moisture content at high tide (time = 3:21 h in Figure 4.7) and low tide (time = 9:36 h in Figure 4.7) are shown in Figure 4.8A and B, respectively. The groundwater level is close to the bed for most parts of the intertidal beach during the tidal cycle and the surface moisture always keeps its maximum value, w_{sat}. Only around x= 240 m, the surface moisture drops below 10% to allow aeolian transport during certain parts of the tide. Qualitatively, this is consistent with suggestions in Brakenhoff et al. (2019) and Schmutz et al. (2019) that the contribution of the intertidal zone as a sand source for aeolian transport is limited.
In general, q_a is less than q_p for $\theta = 15^\circ$, except for the smallest wind velocity $U_{regional}$ = 13 m/s. Then, q_a is smaller than q_p during high tide only (Figure 4.7A). The larger the wind velocity, the larger the difference between q_a and q_p. Similar results can also be seen for $\theta = 45^\circ$ (Figure 4.7B), but not when $\theta = 75^\circ$ (Figure 4.7C). Now, $q_a = q_p$ in all simulations. This (lack of) difference between q_a and q_p is further illustrated in Figure 4.9. Both q_a and q_p, averaged for a single tide, increase when the wind becomes more alongshore, and the wind speed increases. For q_p (Figure 4.9A), the difference with θ is caused by the wind speed correction while for q_a, θ also affects the maximum fetch. When the angle of the wind is almost alongshore, the critical fetch length F_c is reached and exceeded even at high tide, which causes q_a and q_p to be the same. Little to no potential and actual transport can be expected for small wind velocities no matter the direction. Figure 4.9C shows the standard deviation in q_a. A zero standard deviation implies q_a does not vary with the tide. This happens when the wind is (almost) alongshore. The critical fetch is then reached during the entire tidal cycle. With oblique winds, the maximum fetch length varies greatly, allowing the critical fetch to be (almost) reached only during low tide. This results in the largest standard deviations. With cross-shore winds, the maximum fetch length still varies, but it will do so less than for oblique winds, and, consequently, the standard deviation reduces again.

4.3 Results

The most common regional wind speed during the studied time period from October 2011 to March 2012 was around 5 m/s (Figure 4.10a), while the average regional wind speed was 6.6 m/s. The largest wind speed encountered was 24 m/s. The dominant wind direction was south-west, followed by nearly westerly winds (Figure 4.10b). Westerly winds also showed a relatively large percentage of strong winds (>13.5 m/s).

Table 4.3 displays the number of days with transport sorted according to their largest 10-min-averaged wind velocity measured during daylight hours and their strongest visual signs of transport. A few days (November 10, 17, and 21) could not be studied as fog obscured the beach during the entire day. Most of the 183 days show either no (class 0, 126 days) or

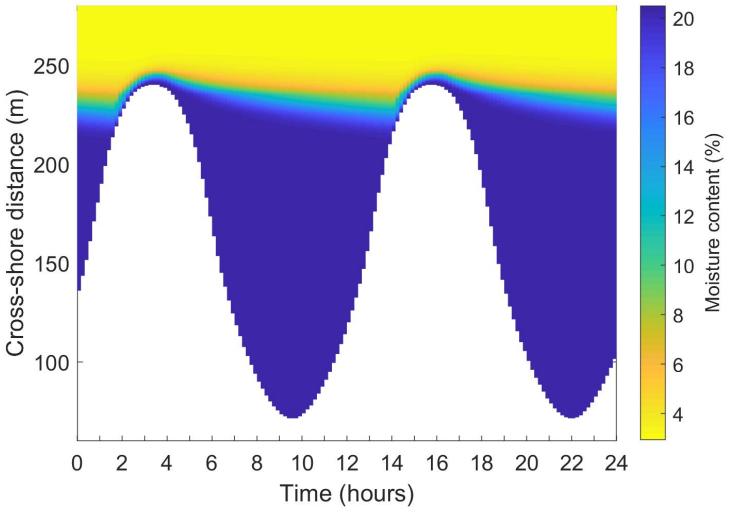

Figure 4.6: Surface moisture model output for a 12.5 h tide with an amplitude of 1.5 m, a wave height of 1.2 m, a wave period of 5 s, and using the parameters and bed profile for Egmond aan Zee. The figure depicts the model output for day 30 of the studied time period. The cross-shore distance runs from the sea (**bottom** of the figure) to the dunes (**top** of figure).

Table 4.3: Days sorted according to their wind class (Table 4.1) and visual transport class (Figure 4.3), with the total number of days for each class and the corresponding percentage.

	Visual Transport Class						
Wind Class	0	1	2	3	4	Total	Percentage
1	84	1	1	1	0	87	47.5%
2	20	4	4	1	10	39	21.3%
3	15	5	1	3	5	29	15.8%
4	7	4	1	3	13	28	15.3%
Total	126	14	7	8	28	183	
Percentage	68.8%	7.7%	3.8%	4.4%	15.3%		

substantial visual signs (class 4, 28 days) of aeolian transport. According to Chapter 3, strong winds but no or limited transport indicate supply-limited conditions at the beach. How large the wind speed has to be for limited transport depends on the strength of the visual aeolian transport; a transport day with no visual sign of transport is considered limited when the wind speed is above the threshold of transport ($\approx$8 m/s for Egmond aan Zee). The wind speed must be larger when stronger visual signs are present. That means that all days of visual transport class 0 in Table 4.3, many of visual transport class 1, and some of visual transport class 2 and 3 are probably limited.

Figure 4.11A shows the hourly average predicted potential and actual transport during daylight hours, together with the strongest visual classification of Argus imagery of the corresponding day. The corresponding wind direction and velocity is shown in Figure 4.11B. Visual signs of aeolian transport were especially common in the end of November and in

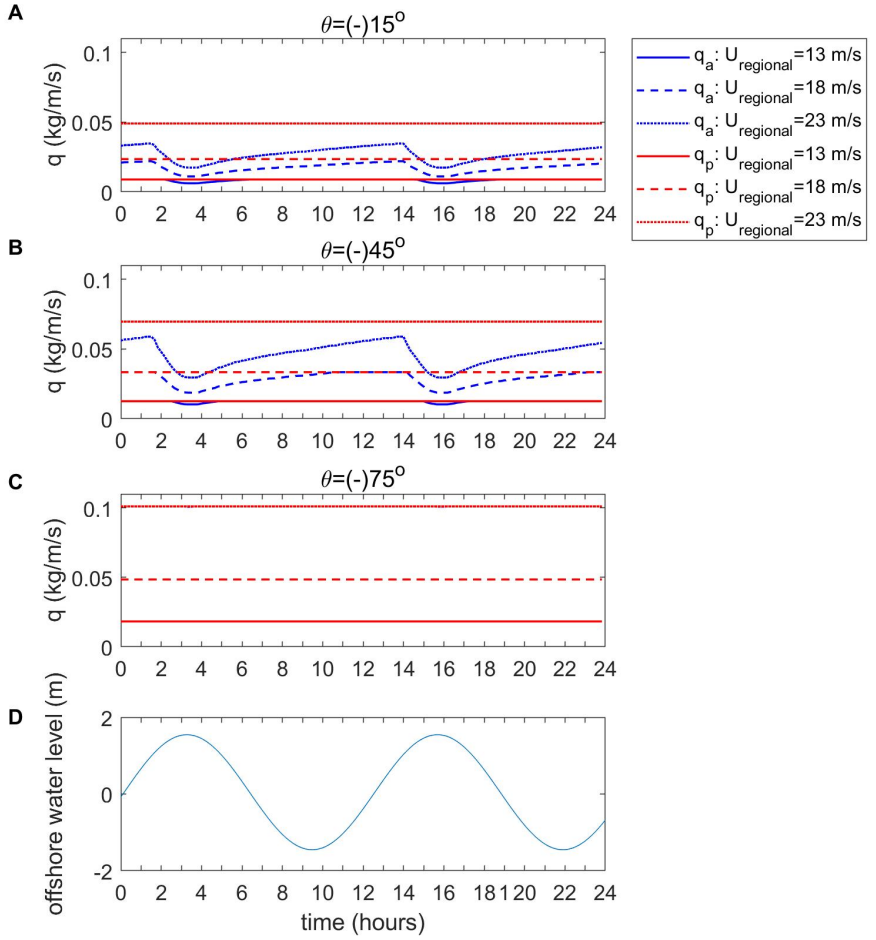

Figure 4.7: Aeolian transport rate q_a as calculated by Aeolus and the potential transport rate q_p based on wind velocity alone at $x \approx 260$ m ($z_{up} = 2.5$ m) for (**A**) $\theta = 15°$, (**B**) $\theta = 45°$, and (**C**) $\theta = 75°$. This transport does not take the cosine effect into account. (**D**) shows the tide for reference.

December 2011, during which the wind was relatively strong. March 2012, in contrast, had weak winds and contained only a few Argus images with visual transport. Offshore winds usually do not create aeolian bedform, which was the case for most days in November. This corresponds qualitatively with the model predictions, which are largest during the second half of November and December. The day with the largest average predicted potential and predicted actual transport is 3 January 2012, reaching 265.4 and 251.2 kg/m/h, respectively. The intensity of the visual signs of aeolian transport on the Argus images generally corresponds with the amount of predicted actual transport, with a stronger visual class generally having a larger predicted actual transport. There are, however, several days (e.g., October

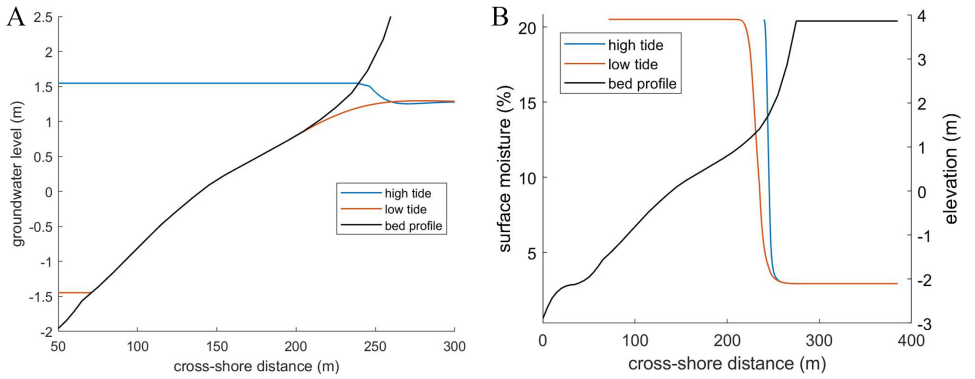

Figure 4.8: (**A**) Groundwater level during high and low tide and (**B**) surface moisture during high and low tide modelled by Aeolus.

Table 4.4: Mean q_a/q_p for the days from Table 4.3. When there is no number, there either are no days that fall within this wind and visual transport class or q_a and q_p are zero. The numbers between parentheses show the number of days where q_a and q_p are non-zero and the total number of days in that class.

	Visual Transport Class				
Wind Class	0	1	2	3	4
1	1.00 (2 out of 84)	- (0 out of 1)	- (0 out of 1)	- (0 out of 1)	- (0 out of 0)
2	0.94 (11 out of 20)	0.99 (3 out of 4)	0.98 (4 out of 4)	- (0 out of 1)	1.00 (10 out of 10)
3	0.77 (10 out of 15)	0.91 (5 out of 5)	0.91 (1 out of 1)	0.98 (3 out of 3)	1.00 (5 out of 5)
4	0.46 (6 out of 7)	0.76 (4 out of 4)	0.88 (1 out of 1)	0.98 (3 out of 3)	0.98 (13 out of 13)

5, 6, 7, and 12, 2011), for which q_a was predicted to be relatively large (≈50 kg/m/h, which was almost the same as q_a on those days), but Argus showed minimal signs of aeolian activity (class 1). The other way around, with small q_a (≈10 kg/m/h), but strong visual signs of transport (class 4), happened occasionally too (e.g., October 21, 26, and 30).

On 30 of the total 183 days the model predictions and Argus observations did not agree in the sense that Argus showed no transport but q_a was non-zero. These mismatches tend to occur on days with little transport, as on 27 days the potential transport was less than 10% of the maximum predicted potential transport. This may imply that small transport rates are not well visible, and are thus incorrectly classified as transport class 0. On 5 days, visual signs of transport were present, but the model predicted zero q_a. These mismatches will be examined further in the Discussion section of this chapter.

The ratio of q_a/q_p depends on the wind speed and direction. The wind rose in Figure 4.12a is based on wind data with $q_a/q_p < 0.8$ and in Figure 4.12b with $q_a/q_p \geq 0.8$. When q_a/q_p <0.80, the wind is mostly strong and predominantly onshore directed. This wind direction is the most common for visual transport class 0 with wind class 3 and 4. Alongshore winds, on the other hand, are almost completely absent in this wind rose. The situation

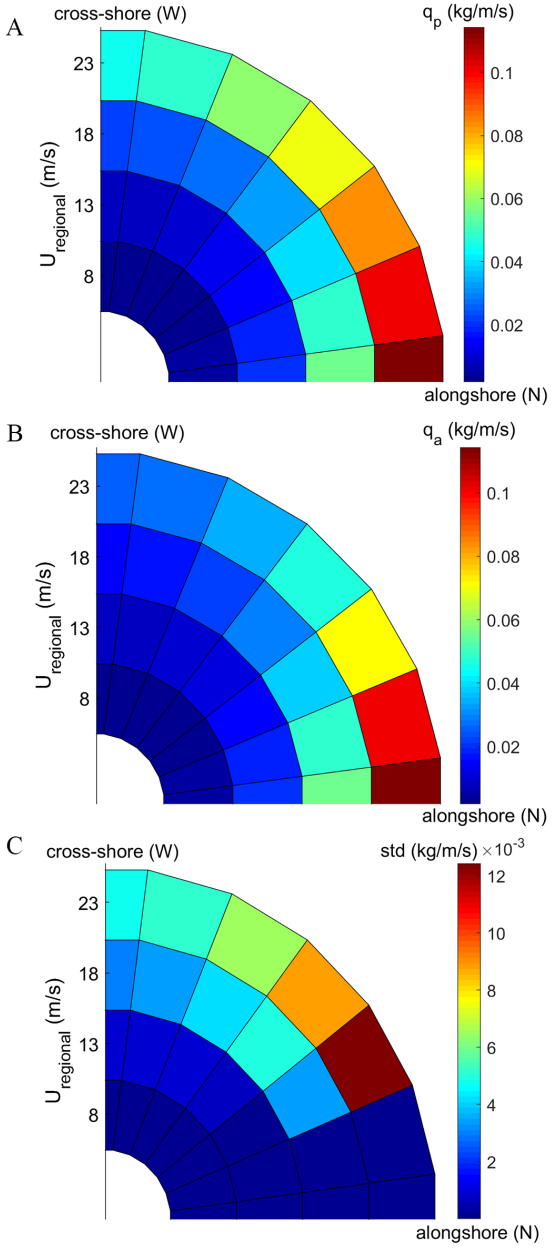

Figure 4.9: (**A**) Mean potential aeolian transport rate q_p for various wind velocities and directions, (**B**) mean actual aeolian transport rate q_a, and (**C**) the standard deviation in q_a, calculated for a single tide and various wind velocities and directions. There are 4 values for the regional wind velocity, which increase from inner to outer ring, and 7 different wind directions.

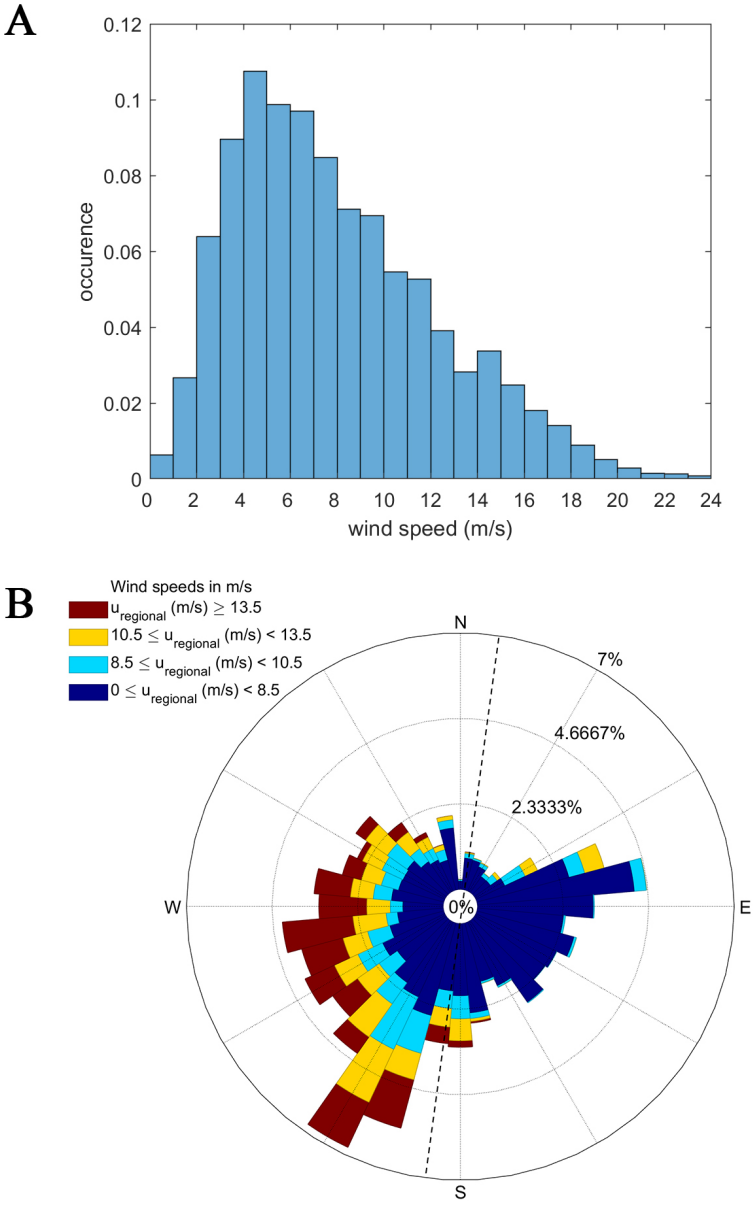

Figure 4.10: (**a**) Histogram of the wind speed and (**b**) a windrose showing the direction and speed of the wind at the KNMI weather station in IJmuiden from October 2011 to March 2012. The coastline has an approximate north-south orientation.

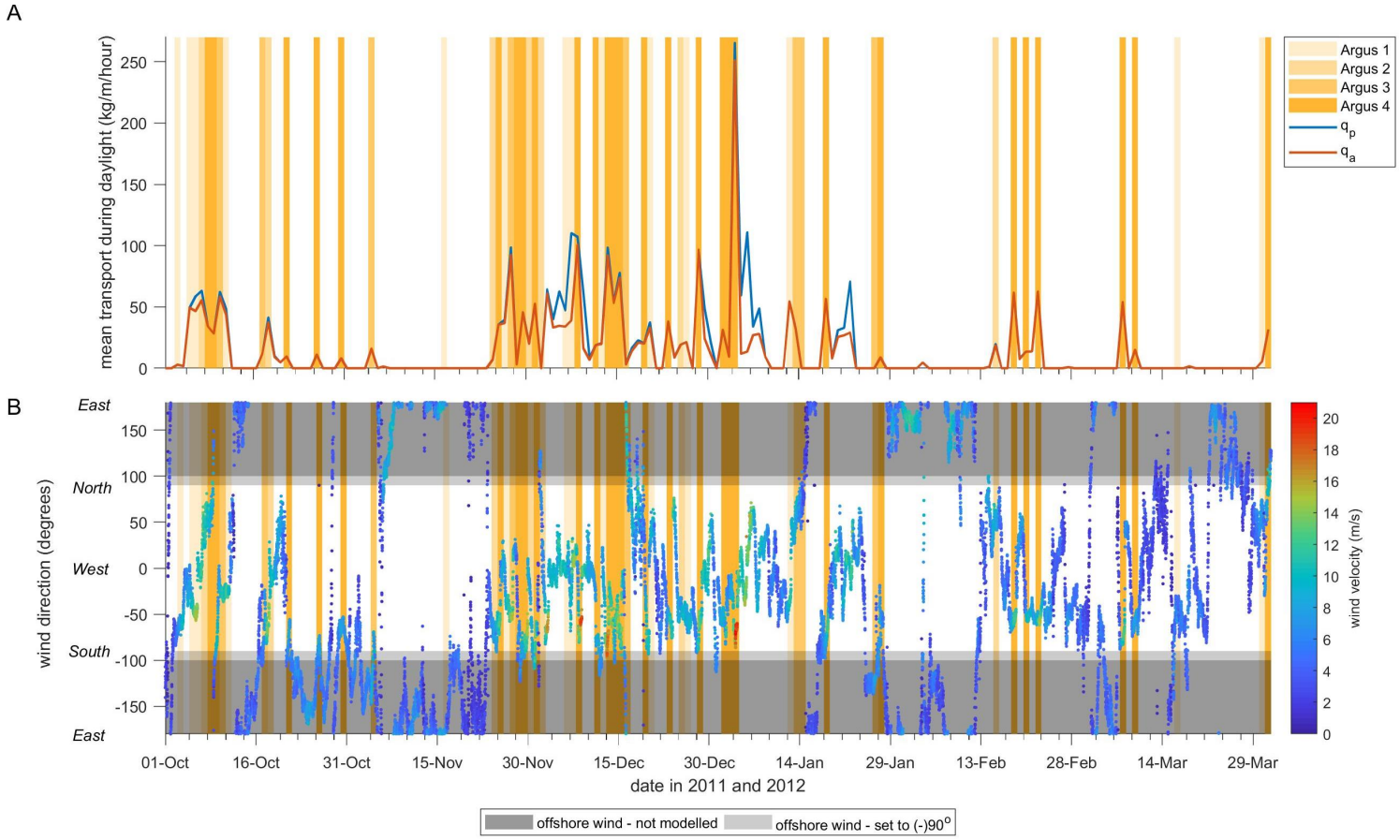

Figure 4.11: (**A**) Time series of predicted hourly average potential and actual transport (daylight hours only) and the strongest observed visual transport for each day. (**B**) the corresponding wind direction and velocity. Aeolus cannot model offshore wind. Winds that were offshore, but nearly alongshore (with θ between (-)90° and (-)100°) were set to θ = (-)90°.

with q_a/q_p $\geq$0.80 corresponds to winds with a predominantly alongshore direction. The few days when the wind blew onshore (from the west), the wind velocity generally did not exceed 12 m/s. Relatively small wind velocities ($<$9.5 m/s) are more common here than in Figure 4.12a. These findings are largely consistent with the results from the synthetic runs. It also corresponds to the findings in Chapter 3. The wind direction is important during large wind speeds; only under alongshore winds the fetch length will be long enough for unlimited transport.

4.4 Discussion

4.4.1 Model performance

The dataset from October 2011 to March 2012 of the Argus video monitoring station at Egmond aan Zee was classified according to their visual signs of aeolian transport days. Their timing and class were compared with the aeolian transport rates predicted by the Aeolus model. The visual signs of aeolian transport on the Argus images coincided well with Aeolus for most days (148 out of 183). The model gave limited transport rates (i.e., when q_a/q_p is $<$0.80 in this research) for winds with a predominantly cross-shore direction and larger wind velocities ($\geq$13 m/s). This is qualitatively consistent with other narrow beach studies (Bauer and Davidson-Arnott, 2002; Delgado-Fernandez and Davidson-Arnott, 2011).

On 30 days Aeolus predicted non-zero transport rates while no transport was visible on the Argus imagery. For most (27) of these days, average transport rates were predicted to be small ($<$25 kg/m/h using daylight hours only), and it is possible that these small rates leave no visual signature on the Argus imagery. Five of the 27 days showed signs of rain or snow, or had very low temperatures (presumably causing a frozen beach), which may have prevented aeolian transport. The Aeolus model does not incorporate these limiting factors. The present results suggest it may be worthwhile to include these meteorological variables to filter out the days of zero transport, in a similar fashion as in Delgado-Fernandez (2011).

There were 3 periods in the dataset when Argus imagery showed no sign of aeolian transport while Aeolus predicted relatively strong transport rates ($\geq$25 kg/m/h). In all these cases, the Argus images were difficult to interpret, and it is thus possible that these classes 0 were incorrectly classified as such. On the first of these periods, December 3 to 5, 2011, the imagery showed contrast between dark, wet sand, and light, dry sand that grew in area. This was interpreted as drying of the sand, and therefore a visual transport class 0, but it could have been caused by transported sand too. Furthermore, it was raining, which might have hindered the development of sand strips. The second period, January 6 and 7, 2012, might have signs of transport next to a small scarp in the dunefront, but again, the Argus images were difficult to interpret. The third period, January 20 to 22, 2012, suffers from Argus images taken under relatively bad light conditions, which makes it hard to discern small traces of transport.

Five days showed visual transport while the Aeolus model predicted zero q_a. For two of these days, 2 December 2012, and 16 March 2012, the Argus imagery might have been classified incorrectly as their interpretation was difficult. The situation on 16 November 2011 was classified as visual transport class 1, showing only a few visual traces of aeolian transport. Overall, we do not consider this mismatch to be a large error, as the difference between no and little transport here is small. The images of 14 January 2012 on the other hand, showed a medium strong visual sign of transport (class 3), even though the wind velocity did not exceed the threshold of motion. The period of visual aeolian transport lasted no more than an hour. The wind causing it might have been too local to be registered by the weather station in IJmuiden, and therefore resulted in a q_a of zero. Also, wind gusts above the threshold may have caused some transport, but gustiness is not included in Aeolus. The images of 26 January

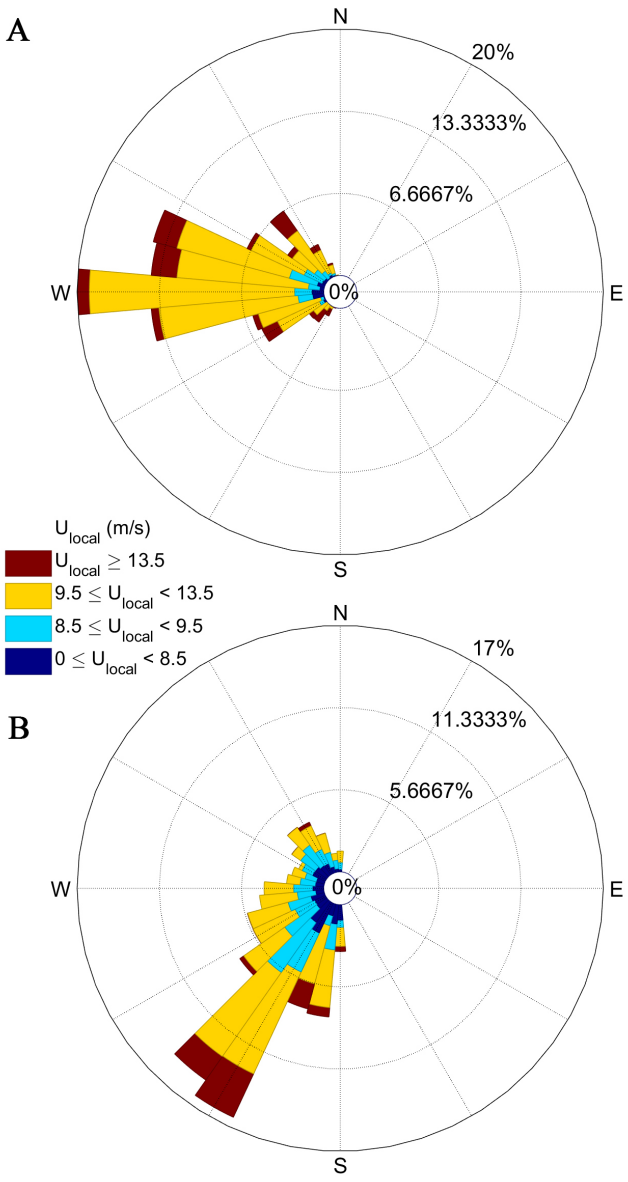

Figure 4.12: (**a**) Wind rose consisting of transport when q_a/q_p <0.80 and (**b**) when q_a/q_p ≥0.80.

2012 showed strong signs of transport (class 4). The wind direction was larger than 100° for most of the day, meaning its transport rate was set to zero by Aeolus. On this day, the days when the wind direction was less than 100°, the wind velocity was below the threshold of motion. This case shows that the threshold of 100° might not have been large enough to include all days that cause alongshore aeolian transport. Offshore winds that have a more cross-shore direction usually do not cause visible signs of aeolian transport at the Egmond study site, which makes Aeolus work reasonably well for this site. This might not be the case for other beaches, where studying and modelling aeolian transport events by offshore events, as was done by Jackson et al. (2011) and Delgado-Fernandez et al. (2013), is far more essential. Overall, most Argus-Aeolus mismatches are thus induced by poor classification of Argus imagery, where the visual signs of aeolian transport are too small to be observed properly. For a few cases, precipitation and frost could be the cause of a mismatch. Exceeding the wind direction threshold was the cause of a mismatch for one day.

Finally, we note that the days with strong signs of aeolian transport did not always coincide with large predicted transport rates (Figure 4.11). Underdeveloped or no sand strips (class 0, 1, and 2), however, do seem to be more common when q_a differs strongly from q_p, which can be seen for October 5 and 6, December 5 to 7, January 4 to 7, and January 20 to 22. The development of sand strips might be hindered by a moist surface or a short fetch during these days, meaning that well-developed signs of aeolian transport are more likely to appear on days with unhindered sand transport, not necessarily on days with large potential transport rates.

4.4.2 Relevance of days with limited transport

Although, as indicated in Table 4.4, the ratio of q_a to q_p is often large, the days when q_a is well below q_p do have a large influence on the cumulative transport in the study period. This is further illustrated with Figure 4.13. The total q_p and q_a from October 2011 to March 2012 (including night hours) is 6.6×10^4 kg/m and 5.2×10^4 kg/m, respectively. The amount of sand that reaches the dune foot (implementing the cosine effect) is 3.7×10^4 kg/m and 2.7×10^4 kg/m for q_p and q_a, respectively. This amount is larger than observed (see also de Winter et al. (2020)), as the dune volume at this site increases with 2.3×10^4 kg/m/year during accretion periods (Donker et al., 2018). An interesting future step is to calculate aeolian transport rates in supply-limited conditions, like the AeoLis model developed by Hoonhout and Vries (2016).

Both q_a and q_p follow a comparable cumulative trend, but their difference does not increase gradually with time. Instead, only a few individual days seem to invoke sudden, substantial differences (e.g., 5 to 9 December 2011 and 3 January 2012). It is interesting to note that only parts of these days had limited transport. During the days in December, the wind was strong (>11 m/s) and fluctuated in direction. When it was (close to) cross-shore, it caused limited transport. January 3 started with very strong winds of ≈20 m/s. Since these winds were shore-oblique, the fetch length was close to the critical fetch length, causing q_a/q_p to fluctuate between 1.00 (low tide) and 0.80 (high tide). Only when the wind changed to a more cross-shore direction at the end of the day, q_a/q_p dropped to 0.45. This further stresses that the limitation in only a few days with large potential transport may have a profound effect on long-term aeolian transport. Future work is needed to test the generality of this finding, including in-depth analyses of these complex events and the possibility of increasing the temporal resolution of visual transport classifications from daily to hourly.

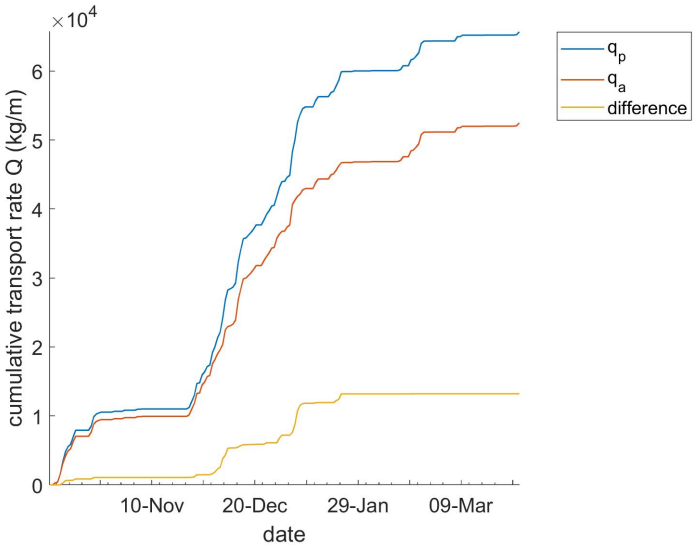

Figure 4.13: Cumulative sum of Q_a and Q_p, and their difference.

4.5 Conclusions

The Aeolus model was developed to make better predictions of aeolian sand transport rates on narrow beaches by including wind- and moisture-induced fetch effects. To test if the model predicts the timing and transport-limited nature of aeolian transport events correctly, its results were compared to Argus images collected during a six-month winter period at Egmond aan Zee (the Netherlands). The medium to strong transport events predicted by Aeolus usually coincided with strong visual signs of aeolian transport in the images. Consistent with visual signs of limited transport, Aeolus sometimes predicted the actual transport to be smaller than the potential transport. Strong differences are more common for strong and onshore winds. Furthermore, it was observed that strong visual signs of aeolian transport overlapped with either equal actual and potential transport (i.e., no limitation), or when the actual transport was relatively large. Mismatched days usually had no visual sign of aeolian transport on the corresponding Argus images and only small transport rates predicted by Aeolus. It is possible that these aeolian transports are too small to be seen on Argus, or that a limiting factor not taken into account by Aeolus, like rain or snow, was enough to end this small amount of aeolian transport. This semi-quantitative research shows that overall, the Aeolus model predicts the timing of sand transport well for a long, multiple-month time period.

Chapter 5

Synthesis

Foredune growth predictions based on aeolian transport equations (Bagnold, 1941) often overestimate observed growth rates (Delgado-Fernandez, 2011; Keijsers et al., 2014) over longer time scales (months to years), especially on narrow beaches. This transport contributes to the growth of dunes, which provide protection against marine flooding and contributes to a diverse ecosystem in the dunes landward of the foredune. Therefore, the main aim of this thesis was to better understand the timing of aeolian transport on a narrow beach, and to identify and elucidate key factors that determine this timing, with a focus on timescales from months to years. To do this, three research questions were defined. A key dataset was collected by Argus, a coastal video monitoring system, which contains high resolution images and spanned a period of multiple years. Aeolian transport often results in sand strips, common bedforms in wet aeolian systems, and streamers, which can be seen on the Argus imagery. Characteristics of sand strips have been studied to understand their dependency on wind direction and velocity (Chapter 2). Subsequently, video monitoring has been used to find moments of limited and unlimited transport in order to investigate how limiting factors influence transport on a timescale of years (Chapter 3). Lastly, a newly developed aeolian sediment transport model, Aeolus, has been qualitatively tested with the use of coastal video imagery (Chapter 4). Below, the findings in Chapters 2 to 4 are summarised and discussed, and suggestions for future research are provided.

5.1 Main findings

Many factors, including moisture content, algae and salt crusts, and lag deposits hinder aeolian transport and imply that a rather long critical distance in the downwind direction is needed before the aeolian transport reaches its maximum (potential) value. However, as the beach at Egmond aan Zee, the study site of this research, is narrow (<100 m), it is expected that this distance is not always reached. Therefore, the maximum available distance (fetch) strongly influences the answers of the research questions. Potential aeolian sand transport can only be reached when the fetch is longer than the critical distance, in other words, when the wind direction is (almost) alongshore. Under cross-shore winds, the available fetch may be too low and the aeolian sand transport potential is thus never reached. This can explain a significant part of the mismatch between predicted aeolian transport rates and measured deposition on the foredune. Stronger winds cause a higher potential transport, but also need a longer fetch, which means the wind direction has an even larger impact.

1. *What are the physical characteristics of sand strips on a narrow beach under a wide range of wind conditions?*

This question, answered in Chapter 2, required Argus images with well-developed sand strips. Images were selected based on wind velocity, as sand is not transported during low wind velocities. This threshold was determined by inspecting all Argus images taken from October 2011 to March 2012. In these images, signs of aeolian sediment transport start to appear at (regional) wind velocities of 7 to 8 m/s. A wind velocity of 8 m/s was therefore used as a threshold to filter Argus images taken between 2005 and 2012. Additionally, these events had to last at least 3 hours to be considered significant. From these events, only the days with well-developed sand strips were chosen, from which an area with sand strips was cropped to quantify their wavelength and migration speed. The image was rotated before cropping to make the migration direction of the sand strips parallel to the upper/lower boundary of the cropped area. Each horizontal pixel row was then used for correlation computations; auto-correlation was used to find the wavelength, and cross-correlation was used to find their migration velocity, using two subsequent hourly images.

During the selection procedures, it was observed that sand strips develop faster under strong winds. They often start out as small patches of sand that grow wider and broader until they form sand strips, but they can also reactivate from old sand strips. The development time can take several hours or be below one hour. The direction of the wind plays a critical role in their development as well. Cross-shore winds cause sand strips to remain underdeveloped or not to develop at all, while alongshore winds result in well-developed sand strips, even at low wind velocities just above the threshold of motion. When the selection was completed, it was found that well-developed sand strips on Egmond beach have an average wavelength of 12.0 m and an average migration velocity of 1.24 m/hour, with a standard deviation of 2.8 m and 0.78 m/h, respectively. The wavelength and migration velocity depend only weakly on the wind velocity ($r = 0.38$ and 0.35, respectively).

2. *How do transport limiting factors affect aeolian sand transport on long time scales at a narrow beach?*

Strong winds do not always cause large aeolian transport rates, which means the transport is less than the potential rate. This is called limited transport in this thesis. Chapter 3 studies the transport-limiting factors by finding days with limited and unlimited transport. The first step in selecting these days was finding moments of potential transport first, where the maximum, hourly mean wind velocity of a day exceeds the threshold velocity for transport found in Chapter 2. The Argus images corresponding to the moments of potential transport were classified according to the developmental stage of the sand strips. Class 0 shows no transport, while class 1 shows the earliest stage of these bedforms, where they start as small patches of sand. These patches grow together and form zebra stripe-like patterns (classes 2 and 3) that eventually cover the entire beach (class 4). Meanwhile, the wind velocity was sorted in four classes, ranging from weak to strong winds. The moments of transport were marked as either limited or unlimited based on their wind velocity class and Argus image class. All moments with well-developed sand strips were considered unlimited, while all moments with no visual traces of transport were considered limited. For the moments with some visual transport (Argus class 1, 2, and 3), the discrimination between limited and unlimited depended on wind velocity. A moment with relatively strong winds but with little visual transport is most likely subjected to transport limiting factors. However, sand strips need time to develop, and an Argus image with little visible sand transport could also indicate that sand strip formation has just started. Therefore, Argus images from the hours preceding the hour with the highest mean wind velocity of the day were searched for traces of transport. If transport occurred earlier, but not during the studied hour, then transport is limited. Smaller signs of transport were considered unlimited under relatively low wind velocities, as those are more likely to be signs of sand

strips in development, not of hindered transport. Sand strips can develop quickly (sometimes under an hour) during high wind velocities, so here, small signs of transport are more likely to be caused by limiting factors.

Wind speed, direction and temperature were the most prominent weather characteristics that showed a difference between limited (241) and unlimited (467) events. The wind was more often cross-shore (westerly for Egmond beach) and had generally a higher velocity ($\geq$12 m/s) for limited transport events. Sometimes, these strong winds caused such a high storm surge that a large part of or even the total beach was flooded and aeolian transport obviously ceased to exist. Unlimited transport events, on the other hand, occurred under lower wind velocities as well and had an (almost) alongshore wind direction. It was also found that some limited events were only limited during high tide and showed unlimited transport when the tide was low. This indicates that the fetch length strongly influences transport on a narrow beach. It was also observed that unlimited events were relatively more common in summer months. A potential reason for this is stronger evaporation, but it remains unclear if this is truly the case.

3. *Can a fetch model, building on the work of Delgado-Fernandez (2011), predict the timing of limited and unlimited aeolian sediment transport correctly?*

The answer to this question is described in Chapter 4. The Argus images taken between October 2011 and March 2012 were investigated for signs of aeolian sediment transport. This period of time was then modelled with Aeolus, a fetch-based transport model based on the conceptual work of Bauer and Davidson-Arnott (2002), who proposed a series of explicit equations for aeolian sediment transport rates. This framework was later tested and improved by Delgado-Fernandez (2011) by using data from a 9-month field campaign at Greenwich Dunes, Canada. Aeolus takes it a step further, using a spatially varying moisture content where the extended model by Delgado-Fernandez (2011) extracted a uniform moisture content for the beach from video imagery. Aeolus determines the groundwater level based on (tidal) water level data and determines a surface moisture content using a soil water retention curve. Furthermore, Aeolus uses water level data and a beach profile to determine the width of the beach, where the Delgado-Fernandez model was based on video imagery. This video monitoring is no longer necessary to drive Aeolus, making it more generally applicable.

It was found that the timing of non-zero Aeolus coincides quite well with the timing of transport as visible on the Argus images. Strong prediction differences between the actual transport rate as predicted by Aeolus and the potential transport rate based on wind-only models were more common for strong, cross-shore winds. A strong difference indicates limited transport. These results correspond with the findings in Chapter 3, where it was also found that moments of transport are more often limited under these circumstances.

Thirty of the 183 examined days had no visual signs of aeolian transport on the Argus imagery, while Aeolus predicted non-zero transport. For 27 of the 30 mismatched days, only a little transport resulted from the Aeolus calculations, which is probably too small to be seen on the Argus images. For the moments of larger predicted transport, the Argus imagery was unclear and could have been classified incorrectly. Of the 27 days, 5 days showed signs of rain or snow, or had very low temperatures, presumingly causing the beach to be frozen. This factors are not incorporated in Aeolus and could have hindered aeolian transport.

On 5 days, visual signs of transport were present, but the Aeolus model predicted zero sand transport. Again, this can be the result of incorrect classification due to unclear Argus imagery. One day though showed medium strong visual signs of transport while

the wind velocity was below the threshold of motion. The bedforms might have been formed by a wind too local to be registered by the weather station in IJmuiden, or by wind gusts. Gustiness is not included in Aeolus.

5.2 Discussion and perspectives

Chapters 2 and 3 have shown that visual signs of aeolian transport can be gathered relatively easily with high temporal resolution for a long duration using video monitoring. The Argus imagery at Egmond aan Zee, for example, spans from 1998 to 2015, consisting of three types of photos for five cameras taken every 30 minutes. The original purpose of Argus was to study nearshore phenomena (Holman and Stanley, 2007), but it has been used here to study the intertidal and upper (dry) beach, offering potential for further development in the field of coastal aeolian research. Other aeolian studies based on video monitoring include Delgado-Fernandez and Davidson-Arnott (2011), Montreuil et al. (2018), and Williams et al. (2018). Chapter 2 particularly focussed on sand strips, but video monitoring does not have to be limited to these bedforms. For example, moments of aeolian sediment transport was visually observed and selected as well by Guimarães et al. (2016) at Cassino Beach, Brazil, where the bedforms were ephemeral dunes, larger than sand strips and with a slipface. Sherman et al. (2013b) used a video monitoring system close to the ground (at 2 m) to study streamers at the beach of Jericoacoara, Brazil, indicating that instantaneous high-resolution data can also be used to examine detailed aeolian processes. Baas and Van den Berg (2018) had a similar system to extract displacement vectors of streamers, using a black surface for extra contrast for the camera.

All these studies, and this thesis, illustrate the suitability and usefulness of video imagery to study aeolian processes and dynamics, from temporal scales of seconds to years. As such, it provides a welcome addition to more standard equipment, such as anemometers and sand catchers, to study aeolian processes. Delgado-Fernandez and Davidson-Arnott (2011) used video monitoring during their nine-month research at Greenwich Dunes, Canada, to determine the moisture content of the beach, using the surface brightness of the images, and to classify moments of aeolian transport. This was done by combining the imagery with data from in situ measurements. Williams et al. (2018) also combined coastal imagery with in-situ data. Here, they used Argus images taken at the Sand Motor, the Netherlands, to automatically find and classify aeolian streamers. Part of their data overlapped with a field campaign by Hoonhout and de Vries (2017). Combining those datasets showed that images with traces of transport generally relate to high particle counts. The research in this thesis did not compare video images to measured transport data because the cameras of the Argus tower at Egmond stopped working before this could be done. A future step would be, like Williams et al. (2018), to look for a relation between visual transport intensity and actual transport rate. The images could then be used to estimate aeolian sediment transport without needing to visit the field site. As was done in Chapter 4, comparing the results with Aeolus is also a possibility, but this requires a quantitative test of the model first.

Additionally, other significantly different field sites could be studied with Argus or video imagery in general. Interesting opportunities may also arise from the use of smartphones or webcams (e.g. www.solarcam.fr/en) or the use of citizen science (Harley et al., 2019). This thesis has focused on one beach, which is characterised by its narrow width and a steep, high (20-25 m) foredune. The wind direction strongly influences the amount of transported sand and the development of aeolian bedforms at this site. Studying Argus images for traces of aeolian transport of other beaches will show how limiting factors affect aeolian transport differently, or if other limiting factors play a more important role. This thesis has shown that, as soon as the wind velocity has surpassed a threshold and is (almost) alongshore, the

sand strip wavelength and migration velocity do not show a strong change with increasing wind velocity. Studying other beaches might reveal a correlation between sand strip characteristics and, for example, grain size or beach morphology. Additionally, using a local wind station to link sand strip to wind characteristics is strongly advised, as it was found that the migration direction of the sand strips turned alongshore when the regional wind measured by the nearby 'regional' weather station was oblique, indicating wind steering by the steep, high foredune at Egmond. Video monitoring can be applied to any coastal area, as long as the vantage point is high and the beach is well in view. There must be a strong colour contrast between the dry (light-coloured) transported sand, and the dark (moist) sand of the surface in order to see sediment transport, which generally means only the intertidal area can be studied.

The Aeolus model can contribute greatly to understanding the coastal zone, but like Argus, it can profit from aeolian transport measurements, as Chapter 4 only inspected the timing of the model. The measurements for this future research can be in the form of downwind arrays of sediment traps (Rasmussen and Mikkelsen, 1998; Dong et al., 2004; Sterk and Raats, 1996; Basaran et al., 2011; Mendez et al., 2011), laser samplers (Hugenholtz and Barchyn, 2011; Sherman et al., 2011), acoustic samplers (Spaan and Van den Abeele, 1991; Yurk et al., 2013; Ellis et al., 2009; Schönfeldt, 2012), piezoelectric samplers (Stout, 1998; Baas, 2004; de Winter et al., 2018) and pressure sensitive samplers (Ridge et al., 2011). The best method to improve the model is to test it for various conditions. This can be achieved by doing fieldwork at different moments of a year, when wind and beach conditions are different. Alternatively, predicted transport rates at the beach-dune transition can be compared to sand deposition on the foredune, assuming that no sand gets transported further into the dunes.

A different study site results for different parameters for Aeolus as well. For example, the Egmond beach consists of well-sorted sand with a grainsize of 240 μm. A different grain size affects how the groundwater level responds to changes in seawater level (Schmutz and Namikas, 2013; Smit, 2019). The beach profile and wind conditions will probably not be the same either. The best results are obtained when an on-site weather station is used, but if that is not possible, the correction factor used by Aeolus to turn regional into local wind must be fitted for the current site. Furthermore, de Winter et al. (2020) found that the regional wind direction does not match the wind direction at the dune foot at Egmond aan Zee. Aeolus already has a correction factor for this, and turns the wind at Egmond aan Zee in a more alongshore direction (which is especially the case for oblique, 45° winds). This was not used in this research, as it focused on total rather than cross-shore transport. When Aeolus is applied to other beaches, this correction factor might be different, becoming smaller when the dunes are lower and less steep. de Winter et al. (2020) indicated that Computational Fluid Dynamics could be used in a number of synthetic runs to explore how the foredune affects winds flow on the beach and hence to derive correction factors for the topographically altered winds.

Additionally, Aeolus can be made more accurate when more factors that limit transport, like rain and snow, are incorporated. This study has already shown that rain is important for transport at Egmond aan Zee. During days with rain, the Argus images show that aeolian transport comes to a halt or becomes less intense. As was found by Arens (1996), the threshold for aeolian transport increases when rain is present, or transport shuts down completely during intense rain. Another extension may be to consider more patchy moisture conditions or moisture pattern influenced by sandbar morphology (Smit et al., 2019).

Both Aeolus and Argus help understanding the wind-driven processes at the coast. The Aeolus model predicts the amount of sand that will be deposited at the dune foot, which is used for dune growth and recovery from erosion events. If this sand is allowed to blow beyond the foredune, it can affect a larger area. Not only will this increase the height of the

hinterland, making it less prone to flooding in case the foredune fails, it will also add to a more diverse, dynamic ecosystem (Martínez et al., 2013; Arens et al., 2013; Meerkerk et al., 2007). The sand will bury existing vegetation which allows rare pioneer vegetation to settle (Schwarz et al., 2019). Before this can be done, though, the marram grass covering the dunes has to be removed, as vegetation traps the sand and thus blocks the onshore sand transport pathway. Notches can be dug to stimulate sand transport even further, as was done at the Dutch National Park Zuidkennemerland (Ruessink et al., 2018a). It is up to policy makers to take steps to this kind of coastal management. It might feel contradicting to remove marram grass, which was planted in the first place to make the dunes grow in height and form a better protection against flooding, but this mindset is slowly changing. Decades ago, the coastal zone was purely seen as a defence against coastal flooding. Protective measures were hard structures in the such as seawalls, breakwaters, or groins which kept the hinterland safe, but harmed natural processes and biodiversity. Now, however, a shift has been made to 'soft' measures that protect against flooding and work together with nature (Borsje et al., 2011; Charlier et al., 2005). These include, for example, sand nourishments to broaden and heighten the beach, where natural processes can transport the sand towards the dunes. With climate change and a rising sea level, such forms of protection become more important than ever. Luckily, we discover more ways to keep coasts safe and ecologically rich and diverse. We only need to change our mindset to use them.

References

Aagaard, T., A. Kroon, S. Andersen, R. M. Sørensen, S. Quartel, and N. Vinther (2005). Intertidal beach change during storm conditions; Egmond, The Netherlands. *Marine Geology* 218.1, pp. 65–80.

Aarninkhof, S. G. J., I. L. Turner, T. D. T. Dronkers, M. Caljouw, and L. Nipius (2003). A video-based technique for mapping intertidal beach bathymetry. *Coastal Engineering* 49.4, pp. 275–289.

Anderson, R. S. and P. K. Haff (1988). Simulation of eolian saltation. *Science* 241.4867, pp. 820–823.

Arens, S. M., J. P. Mulder, Q. L. Slings, L. H. Geelen, and P. Damsma (2013). Dynamic dune management, integrating objectives of nature development and coastal safety: examples from the Netherlands. *Geomorphology* 199, pp. 205–213.

Arens, S. M. (1994). Aeolian processes in the Dutch foredunes.

Arens, S. M. (1996). Patterns of sand transport on vegetated foredunes. *Geomorphology* 17.4, pp. 339–350.

Avis, A. and R. Lubke (1996). Dynamics and succession of coastal dune vegetation in the Eastern Cape, South Africa. *Landscape and Urban Planning* 34.3-4, pp. 237–253.

Baas, A. C. W. (2004). Evaluation of saltation flux impact responders (Safires) for measuring instantaneous aeolian sand transport intensity. *Geomorphology* 59.1-4, pp. 99–118.

Baas, A. C. W. and D. J. Sherman (2005). Formation and behavior of aeolian streamers. *Journal of Geophysical Research: Earth Surface* 110.F3.

Baas, A. C. W. and F. Van den Berg (2018). Large-Scale Particle Image Velocimetry (LSPIV) of aeolian sand transport patterns. *Aeolian research* 34, pp. 1–17.

Baas, A. C. W. and D. J. Sherman (2006). Spatiotemporal variability of aeolian sand transport in a coastal dune environment. *Journal of Coastal Research*, pp. 1198–1205.

Baas, J. H. (1994). A flume study on the development and equilibrium morphology of current ripples in very fine sand. *Sedimentology* 41.2, pp. 185–209.

Baas, J. H., A. P. Oost, O. K. Sztano, P. L. Boer, and G. Postma (1993). Time as an independent variable for current ripples developing towards linguoid equilibrium morphology. *Terra Nova* 5.1, pp. 29–35.

Baddock, M. C., J. M. Nield, and G. F. S. Wiggs (2017). Early-stage aeolian protodunes: Bedform development and sand transport dynamics. *Earth Surface Processes and Landforms*.

Bagnold, R. A. (1941). *The Physics of Blown Sand and Desert Dunes*. Dover Publications, Inc.

Basaran, M, G Erpul, O Uzun, and D Gabriels (2011). Comparative efficiency testing for a newly designed cyclone type sediment trap for wind erosion measurements. *Geomorphology* 130.3-4, pp. 343–351.

Bauer, B. O., R. G. D. Davidson-Arnott, P. A. Hesp, S. L. Namikas, J. Ollerhead, and I. J. Walker (2009). Aeolian sediment transport on a beach: Surface moisture, wind fetch, and mean transport. *Geomorphology* 105.1, pp. 106–116.

Bauer, B. O. and R. G. D. Davidson-Arnott (2002). A general framework for modeling sediment supply to coastal dunes including wind angle, beach geometry, and fetch effects. *Geomorphology* 49.1, pp. 89–108.

Bauer, B. O., R. G. Davidson-Arnott, K. F. Nordstrom, J. Ollerhead, and N. L. Jackson (1996). Indeterminacy in aeolian sediment transport across beaches. *Journal of Coastal Research*, pp. 641–653.

Bauer, B. O., R. G. Davidson-Arnott, I. J. Walker, P. A. Hesp, and J. Ollerhead (2012). Wind direction and complex sediment transport response across a beach–dune system. *Earth Surface Processes and Landforms* 37.15, pp. 1661–1677.

Bird, E. C. (2011). *Coastal geomorphology: an introduction*. John Wiley & Sons.

Borsje, B. W., B. K. van Wesenbeeck, F. Dekker, P. Paalvast, T. J. Bouma, M. M. van Katwijk, and M. B. de Vries (2011). How ecological engineering can serve in coastal protection. *Ecological Engineering* 37.2, pp. 113–122.

Brakenhoff, L. B., Y. Smit, J. J. Donker, and G. Ruessink (2019). Tide-induced variability in beach surface moisture: Observations and modelling. *Earth Surface Processes and Landforms* 44.1, pp. 317–330.

Castelle, B., V. Marieu, S. Bujan, K. D. Splinter, A. Robinet, N. Sénéchal, and S. Ferreira (2015). Impact of the winter 2013–2014 series of severe Western Europe storms on a double-barred sandy coast: Beach and dune erosion and megacusp embayments. *Geomorphology* 238, pp. 135–148.

Chapman, V. J. (2016). *Coastal vegetation*. Elsevier.

Charlier, R. H., M. C. P. Chaineux, and S. Morcos (2005). Panorama of the history of coastal protection. *Journal of Coastal Research*, pp. 79–111.

Davidson-Arnott, R. G. D. and B. O. Bauer (2009). Aeolian sediment transport on a beach: Thresholds, intermittency, and high frequency variability. *Geomorphology* 105.1–2, pp. 117 –126. DOI:HTTP://DX.DOI.ORG/10.1016/J.GEOMORPH.2008.02.018.

Davidson-Arnott, R. G. D. and M. N. Law (1990). Seasonal patterns and controls on sediment supply to coastal foredunes, Long Point, Lake Erie. *Coastal dunes: form and process*, pp. 177–200.

Davidson-Arnott, R. G. D. and M. N. Law (1996). Measurement and prediction of long-term sediment supply to coastal foredunes. *Journal of Coastal Research*, pp. 654–663.

Davidson-Arnott, R. G. D., K. MacQuarrie, and T. Aagaard (2005). The effect of wind gusts, moisture content and fetch length on sand transport on a beach. *Geomorphology* 68.1, pp. 115–129.

Davidson-Arnott, R. and J. Dawson (2001). Moisture and fetch effects on rates of aeolian sediment transport, Skallingen, Denmark. In: *Proceedings Canadian Coastal Conference*. Canadian Coastal Science and Engineering Association Ottawa, Canada, pp. 309–321.

Davidson-Arnott, R. G. D., Y. Yang, J. Ollerhead, P. A. Hesp, and I. J. Walker (2008). The effects of surface moisture on aeolian sediment transport threshold and mass flux on a beach. *Earth Surface Processes and Landforms* 33.1, pp. 55–74.

De Vries, S., S. M. Arens, M. A. de Schipper, and R. Ranasinghe (2014). Aeolian sediment transport on a beach with a varying sediment supply. *Aeolian Research* 15, pp. 235–244. DOI:10.1016/J.AEOLIA.2014.08.001.

De Winter, R. C., F. Gongriep, and B. G. Ruessink (2015). Observations and modeling of alongshore variability in dune erosion at Egmond aan Zee, the Netherlands. *Coastal Engineering* 99, pp. 167–175. DOI:10.1016/J.COASTALENG.2015.02.005.

De Winter, W., B. Ruessink, and J. Donker (2018). The influence of beach-foredune morphology on local wind characteristics.

De Winter, W., J. Donker, G. Sterk, J. Van Beem, and G. Ruessink (2020). Regional versus local wind speed and direction at a narrow beach with a high and steep foredune. *PLoS One* 15.1.

De Winter, R. C. and B. G. Ruessink (2017). Sensitivity analysis of climate change impacts on dune erosion: case study for the Dutch Holland coast. *Climatic Change* 141.4, pp. 685–701.

Delgado-Fernandez, I. (2010). A review of the application of the fetch effect to modelling sand supply to coastal foredunes. *Aeolian Research* 2.2-3, pp. 61–70. DOI:10.1016/J.AEOLIA.2010.04.001.

Delgado-Fernandez, I. (2011). Meso-scale modelling of aeolian sediment input to coastal dunes. *Geomorphology* 130.3-4, pp. 230–243.

Delgado-Fernandez, I. and R. G. D. Davidson-Arnott (2011). Meso-scale aeolian sediment input to coastal dunes: The nature of aeolian transport events. *Geomorphology* 126.1-2, pp. 217–232. DOI:10.1016/J.GEOMORPH.2010.11.005.

Delgado-Fernandez, I., R. G. D. Davidson-Arnott, and J. Ollerhead (2009). Application of a Remote Sensing Technique to the Study of Coastal Dunes. *Journal of Coastal Research* 255.255, pp. 1160–1167. DOI:10.2112/09-1182.1.

Delgado-Fernandez, I., D. W. Jackson, J. A. G. Cooper, A. C. Baas, J. M. Beyers, and K. Lynch (2013). Field characterization of three-dimensional lee-side airflow patterns under offshore winds at a beach-dune system. *Journal of Geophysical Research: Earth Surface* 118.2, pp. 706–721.

Dong, Z., H. Sun, and A. Zhao (2004). WITSEG sampler: a segmented sand sampler for wind tunnel test. *Geomorphology* 59.1-4, pp. 119–129.

Donker, J., M. van Maarseveen, and G. Ruessink (2018). Spatio-temporal variations in foredune dynamics determined with mobile laser scanning. *Journal of Marine Science and Engineering* 6.4, p. 126.

Durán, O. and L. J. Moore (2013). Vegetation controls on the maximum size of coastal dunes. *Proceedings of the National Academy of Sciences* 110.43, pp. 17217–17222. DOI:10.1073/PNAS.1307580110.

Eamer, J. B. R. and I. J. Walker (2010). Quantifying sand storage capacity of large woody debris on beaches using LiDAR. *Geomorphology* 118.1, pp. 33–47.

Edwards, B. L. and S. L. Namikas (2009). Small-scale variability in surface moisture on a fine-grained beach: implications for modeling aeolian transport. *Earth Surface Processes and Landforms* 34.10, pp. 1333–1338. DOI:10.1002/ESP.1817.

Elbelrhiti, H. (Feb. 2012). Initiation and early development of barchan dunes: A case study of the Moroccan Atlantic Sahara desert. *Geomorphology* 138.1, pp. 181–188. DOI:10.1016/J.GEOMORPH.2011.08.033.

Ellis, J. T., R. F. Morrison, and B. H. Priest (2009). Detecting impacts of sand grains with a microphone system in field conditions. *Geomorphology* 105.1-2, pp. 87–94.

Ewing, R. C. and G. Kocurek (2010). Aeolian dune-field pattern boundary conditions. *Geomorphology* 114.3, pp. 175–187.

Ewing, R. C., G. Kocurek, and L. W. Lake (2006). Pattern analysis of dune-field parameters. *Earth Surface Processes and Landforms* 31.9, pp. 1176–1191.

Gares, P. A. (1988). Factors affecting eolian sediment transport in beach and dune environments. *Journal of coastal research* Special Issue No. 3 Dune/beach interaction, pp. 121–126.

Gillette, D. A., G. Herbert, P. H. Stockton, and P. Owen (1996). Causes of the fetch effect in wind erosion. *Earth Surface Processes and Landforms* 21.7, pp. 641–659.

Guimarães, P. V., P. S. Pereira, L. J. Calliari, and J. T. Ellis (2016). Behavior and identification of ephemeral sand dunes at the backshore zone using video images. *Anais da Academia Brasileira de Ciências* 88, pp. 1357–1369. DOI:10.1590/0001-3765201620150656.

Hage, P. M. (2014). Video monitoring of meso-scale aeolian activity on a narrow beach. To be found in https://dspace.library.uu.nl/handle/1874/301331. MA thesis. Utrecht University.

Harley, M. D., M. A. Kinsela, E. Sánchez-García, and K. Vos (2019). Shoreline change mapping using crowd-sourced smartphone images. *Coastal Engineering* 150, pp. 175–189.

Hesp, P. (2012). Surfzone-beach-dune interactions.

Hesp, P. (2002). Foredunes and blowouts: initiation, geomorphology and dynamics. *Geomorphology* 48.1-3, pp. 245–268.

Hesp, P. A. and S. M. Arens (1997). Crescentic dunes at Schiermonnikoog, the Netherlands. *Earth Surface Processes and Landforms* 22.

Holland, K. T., R. A. Holman, T. C. Lippmann, J. Stanley, and N. Plant (1997). Practical use of video imagery in nearshore oceanographic field studies. *IEEE Journal of oceanic engineering* 22.1, pp. 81–92.

Holman, R. A. and J. Stanley (June 2007). The history and technical capabilities of Argus. *Coastal Engineering* 54.6-7, pp. 477–491. DOI:10.1016/J.COASTALENG.2007.01.003.

Holman, R. A. and A. H. Sallenger (1986). High-energy nearshore processes. *Eos, Transactions American Geophysical Union* 67.49, p. 1369. DOI:10.1029/EO067I049P01369.

Hoonhout, B. M. and S. de Vries (2017). Field measurements on spatial variations in aeolian sediment availability at the Sand Motor mega nourishment. *Aeolian Research* 24.2017, pp. 93–104. DOI:10.1016/j.aeolia.2016.12.003.

Hoonhout, B. M. and S. d. Vries (2016). A process-based model for aeolian sediment transport and spatiotemporal varying sediment availability. *Journal of Geophysical Research: Earth Surface* 121.8, pp. 1555–1575.

Houser, C. (Oct. 2009). Synchronization of transport and supply in beach-dune interaction. *Progress in Physical Geography* 33.6, pp. 733–746. DOI:10.1177/0309133309350120.

Hsu, S. A. (1971). Wind stress criteria in eolian sand transport. *Journal of Geophysical Research* 76.36, pp. 8684–8686.

Hsu, S. A. (1974). Computing Eolian Sand Transport from Routine Weather Data. In: *Coastal Engineering 1974*, pp. 1619–1626. DOI:10.1061/9780872621138.097. eprint: https://ascelibrary.org/doi/pdf/10.1061/9780872621138.097.

Hugenholtz, C. H. and T. E. Barchyn (2011). Laboratory and field performance of a laser particle counter for measuring aeolian sand transport. *Journal of Geophysical Research: Earth Surface* 116.F1.

Huizer, S, M. Karaoulis, G. Oude Essink, and M. Bierkens (2017). Monitoring and simulation of salinity changes in response to tide and storm surges in a sandy coastal aquifer system. *Water Resources Research* 53.8, pp. 6487–6509.

ITU-R (2011). *ITU-R Recommendation BT.601-7: Studio encoding parameters of digital television for standard 4: 3 and wide-screen 16: 9 aspect ratios*. ITU.

Jackson, D., J. Beyers, K. Lynch, J. Cooper, A. Baas, and I. Delgado-Fernandez (2011). Investigation of three-dimensional wind flow behaviour over coastal dune morphology under offshore winds using computational fluid dynamics (CFD) and ultrasonic anemometry. *Earth Surface Processes and Landforms* 36.8, pp. 1113–1124.

Jackson, N. L., D. J. Sherman, P. A. Hesp, A. H. F. Klein, F. Ballasteros Jr, and K. F. Nordstrom (2006). Small-scale spatial variations in aeolian sediment transport on a fine-sand beach. *Journal of Coastal Research* 1.Special Issue No. 39. Proceedings of the 8th International Coastal Symposium (ICS 2004), pp. 379–383.

Jackson, N. L. and K. F. Nordstrom (1997). Effects of Time-dependent Moisture Content of Surface Sediments on Aeolian Transport Rates Across a Beach, Wildwood, New Jersey, USA. *Earth Surface Processes and Landforms* 22.7, pp. 611–621.

Jackson, N. L. and K. F. Nordstrom (1998). Aeolian transport of sediment on a beach during and after rainfall, Wildwood, NJ, USA. *Geomorphology* 22.2, pp. 151–157.

Kadib, A. A. (1965). *A function for sand movement by wind*. Tech. rep. California University Berkeley Hydraulic Engineering Lab.

Kang, H.-Y., P. Nielsen, and D. J. Hanslow (1994). Watertable overheight due to wave runup on a sandy beach. In: *Coastal Engineering 1994*, pp. 2115–2124.

Kawamura, R. (1951). Study on sand movement by wind. *Rept. Inst. Sci. Technol.* 5, pp. 95–112.

Keijsers, J. G. S., A. Poortinga, M. J. P. M. Riksen, and J. Maroulis (2014). Spatio-temporal variability in accretion and erosion of coastal foredunes in the netherlands: Regional climate and local topography. *PloS one* 9.3, e91115.

Kocurek, G., M. Townsley, E. Yeh, K. G. Havholm, and M. L. Sweet (1992). Dune and Dune-Field Development on Padre Island, Texas, with Implications for Interdune Deposition and Water-Table-Controlled Accumulation. *Journal of Sedimentary Research* Vol. 62.4, pp. 622–635. DOI:10.1306/D4267974-2B26-11D7-8648000102C1865D.

Kocurek, G., R. C. Ewing, and D. Mohrig (2010). How do bedform patterns arise? New views on the role of bedform interactions within a set of boundary conditions. *Earth surface processes and landforms* 35.1, pp. 51–63.

Kooijman, A. (2008). Environmental problems and restoration measures in coastal dunes in the Netherlands. In: *Coastal Dunes*. Springer, pp. 243–258.

Kopp, R. E., R. M. Horton, C. M. Little, J. X. Mitrovica, M. Oppenheimer, D. Rasmussen, B. H. Strauss, and C. Tebaldi (2014). Probabilistic 21st and 22nd century sea-level projections at a global network of tide-gauge sites. *Earth's Future* 2.8, pp. 383–406.

Kulp, S. A. and B. H. Strauss (2019). New elevation data triple estimates of global vulnerability to sea-level rise and coastal flooding. *Nature communications* 10.1, pp. 1–12.

Lettau, K (1978). Experimental and micrometeorological field studies of dune migration. *Exploring in the World's driest climate*, pp. 110–147.

Lippmann, T. C. and R. A. Holman (1989). Quantification of sand bar morphology: A video technique based on wave dissipation. *Journal of Geophysical Research: Oceans* 94.C1, pp. 995–1011.

Lithgow, D et al. (2013). Linking restoration ecology with coastal dune restoration. *Geomorphology* 199, pp. 214–224.

Luijendijk, A., G. Hagenaars, R. Ranasinghe, F. Baart, G. Donchyts, and S. Aarninkhof (2018). The state of the world's beaches. *Scientific reports* 8.1, p. 6641.

Lynch, K., D. Jackson, and J. A. G. Cooper (2016). The fetch effect on aeolian sediment transport on a sandy beach: a case study from Magilligan Strand, Northern Ireland. *Earth Surface Processes and Landforms* 41.8, pp. 1129–1135.

Martínez, M. L. and N. P. Psuty (2004). *Coastal dunes*. Springer.

Martínez, M. L., P. A. Hesp, and J. B. Gallego-Fernández (2013). Coastal dunes: human impact and need for restoration. In: *Restoration of coastal dunes*. Springer, pp. 1–14.

Masselink, G., B. Castelle, T. Scott, G. Dodet, S. Suanez, D. Jackson, and F. Floc'h (2016). Extreme wave activity during 2013/2014 winter and morphological impacts along the Atlantic coast of Europe. *Geophysical Research Letters* 43.5, pp. 2135–2143.

Masselink, G., A. Kroon, and R. G. D. Davidson-Arnott (2006). Morphodynamics of intertidal bars in wave-dominated coastal settings—a review. *Geomorphology* 73.1, pp. 33–49.

McKenna Neuman, C. and G. Langston (2006). Measurement of water content as a control of particle entrainment by wind. *Earth Surface Processes and Landforms* 31.3, pp. 303–317.

Meerkerk, A., S. Arens, R. Van Lammeren, and H. Stuiver (2007). Sand transport dynamics after a foredune breach: A case study from Schoorl, The Netherlands. *Geomorphology* 86.1-2, pp. 52–60.

Mendez, M. J., R. Funk, and D. E. Buschiazzo (2011). Field wind erosion measurements with big spring number eight (BSNE) and modified wilson and cook (MWAC) samplers. *Geomorphology* 129.1-2, pp. 43–48.

Miot da Silva, G. and P. A. Hesp (2010). Coastline orientation, aeolian sediment transport and foredune and dunefield dynamics of Moçambique Beach, Southern Brazil. *Geomorphology* 120.3-4, pp. 258–278. DOI:10.1016/J.GEOMORPH.2010.03.039.

Montreuil, A.-L., M. Chen, E. Brand, G. Strypsteen, P. Rauwoens, A. Vandenbulcke, A. De Wulf, S. Dan, and T. Verwaest (2018). Dynamics of Surface Moisture Content on a Macro-tidal Beach. *Journal of Coastal Research* 85.sp1, pp. 206–210.

Namikas, S. L., B. L. Edwards, M. C. A. Bitton, J. L. Booth, and Y. Zhu (2010). Temporal and spatial variabilities in the surface moisture content of a fine-grained beach. *Geomorphology* 114.3, pp. 303–310.

Namikas, S. L. and D. J. Sherman (1995). A review of the effects of surface moisture content on aeolian sand transport. In: *Desert aeolian processes*. Springer, pp. 269–293.

Nickling, W. G. and C. M. Neuman (2009). Aeolian sediment transport. In: *Geomorphology of desert environments*. Springer, pp. 517–555.

Nield, J. M. (Sept. 2011). Surface moisture-induced feedback in aeolian environments. *Geology* 39.10, pp. 915–918. DOI:10.1130/G32151.1.

Nield, J. M. and G. F. S. Wiggs (2011). The application of terrestrial laser scanning to aeolian saltation cloud measurement and its response to changing surface moisture. *Earth Surface Processes and Landforms* 36.2, pp. 273–278.

Nield, J. M., G. F. S. Wiggs, and R. S. Squirrell (2011). Aeolian sand strip mobility and protodune development on a drying beach: examining surface moisture and surface roughness patterns measured by terrestrial laser scanning. *Earth Surface Processes and Landforms* 36.4, pp. 513–522.

Nield, J. M. et al. (2013). Estimating aerodynamic roughness over complex surface terrain. *Journal of Geophysical Research Atmospheres* 118.23, pp. 12948–12961. DOI:10.1002/2013JD020632.

Nield, J. M., J. King, and B. Jacobs (Mar. 2014). Detecting surface moisture in aeolian environments using terrestrial laser scanning. *Aeolian Research* 12, pp. 9–17. DOI:10.1016/J.AEOLIA.2013.10.006.

Nielsen, P., G. Davis, J. Winterbourne, and G. Elias (1998). Wave setup and the watertable in sandy beaches. *Technical Report Technical Memo- randum* 88/1.

Nielsen, P. (1990). Tidal dynamics of the water table in beaches. *Water Resources Research* 26.9, pp. 2127–2134.

Nordstrom, K. F. and N. L. Jackson (1992). Effect of source width and tidal elevation changes on aeolian transport on an estuarine beach. *Sedimentology* 39.5, pp. 769–778.

Nordstrom, K. F. and N. L. Jackson (1993). The role of wind direction in eolian transport on a narrow sandy beach. *Earth Surface Processes and Landforms* 18.8, pp. 675–685.

Nordstrom, K. F., N. L. Jackson, and E. Pranzini (2004). Beach sediment alteration by natural processes and human actions: Elba Island, Italy. *Annals of the Association of American Geographers* 94.4, pp. 794–806.

Owen, P. R. (1964). Saltation of uniform grains in air. *Journal of Fluid Mechanics* 20.2, pp. 225–242.

Pachauri, R. K. et al. (2014). *Climate change 2014: synthesis report. Contribution of Working Groups I, II and III to the fifth assessment report of the Intergovernmental Panel on Climate Change*. IPCC.

Pape, L, Y Kuriyama, and B. Ruessink (2010). Models and scales for cross-shore sandbar migration. *Journal of Geophysical Research: Earth Surface* 115.F3.

Pianca, C., R. A. Holman, and E. Siegle (2015). Shoreline variability from days to decades: Results of long-term video imaging. *Journal of Geophysical Research: Oceans* 120.3, pp. 2159–2178. DOI:10.1002/2014JC010329.

Poortinga, A., J. G. Keijsers, J. Maroulis, and S. M. Visser (2014). Measurement uncertainties in quantifying aeolian mass flux: evidence from wind tunnel and field site data. *PeerJ* 2, e454. DOI:10.7717/PEERJ.454.

Quartel, S and B. T. Grasmeijer (2007). Dynamiek van het strand bij Noordwijk aan Zee en Egmond aan Zee en het effect van suppleties. *Rijksinstituut voor Kust en Zee (RIKZ). Opdracht RKZ-1667* september 2006.

Quartel, S, B. G. Ruessink, and A. Kroon (2007). Daily to seasonal cross-shore behaviour of quasi-persistent intertidal beach morphology. *Earth Surface Processes and Landforms* 32.9, pp. 1293–1307.

Rasmussen, K. R. and H. E. Mikkelsen (1998). On the efficiency of vertical array aeolian field traps. *Sedimentology* 45.4, pp. 789–800.

Raubenheimer, B, R. Guza, and S. Elgar (1999). Tidal water table fluctuations in a sandy ocean beach. *Water Resources Research* 35.8, pp. 2313–2320.

Ridge, J. T., A. B. Rodriguez, S. R. Fegley, R. Browne, and D. Hood (2011). A new 'pressure sensitive'method of measuring aeolian sediment transport using a gauged sediment trap (gast). *Geomorphology* 134.3-4, pp. 426–430.

Roelvink, D., A. Reniers, A. Van Dongeren, J. v. T. de Vries, R. McCall, and J. Lescinski (2009). Modelling storm impacts on beaches, dunes and barrier islands. *Coastal engineering* 56.11-12, pp. 1133–1152.

Ruessink, B. G., L. Pape, and I. L. Turner (2009). Daily to interannual cross-shore sandbar migration: Observations from a multiple sandbar system. *Continental Shelf Research* 29.14, pp. 1663–1677. DOI:10.1016/J.CSR.2009.05.011.

Ruessink, B. G., S. M. Arens, M. Kuipers, and J. J. A. Donker (2018a). Coastal dune dynamics in response to excavated foredune notches. *Aeolian Research* 31, pp. 3–17.

Ruessink, B. G., C. Schwarz, P. M. Hage, Y. Smit, W. de Winter, and J. J. A. Donker (2018b). Predicting Potential Aeolian Sand Supply to a High and Steep Foredune. In: *AGU Fall Meeting Abstracts*.

Ruessink, B., C. Schwarz, T. Price, and J. Donker (2019). A Multi-Year Data Set of Beach-Foredune Topography and Environmental Forcing Conditions at Egmond aan Zee, The Netherlands. *Data* 4.2, p. 73.

Sallenger Jr, A. H. (2000). Storm impact scale for barrier islands. *Journal of Coastal Research*, pp. 890–895.

Schmutz, P., T. Briggs, and P. Tereszkiewicz (2019). The utility of an omni-directional photoelectronic sensor device to measure meso-scale variability in aeolian sediment transport activity. *Aeolian Research* 36, pp. 61–67.

Schmutz, P. P. and S. L. Namikas (2013). Measurement and modeling of moisture content above an oscillating water table: implications for beach surface moisture dynamics. *Earth Surface Processes and Landforms* 38.11, pp. 1317–1325.

Schönfeldt, H.-J. (2012). High resolution sensors in space and time for determination saltation and creep intensity. *Earth Surface Processes and Landforms* 37.10, pp. 1065–1073.

Schwarz, C., J. Brinkkemper, and B. G. Ruessink (2019). Feedbacks between biotic and abiotic processes governing the development of foredune blowouts: A review. *Journal of Marine Science and Engineering* 7.1, p. 2.

Scott, T., G. Masselink, T. O'Hare, A. Saulter, T. Poate, P. Russell, M. Davidson, and D. Conley (2016). The extreme 2013/2014 winter storms: Beach recovery along the southwest coast of England. *Marine Geology* 382, pp. 224–241.

Seppälä, M. and K. Lindé (1978). Wind Tunnel Studies of Ripple Formation. *Geografiska Annaler: Series A, Physical Geography* 60.1-2, pp. 29–42. DOI:10.1080/04353676.1978.11879961. eprint: https://doi.org/10.1080/04353676.1978.11879961.

Sherman, D. J. and S. Hotta (1990). Aeolian sediment transport: theory and measurement. *Coastal Dunes: form and process* 17, p. 37.

Sherman, D. J., C. Houser, and A. C. W Baas (2013a). *Electronic Measurement Techniques for Field Experiments in Process Geomorphology*. Vol. 14. Elsevier Ltd., pp. 195–221. DOI:10.1016/B978-0-12-374739-6.00401-2.

Sherman, D. J. and B. Li (Jan. 2012). Predicting aeolian sand transport rates: A reevaluation of models. *Aeolian Research* 3.4, pp. 371–378. DOI:10.1016/J.AEOLIA.2011.06.002.

Sherman, D. J., D. W. Jackson, S. L. Namikas, and J. Wang (1998). Wind-blown sand on beaches: an evaluation of models. *Geomorphology* 22.2, pp. 113–133.

Sherman, D. J., B. Li, E. J. Farrell, J. T. Ellis, W. D. Cox, L. P. Maia, and P. H. G. O. Sousa (2011). Measuring Aeolian Saltation: A Comparison of Sensors. *Journal of Coastal Research* 59.May 2017, pp. 280–290. DOI:10.2112/SI59-030.1.

Sherman, D. J., C. Houser, J. T. Ellis, E. J. Farrell, B. Li, R. G. Davidson-Arnott, A. C. Baas, and L. P. Maia (Jan. 2013b). Characterization of aeolian streamers using time-average videography. *Journal of Coastal Research* 165.65, pp. 1331–1336. DOI:10.2112/SI65-225.1.

Short, A. and P. Hesp (1982). Wave, beach and dune interactions in southeastern Australia. *Marine geology* 48.3-4, pp. 259–284.

Sluijter, R., H. Leenaers, and M. Camarasa (2011). *De Bosatlas van het klimaat*. Data can be found at www.klimaatatlas.nl. Noordhoff uitgevers Groningen, The Netherlands.

Smit, Y. (2019). Surface moisture dynamics on a narrow coastal beach. PhD thesis. Utrecht University.

Smit, Y., J. Donker, and B. Ruessink (2019). Spatiotemporal surface moisture variations on a barred beach and their relationship with groundwater fluctuations. *Hydrology* 6.1, p. 8.

Smit, Y., G. Ruessink, L. B. Brakenhoff, and J. J. A. Donker (2018). Measuring spatial and temporal variation in surface moisture on a coastal beach with a near-infrared terrestrial laser scanner. *Aeolian Research* 31, pp. 19–27.

Sørensen, M. (2004). On the rate of aeolian sand transport. *Geomorphology* 59.1-4, pp. 53–62.

Spaan, W. and G. Van den Abeele (1991). Wind borne particle measurements with acoustic sensors. *Soil technology* 4.1, pp. 51–63.

Sterk, G and P. Raats (1996). Comparison of models describing the vertical distribution of wind-eroded sediment. *Soil Science Society of America Journal* 60.6, pp. 1914–1919.
Stockdon, H. F., R. A. Holman, P. A. Howd, and A. H. Sallenger Jr (2006). Empirical parameterization of setup, swash, and runup. *Coastal engineering* 53.7, pp. 573–588.
Stockdon, H. F., A. H. Sallenger Jr, R. A. Holman, and P. A. Howd (2007). A simple model for the spatially-variable coastal response to hurricanes. *Marine Geology* 238.1-4, pp. 1–20.
Stout, J. E. (1998). Effect of averaging time on the apparent threshold for aeolian transport. *Journal of Arid Environments* 39.3, pp. 395–401.
Svasek, J. N. and J. H. J. Terwindt (1974). Measurements of sand transport by wind on a natural beach. *Sedimentology* 21.2, pp. 311–322. DOI:10.1111/J.1365-3091.1974.TB02061.X.
Sweet, W. V., R. E. Kopp, C. P. Weaver, J. Obeysekera, R. M. Horton, E. R. Thieler, and C. Zervas (2017). Global and regional sea level rise scenarios for the United States.
Tuijnman, Y. (2019). *Soil moisture dynamics and the effects on initiation of aeolian sand transport*. Utrecht University.
Turner, I. L. and P. Nielsen (1997). Rapid water table fluctuations within the beach face: Implications for swash zone sediment mobility? *Coastal Engineering* 32.1, pp. 45–59.
Udo, K., Y. Kuriyama, and D. W. T. Jackson (2008). Observations of wind-blown sand under various meteorological conditions at a beach. *Journal of Geophysical Research: Earth Surface* 113.F4.
Van Enckevort, I. M. J. and B. G. Ruessink (2001). Effect of hydrodynamics and bathymetry on video estimates of nearshore sandbar position. *Journal of Geophysical Research: Oceans* 106.C8, pp. 16969–16979.
Van der Wal, D (1998). Effects of fetch and surface texture on aeolian sand transport on two nourished beaches. *Journal of Arid Environments* 39.3, pp. 533–547.
van Enckevort, I. M. J., B. G. Ruessink, G. Coco, K. Suzuki, I. L. Turner, N. G. Plant, and R. A. Holman (2004). Observations of nearshore crescentic sandbars. *Journal of Geophysical Research C: Oceans* 109.6, pp. 1–17. DOI:10.1029/2003JC002214.
Van Genuchten, M. T. (1980). A closed-form equation for predicting the hydraulic conductivity of unsaturated soils 1. *Soil science society of America journal* 44.5, pp. 892–898.
Walker, I. J., P. A. Hesp, R. G. D. Davidson-Arnott, and J. Ollerhead (2006). Topographic Steering of Alongshore Airflow over a Vegetated Foredune: Greenwich Dunes, Prince Edward Island, Canada. *Journal of Coastal Research* 225.225, pp. 1278–1291. DOI:10.2112/06A-0010.1.
Walstra, D., R Hoekstra, P. Tonnon, and B. G. Ruessink (2013). Input reduction for long-term morphodynamic simulations in wave-dominated coastal settings. *Coastal Engineering* 77, pp. 57–70.
Wiggs, G. F. S., R. J. Atherton, and A. J. Baird (2004). Thresholds of aeolian sand transport: establishing suitable values. *Sedimentology* 51.1, pp. 95–108. DOI:10.1046/J.1365-3091.2003.00613.X.
Wijnberg, K. M. and J. H. J. Terwindt (1995). Extracting decadal morphological behaviour from high-resolution, long-term bathymetric surveys along the Holland coast using eigenfunction analysis. *Marine Geology* 126.1-4, pp. 301–330. DOI:10.1016/0025-3227(95)00084-C.
Williams, I. A., K. M. Wijnberg, and S. J. Hulscher (2018). Detection of aeolian transport in coastal images. *Aeolian research* 35, pp. 47–57.
Wolman, M. G. and J. P. Miller (1960). Magnitude and frequency of forces in geomorphic processes. *The Journal of Geology* 68.1, pp. 54–74.
Wondergem, H. E. (2005). Monitoring dune dynamics in 'De Kerf'(NL) 1997-2003. *VLIZ Special Publication*.
Yurk, B. P., E. C. Hansen, and D. Hazle (2013). A deadtime model for the calibration of impact sensors with an application to a modified miniphone sensor. *Aeolian Research* 11, pp. 43–54.
Zingg, A. (1953). Wind tunnel studies of the movement of sedimentary material. In: *Proceedings of the 5th Hydraulic Conference Bulletin*. Vol. 34. Inst. of Hydraulics Iowa City, pp. 111–135.

Dankwoord/Acknowledgements

De afgelopen jaren vormden een leerzame, fantastische reis die ik, gelukkig, niet in mijn eentje hoefde te maken. Ik heb van alle kanten hulp, inspiratie en, zo nu en dan, de nodige afleiding gekregen. Hiervoor wil ik graag een aantal mensen bedanken.

Natuurlijk is daar Gerben. Zonder hem was dit boekje er niet geweest. Je hebt me de weg gewezen in dit doolhof dat wetenschap heet, maar altijd op zo'n manier dat ik een eigen richting kon kiezen. Hoe je de tijd hebt om naast mij nog veel andere PhD-ers onder je hoede te hebben, je taken voor de universiteit te doen en dan nog zelf het een en ander aan onderzoek te verrichten, begrijp ik nog steeds niet, maar ik heb er ontzettend veel respect voor. Je hielp altijd op een vriendelijke, positieve manier (en ging daar zo ver mee dat je zelfs nooit een rode pen voor correcties gebruikte). Eigenlijk gaat het bedankje verder terug, want jij gaf antwoord op een vraag die me al jaren plaagde: waar is die toren op het strand van Egmond aan Zee nou voor? Dat mijn jaarlijkse vakantiebestemming een hotspot voor onderzoek bleek te zijn, had ik totaal niet verwacht, en het wakkerde mijn interesse voor stranden alleen maar aan. Na het kustenvak in de bachelor ben je ook niet meer van me af gekomen.

Jasper, jij ook bedankt voor alles. Je was een soort tweede Gerben die heel mooi alle puntjes op de i wist te zetten voordat een artikel de deur uit ging. Het was geweldig om met jou in het Aeolus versus Poseidon project te zitten. Dit geldt net zo goed voor Winnie en Yvonne, de andere leden van 'Gerbens harem': jullie zijn tof! Bedankt voor de leuke momenten tijdens conferenties, veldwerk, en gewoon op kantoor. Zilla, we hebben samen mogen prutsen met het Aeolus model en je kwam dingen tegen waar ik erg veel aan heb gehad. Dank je!

Over kantoor gesproken, ik had een aantal geweldige kamergenoten: eerst Joost en Jantien, dan Daan en Anita, en later kwam daar Klaas bij. Dank jullie wel voor de gezelligheid en af en toe nodige afleiding. Jullie maken onderzoek doen zoveel leuker. Also, Anita, thank you for letting Arjen and me stay at your place in San Francisco and being our personal guide! We had a lovely time there, despite my epic blisters caused by all those steep hills.

Ik heb het ontzettend naar mijn zin gehad bij Fysische Geografie en genoten elk moment, van simpele lunchwandeling tot PhD uitje. Ik wil met name de kustengroep noemen. Anita, Klaas, Daan, Winnie, Yvonne, Laura, Jasper, Tim, Joost, Jantien, Anouk, Renske, Nynke, Sepehr, Christian, Gerben, Maarten, en Piet, ik vond het erg leuk om met jullie te werken. Bedankt voor jullie steun en feedback. Marcel, Henk, Bas, Arjen en natuurlijk Chris, zonder jullie was veel onderzoek niet mogelijk geweest. Jullie zijn echte veldwerkhelden.

Ook wil ik Daan, Klaas, Jasper, Joost, Sebastian en Arjen (ja, er worden wat namen herhaald hier) bedanken voor de spelletjesavonden op woensdag. Anouk, jij hoort hier ook bij, al hebben we op het moment van schrijven nog geen bordspel samen gespeeld. Hopelijk komt daar snel verandering in!

Dan is er nog die andere spelletjesgroep: Jesse, Timbaas, Sander, Timbo en (nogmaals) Arjen, bedankt voor de maandelijkse gekkigheid. Escaleren kan je inderdaad leren. Cathy, jij zorgde voor de nodige afleiding in de vorm van verhalen of het brainstormen erover. Louise, ook jij hebt prachtige verhalen in je hoofd zitten waar ik echt meer over moet weten. Ook was het heel fijn dat we onze PhD ervaringen konden uitwisselen. Dan is er Machteld, dankzij jou heb ik ook na mijn PhD wat te doen! And to the 200 rogues on Facebook, you are an awesome family of creative weirdos. I'm happy to be part of it. Hoods up!

En Gul, ik heb je altijd gekend als die vriendelijke man in de pickup truck die mij en mij familie helpt met het vervoeren van (te veel) tassen van en naar ons vakantiehuisje en de gasflessen vervangt, dus ik vond het erg leuk om te horen dat je ook betrokken was bij ons veldwerk in 2015. Die container met onze meetapparatuur erin hebben we goed gebruikt. Mike, it was great to see similar research done on the other side of the planet. Thank you for inviting us for a fantastic dinner with you and your family. You kiwis are too kind (and wonderful chefs!). Kia ora!

Natuurlijk kan ik mijn familie niet vergeten. Het feit dat ik deze studierichting heb gekozen is voor een groot deel te danken aan de fantastische vakanties in Egmond aan Zee. Pap en Mam (al gebruik ik liever Moeders), ook al werd ik een beetje gek wanneer ik weer het verschil moest uitleggen tussen een thesis en een paper, ik ben wel erg blij dat jullie me al die tijd gesteund hebben en zo geinteresseerd waren in mijn onderzoek. Jullie waren soms enthousiaster dan ik, haha! Nikki, jij bleef een stukje nuchterder - op een positieve manier, uiteraard - dus dank daarvoor. Gino moet ik zeker te vriend houden, aangezien jij mogelijk degene bent die mijn thesis in het repository van de universiteit zal zetten.

Dan, last but not least, Arjen, ook al heb ik je al meerdere keren genoemd. Jij was er altijd voor me en probeerde altijd de balans te bewaren. Als ik weer eens 's avonds met mijn onderzoek bezig was herinnerde jij me er aan dat ik ook tijd voor mezelf moest nemen. Of dat strandvakanties toch echt niet zijn bedoeld om sand strips te tellen. Niet dat ik altijd naar je luisterde, maar goed, dat zijn we wel van elkaar gewend. Dank je wel dat je met me mee bent gegaan op deze gekke reis als mijn persoonlijke 'knight in shining armour'. Of wacht, misschien toch niet… Who needs a knight when you can have a Viking!

En mocht je nou denken 'hey, ze heeft mij helemaal niet genoemd!', sorry daarvoor. Je steun waardeer ik zeer, maar als je me een beetje kent dan weet je dat namen onthouden niet mijn sterkste punt is. Mocht je toch heel graag genoemd willen worden in dit dankwoord, dan kan je hier je naam invullen:……

Houten, juli 2020

About the author

Pam Hage was born on the 10th of June 1991 in Kampen. She grew up in Elburg and attended the Nurborgh College Lambert Franckens. In 2009, she started her bachelors in Earth Sciences at Utrecht University. She grew interested in coastal processes and Pam made it the subject of her bachelor thesis, which was a literature study focused on storm occurrences in the Netherlands through the centuries. Pam continued studying coasts as she followed the master programme Earth Surface, and Water and completed an internship at Rijkswaterstaat in 2014, where she calculated storm damage chances for beach pavilions along the Dutch coast. For her master thesis, she used Argus imagery to find moments of limited and unlimited transport. It formed the basis of her PhD study, which Pam started in 2014. In June 2020, she started her new job at Tauw.

Publications

Journal papers

Hage, P.M., B.G. Ruessink, Z.E.M. van Aartrijk, & J.J.A. Donker. (2020), Using Video Monitoring to Test a Fetch-Based Aeolian Sand Transport Model. *Journal of Marine Science and Engineering 8*, 2, 110.

Hage, P.M., B.G. Ruessink & J.J.A. Donker. (2018), Using Argus Video Monitoring to Determine Limiting Factors of Aeolian Sand Transport on a Narrow Beach. *Journal of Marine Science and Engineering 6*, 4, 138.

Hage, P.M., B.G. Ruessink & J.J.A. Donker. (2018), Determining Sand Strip Characteristics Using Argus Video Monitoring. *Aeolian Research 33*, 1-11.

Conference abstracts and proceedings

Ruessink, B.G., C. Schwartz, **P.M. Hage**, Y. Smit, W. de Winter & J.J.A. Donker. (2018), Predicting Potential Aeolian Sand Supply to a High and Steep Foredune. AGU General Assembly 2018, Washington D.C., USA. (poster pres.)

Hage, P.M., B.G. Ruessink & J.J.A. Donker (2018), Using Argus Video Monitoring to Determine Limiting Factors of Aeolian Sand Transport on a Narrow Beach. NCK days 2018 (poster pres.)

Hage, P.M., B.G. Ruessink & J.J.A. Donker (2017), Studying Aeolian Sediment Transport Using Video Monitoring. NCK days 2017 (oral pres.)

de Groot, A., S. de Vries, B. Arens, W. de Winter, J.J.A. Donker, L. Duarte Campos, F. Galiforni Silva, P. Goessen, **P.M. Hage**, B. Hoonhout, J. Keijsers, A. Montreuil, J. Mulder, C. Nolet, P. Rauwoens, M. Riksen, B.G. Ruessink, M. Smit,

Y. Smit, G. Strypsteen, B. van der Valk, M. van Puijenbroek, K.M. Wijnberg & I. Williams (2017), Studying Aeolian Sediment Transport Using Video Monitoring. NCK days 2017 (oral pres.)

Hage, P.M., B.G. Ruessink & J.J.A. Donker (2016), Determining Sand Strip Characteristics Using Argus Video Monitoring. 12th Argus Workshop, Duck, USA (oral pres.)

Hage, P.M., B.G. Ruessink & J.J.A. Donker (2016), Determining Sand Strip Characteristics Using Argus Video Monitoring. 9th ICAR Conference, Mildura, Australia (poster pres.)

Hage, P.M., B.G. Ruessink & J.J.A. Donker (2016), Determining Characteristics of Sand Strips on a Narrow Beach by Using Video Monitoring. NCK days 2016 (poster pres.)

Hage, P.M. & B.G. Ruessink (2015), Video Monitoring of Aeolian Activity on a Narrow Beach. NCK days 2015 (poster pres.)